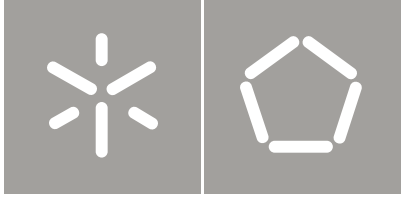

Universidade do Minho
Escola de Engenharia

Mário Simões Correia

Modelling the ejection friction in injection moulding
Estudo do atrito associado à extração de peças moldadas por injeção

Tese de Doutoramento
Ciência e Engenharia de Polímeros e Compósitos

Trabalho efectuado sob a orientação de
António Sérgio Pouzada
António Sousa Miranda
Carlos Alexandre Bento Capela

Janeiro de 2013

Guimarães, ___/___/_____

Assinatura: _____

ACKNOWLEDGEMENTS

This work would have not been possible without the valuable support and help provided by several individuals, institutions and companies. I want to express my gratitude to all of them and refer those whose contributions were of major importance.

First and foremost I would like to thank my supervisor, Professor Pouzada, for the continuous support, availability and encouragement, for his valuable suggestions during all this work. His rigorous work methodology and outmost scientific skills were of great help regarding the scope, organization and the reviewing of all the work involved in this thesis. I can never truly value all the experience and teachings that he provided me during all the time I spent with him. Thank you very much Professor Pouzada!

To Professor Sousa Miranda, co-supervisor of this work, for the theoretical discussions, result analysis and reviewing of this document.

To my colleague of Polytechnic Institute of Leiria and co-supervisor of this work Doctor Carlos Capela for his support, encouragement and friendship.

To the Polytechnic Institute of Leiria for the financial support and leave of lecturing during part of the research period.

I thank the Foundation for Science and Technology, for the research grant SFRH/PROTEC/49301/2008.

To Professor Walter Friesenbichler, from Montanuniversitaet Leoben, Department Polymer Engineering and Science, in Austria, for his interested support, and allowance to use their laboratory space and equipment during the period spent at the Polymer Competence Center Leoben.

I thank Doctor Gerald Berger for his support in the work developed in the Polymer Competence Center Leoben, for many interesting discussions on the demoulding issues and about the characterization of surface roughness.

To CEMUC, Center of Mechanical Engineering of the University of Coimbra, for providing the in-house finite element code DD3IMP.

To Damásio S.A. in Leiria, Portugal in the person of Eng. Hugo Damásio for the possibility of machining the metallic probes.

To Mr. João Ramos from F. Ramada, Aços e Indústrias, for the help on choosing the steels for the metal probes.

To my good friend Marta Oliveira from the Mechanical Engineering Department of University of Coimbra, for her support and friendship, and scientific skill sharing.

To my friend Rui Ruben for his friendship, good mood and help in the development of the computer program for roughness characterization.

To all my colleagues at the Polytechnic Institute of Leiria, especially the colleagues from my Mechanical Engineering Department.

To my PhD colleagues, Pedro Martinho, Joel Vasco, António Selada and João Matias for their fellowship, discussion of ideas and suggestions throughout this period.

To my colleagues of DEM-ESTG/IPLeiria and DEP/UMinho Guimarães, for their direct or indirect contribution to this work, and their continuous help and friendship. Special thanks to Carlos Mota and Carlos Dias of DEM-ESTG/IPLeiria for their help in the laboratory works.

To all my good and trustful friends, who have always supported me and encouraged me to proceed!

To my family (my parents and in-laws) for the magnificent support and encouragement. Without them it wouldn't have been possible to achieve the

objective that I had proposed. These words are for them even if they are written in English. *Obrigado!*

To my sons Maria Sofia and Nuno Luís for the smiles they gave me every morning. For all the days that I have stolen to them to ensure they will have a better future. *O pai ama-vos muito!*

Finally, but not for last... I wish to thank my wife. This research work and the degree achievement itself are entirely dedicated to her. Thank you for supporting me even when I was in a bad mood. I love you Fátima.

ABSTRACT

The quality of parts produced by injection moulding may be affected during the ejection stage of the moulding cycle. At this stage the parts are mechanically forced to separate from the moulding surfaces. The ejection force depends on the shrinkage of the polymer onto the core and on the friction properties of the contacting surfaces at the moment of extraction. As during moulding there is a replication of the part on the mould surface the ejection process is also dependent on the plastic deformation of the moulded material. Ejection takes place in a very short time, hence the static coefficient of friction must be considered for modelling the ejection process.

To understand the contribution of the mechanisms involved in friction during the ejection stage, a mixed approach was developed: analytical simulation for the ploughing component, numerical simulation for the deformation mechanism, and an experimental inference for the adhesion. The study was based on the observation of three materials that are commonly used in injection mouldings: polypropylene, polycarbonate and a blend of polycarbonate/acrylo-nitrile-butadiene. The friction behaviour was studied with two testing methods: a prototype tester that is fitted to a universal testing machine, and an instrumented mould for the characterization of the friction force.

The relevance of roughness, temperature and contact pressure on friction was evidenced, on the actual value of the static coefficient of friction that applies in the demoulding of thermoplastic mouldings.

RESUMO

A qualidade das peças produzidas por moldação por injeção pode ser afetada durante a fase de extração do ciclo de moldação. Nesta fase, as peças são forçadas mecanicamente a separar-se das superfícies do molde. A força de extração depende da contração do polímero e das propriedades de atrito das superfícies em contacto no momento da extração. No processo de injeção uma réplica da peça é gerada sobre a superfície do molde assim, a força de extração é dependente da deformação plástica do material injetado. A extração ocorre num espaço de tempo muito curto, por isso o coeficiente de atrito estático deve ser considerado para a modelação do processo de extração.

Para compreender a contribuição dos mecanismos envolvidos no atrito durante a fase de extração, uma abordagem mista foi desenvolvida: simulação analítica para a componente de sulcagem, simulação numérica do mecanismo de deformação e inferência experimental da componente da adesão. O estudo foi baseado na observação de três materiais de uso corrente em peças injetadas: polipropileno, policarbonato e uma mistura de PC/acrilo-nitrilo-butadieno. O comportamento em atrito foi estudado recorrendo a dois métodos diferentes de ensaio: um protótipo que está acoplado a uma máquina de ensaio universal e um molde instrumentado para a caracterização da força de atrito.

A relevância da temperatura, rugosidade e pressão de contacto no atrito foi evidenciada para os valores reais do coeficiente de atrito estático que ocorre na desmoldagem de componentes termoplásticos.

TABLE OF CONTENTS

1. INTRODUCTION

Today thermoplastics are the most widely used materials for applications ranging from non-critical packaging products to very demanding technical parts. These parts are frequently made by injection moulding. In the injection moulding cycle, the mechanical process of ejection of the parts may affect their quality; at this stage the parts are mechanically forced to separate from the moulds. This ejection force may be quite high if the parts are moulded over deep cores.

The design of the ejection system depends on factors such as the draft angles, the surface finish, and the properties of the moulding material at the ejection temperature (Pouzada, Ferreira *et al.* 2006). The geometry and the location of the ejector pins depend significantly on the shape of the part and the architecture of the cooling system. Nevertheless, the most important factor for designing the ejection system is the ejection force that varies with materials and the processing conditions (Pontes, Pantani *et al.* 2002). The ejection system must not fail during production, since this will lead to the interruption of the production run or the damage of the mould (Araújo and Pouzada 2002).

The friction force that develops between the polymer moulding surface and the mould surface of the mould results from the polymer shrinkage part onto the mould. Furthermore the polymer surface tends to replicate the mould surface texture, this may become an additional problem in the ejection stage. The more intimate contact caused by the shrinkage and the replication, in the case of

chemical affinity between the moulding and mould materials, may originate adhesion that has to be overcome upon ejection.

The optimisation of the injection mould systems requires that the frictional behaviour of the mouldings during ejection is known and predictable (Araújo and Pouzada 2002; Pontes, Pantani *et al.* 2002; Pouzada, Ferreira *et al.* 2006).

The quality of parts produced by injection moulding may be affected during the ejection stage of the moulding cycle. At this stage the parts are mechanically forced to separate from the moulding surfaces. The ejection force depends on the friction properties of the contacting surfaces at the moment of extraction. As during moulding there is a replication of the part over the mould surface, the ejection process is also dependent on the yield strength and the plastic deformation of the moulded material. The duration of the extraction process is very short in time, thus the friction coefficient relevant for modelling the process is the static coefficient of friction (Pouzada, Ferreira *et al.* 2006).

The concerns of this study are in modelling the friction during the ejection stage. Basically the phenomenon that occurs here is the interaction between two surfaces, the moulding surface and the new plastic surface formed. To make the ejection of the plastics part, it is necessary to push it out from the mould cavity. It is necessary to wait that plastics part reaches a defined temperature. The choice of that temperature (ejection temperature) is very important. That is the difference from getting a good plastics part or a deformed or even destroyed plastics part. As ejection occurs while the mouldings are at elevated temperature, excessive or unbalanced demoulding forces may cause localized and gross deformation of the part, leading to part inefficiency (Pouzada, Ferreira *et al.* 2006). Thus, to eject the plastics part from the mould it is fundamental to know how the behaviour of this tribological system will be. The composition of this tribological system is: mould material, moulding material and the surfaces. During the injection processes, the temperature variations do not influence the behaviour of the mould (in most

cases it is a metallic mould), but in the plastics moulding many changes occur during the injection moulding process. The polymer in the moulding, starts by being solid, then melts and finally cools down to the solid state again. So for the plastics part there is a complete thermomechanical cycle that causes big differences in the mechanical properties during the injection moulding cycle. The contact pressure, roughness and mechanical properties of contacting materials pair have a relevance action in the coefficient of friction.

The structure of this thesis is as follows: firstly, there is this introductory chapter, where it is explained the motivation to study this problem and what are the most important involved variables. This is followed by the review of the state of the art, Chapter 2, of the injection moulding process and ejection issues. At this stage some considerations are made about friction, friction models and roughness characterization.

In Chapter 3 the proposed model based on material properties and roughness is described. This model is a three-term model, including the various components of friction: ploughing, deformation and adhesion.

The fourth chapter describes the experimental methods. These include the materials, samples used in the friction tests and the equipment used to do the characterization of the mechanical properties. The samples used in the Mouldfriction prototype apparatus were made by injection moulding at the University of Minho. At the Montanuniversitaet Leoben it was used their instrumented injection mould. Also in this chapter is described the equipments used for the topography characterization. The chapter closes with the description of the simulation software used.

In Chapter 5 it is made the presentation and discussion of results. Tests were carried out to obtain the mechanical properties of the plastics material at various ejection temperatures, and the friction force evolution. It was possible

to compare the variation of friction force with the contact pressure, temperature and roughness.

Finally, the main conclusions are drawn and recommendations for further work are proposed.

2. STATE OF THE ART

2.1 Injection Moulding

Plastics are used in a wide range of applications in engineering products such as gears, cams and bearings in substitution of metallic parts have gained an increased importance (Zhang 1998). Many of these products are made by injection moulding of engineering thermoplastics. To obtain the best performance of these products, for instance longer life time and reduced energy consumption, both tribological properties and processing conditions must be tuned up (Apichartpattanasiri, Hay *et al.* 2001).

Injection moulding is the most used process due to its flexibility for replicating complex shapes at fast production rates. During this process, the polymer undergoes a complex thermomechanical history, which influences the mechanical properties and the final dimensions (with respect to the corresponding mould dimensions) of the part (Titomanlio and Jansen 1996; Viana, Cunha *et al.* 2001).

The process encompasses four stages: filling, packing, cooling and ejection. Ejection is critical when complex geometry parts are produced and distortion or denting may be caused by the ejectors (Araújo and Pouzada 2002).

The performance properties of the part depend on the manufacturing conditions. The close relationship between processing conditions and mechanical properties was observed in amorphous and semi-crystalline

polymers, as for example (Schmidt, Opfermann *et al.* 1981). In injection moulding the thermal and the mechanical phenomena are strongly coupled. This thermomechanical environment is characterized by high-temperature gradients and stress levels and their local variations in the space domain of the moulding (Viana, Billon *et al.* 2004).

2.2 Shrinkage

The shrinkage of the moulding is an aspect of utmost engineering importance as it influences not only the dimensional accuracy of the product but also the ejection process from the mould. In the case of semi-crystalline materials where the shrinkage is higher than in amorphous polymers the prediction of shrinkage justifies complex consideration of the processing conditions and the molecular structure of the material (Schmidt, Opfermann *et al.* 1981; Pontes, Oliveira *et al.* 2002).

The demoulding force can be worked out using a suitable coefficient of friction and the normal force. According to Burke and Malloy (Burke, Malloy *et al.* 1991) shrinkage is the result of two separate phenomena: thermal contraction and directional distortion. The thermal contraction is volumetric in nature and is due to the reduction of the mean inter-atomic distance as temperature changes. The directional distortion is a result of the orientation of the polymer molecules during flow and their subsequent relaxation back to a coiled state when the flow ends.

Shrinkage is material dependent and varies significantly from amorphous to semi-crystalline polymers it being greater for semi-crystalline than for amorphous polymers which have more gradual volume contraction (Schmidt, Opfermann *et al.* 1981). The cooling rate, the glass transition temperature (with the substantial change of the shrinkage coefficient), the use of additives in the material and the degree of crystallization are other parameters that affect the overall shrinkage (Delaney, Bissacco *et al.* 2012). The shrinkage is affected by

the flow-induced residual stresses and orientation, the flow-induced crystallization and the heat transfer. These factors are influenced by processing parameters such as packing pressure, packing time, melt temperature, mould temperature, injection speed, and material properties as well as geometric constraints (Kwon, Isayev *et al.* 2006). The anisotropic shrinkage cannot be predicted based only on volume shrinkage. It is greatly influenced by ejection temperature, is material dependant, and is very different in amorphous and semicrystalline polymers. Larger gates, long holding times, and high holding pressures in the injection moulding process can compensate for the shrinkage of the part (Pontes, Pantani *et al.* 2001; Pontes, Pantani *et al.* 2002; Kinsella 2004). In particular Pontes and co-workers focused on tubular mouldings where the shrinkage effects tend to be more evident. An early experimental study of shrinkage in injection moulded products was made by Jansen *et al.* (Jansen, Pantani *et al.* 1998). They found that if a constraint prevents the in-mould shrinkage to take place, the final shrinkage may decrease if the holding pressure and time are small.

A numerical and experimental study for the determination of the ejection force using boxes of polycarbonate was carried out by Wang *et al*. (Wang, Kabanemi *et al.* 2000). This study concluded that during solidification the box conforms to the mould core geometry, while it deforms right after ejection. The core provides constraining forces to prevent free shrinkage and warpage of the box before it is ejected. During ejection, friction forces are induced at the mould-part interface, so the ejection force provided by the ejector pins is basically required to overcome friction and to remove the box (Figure 2.1). Therefore the analysis of the ejection process must be based on the constraining and friction forces resulting from mould-part interaction during solidification and ejection.

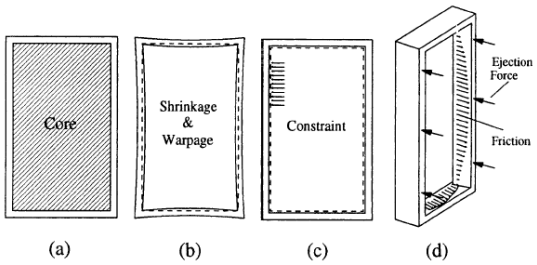

Figure 2.1: Mechanism of part ejection during injection moulding of plastics: (a) before ejection; (b) after ejection, (c) constraint by mould; (d) ejection (Wang, Kabanemi *et al.* 2000)

2.3 Replication

Injection moulding of plastics is basically a replication process. The main objective is obtaining a replica of the impression, the space that will be filled by the molten plastics. The critical steps in the replication processes are the filling, holding and demoulding of the moulded parts.

In injection moulding, during solidification, the plastics part shrinks onto the core while in the molten or very deformable state. As a consequence the moulding surface tends to replicate the topography of the moulding block core (Ferreira, Costa *et al.* 2004), Figure 2.2.

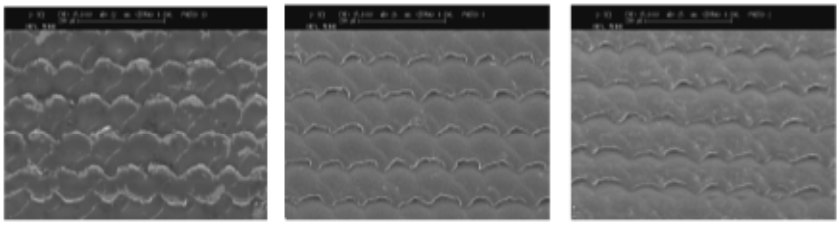

Figure 2.2: SEM images: 1- of the steel moulding surface, 2 – of polycarbonate sample surface and 3 - polypropylene surface sample, (Ferreira, Costa *et al.* 2004)

The replication effect is not usually considered in tribological studies and processes but plays a fundamental role in the ejection process of injection mouldings (Pouzada, Ferreira *et al.* 2006).

2.4 Ejection in injection moulding

The demoulding step in the injection moulding process is the last of the moulding cycle. The demoulding stage is a critical issue recognized in injection moulding technology by many authors *e.g.;* (Heckele and Schomburg 2004; Derdouri, Ilinca *et al.* 2005), who highlight that most replication problems are not caused by the filling of the mould but by demoulding.

The location of the pin ejectors and the definition of its geometry depend significantly on the geometry of the part and the architecture of the cooling system. However, the most important for the dimensioning of the ejection system is the ejection force that varies with the materials and the processing conditions (Pontes, Pantani *et al.* 2002). Ejection is critical when complex geometry parts are produced and distortion or denting is caused by the ejectors (Araújo and Pouzada 2002), to avoid these problems Araújo *et al.* (Araújo, Pontes *et al.* 2003) recommended that efficient ejection systems should be designed for injection moulds. Hu and Massod (Hu and Masood 2002) developed an Intelligent Cavity Layout Design System (ICLDS) for multiple cavity injection moulds. From a practical point of view the system developed

can be used as a tool for designer to implement cavity layout design of injection mould at concept design stage. To prevent the part deformation or the damage of the moulding by the ejector pins, a method for the determination of the layout and size of the ejector pins was proposed by Kwak *et al.* (Kwak, Kim *et al.* 2003).

Pontes *et al.* (Pontes, Brito *et al.* 2004) performed a series of mouldings with polypropylene materials and showed that high viscosity grades lead to higher demoulding force. Usually the ejector pins cause a vestige in the part, but in some products this is not acceptable and the design of the ejection system must be considered with special attention (Pontes and Pouzada 2004).

Demoulding is particularly problematic for replication of microcomponents or components with microfeatures. Microparts are defined as those which have a mass in the range of a few milligrams, have features in the micrometre range or larger parts with dimensional tolerances in the micrometre range. Due to their small size such microparts and their replication tooling are physically weaker and thus both the tools and parts are more prone to physical damage. Breakage of a part within a mould can lead to additional problems since the residue may embed itself in subsequent parts, cause inadequate filling and potentially further damage to the replication tooling (Delaney, Bissacco *et al.* 2012).

In the case of micromoulds to complete the filling process the mould temperature is kept above the T_g of the polymer to ensure the flow of the melt into all impression features during the injection process. Upon complete filling, the mould temperature decreases rapidly to the ejection temperature of the part. This ensures the total replication of the part onto the mould surface (Attia and Alcock 2011).

In the case of the demoulding of microscale hot embossed pillar-type structures this is also complex because these structures have a reduced structural strength

(Guo, Liu *et al.* 2007). In Figure 2.3 the main demoulding forces in pillar-type structures are highlighted.

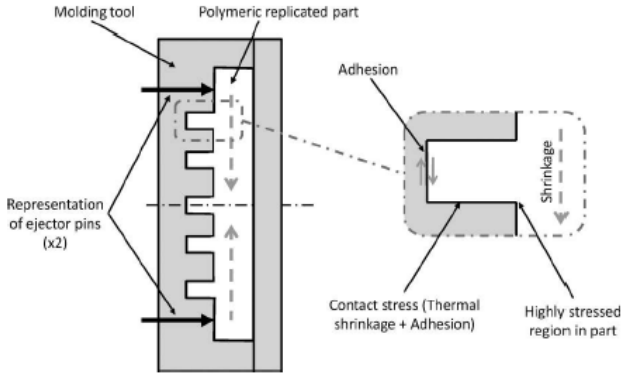

Figure 2.3: Main demoulding forces in pillar-types structures (Delaney, Bissacco *et al.* 2012)

In other types of replication processes similar concerns have been raised regarding demoulding such as thermal imprint lithography (Song, You *et al.* 2008), hot embossing (Worgull, Kabanemi *et al.* 2007) and the automation of the powder injection moulding process (Fleischer and Dieckmann 2006). Even in these cases of replication processes it is suggested that there is an interlocking between the mould tool and the moulding part surfaces. To do the demoulding the degree of replication should be known, the relative velocity of the surfaces and the overall pressure distribution.

The surface roughness is a characteristic of all engineering surfaces. From the machining process to generate the surface of the replication tools imperfections, such as burrs, will appear on the surface resulting on undesired material beyond the desired machined features (Ko and Dornfeld 1991). The existence of these imperfections on the surface results in an increase of the demoulding forces in the case of hot embossing (Schaller, Heckele *et al.* 1999). After the hot-embossing replication, when the part is pushed relative to the replication tool, either the tool or the replicated part must deform sufficiently to allow the demoulding to occur.

Zentay *et al.* modelled the demoulding force for polyurethane seat-like foams to design robot grippers for the automation of the process (Zentay, Zoller *et al.* 1999). If the parameters of the production are not set precisely the demoulding force can be much greater than calculated. This is because adhesion force acts between the mould and the foam (Zentay, Zoller *et al.* 1999).

2.4.1 Materials

The mechanical properties of the materials involved in the ejection of moulded polymers may vary substantially by some orders of magnitude. Typically moulding blocks are made from alloy steels with elastic modulus around 200 GPa, whereas the plastics mouldings are in the order of 1-2 GPa (Crawford 1998).

In specific cases of rapid tooling, which is a field that is gathering increasing interest non-metallic materials with modulus of around 10 GPa are typical (Kinsella 2004; Kinsella, Lilly *et al.* 2005; Gonçalves, Salmoria *et al.* 2007).

The relationship between the draft angle and surface roughness were investigated for stereolithography moulds by Cedorge and Colton (Cedorge and Colton 2000). Experimental demoulding properties were presented by An and Chen (An and Chen 2005) by measuring demoulding force and surface roughness to evaluate tool life and failure mechanism in order to obtain a working range for the process parameters. Due to the good geometric precision Westphal *et al.* also used stereolithography in the manufacture of hybrid mould moulding blocks and studied the performance and friction properties of this combination of materials (Westphal, Pouzada *et al.* 2006).

Using the benefits of the rapid prototyping processes Majewski and Hopkinson (Majewski and Hopkinson 2003; Majewski and Hopkinson 2004) studied the effect of tool finishing on ejection forces using direct metal laser sintered tools. Martinho *et al.* used various rapid prototyping techniques to produce mould

inserts (Martinho, Cardon *et al.* 2008). In their research the ejection aspects associated to hybrid injection moulds were assessed.

Also Pontes *et al.* analysed the performance, especially in ejection of this type of tools (Pontes, Queiros *et al.* 2010). Hybrid moulds with rapid prototyped moulding zones by stereolithography (Ribeiro Jr., Hopkinson *et al.* 2004), or by vacuum casting of steel fibre reinforced epoxy composites (Sabino-Netto, Salmoria *et al.* 2008) were used to study the friction behaviour during the demoulding process.

This wide variation of the data coupled with the replication that occurs in injection moulding may definitely determine the tribological mechanisms associated to the ejection process. Moulders and mouldmakers have to know the mechanisms existent in the several components of the mould tool. The understanding of the wear mechanisms that link them to the design features may avoid or reduce the wear and extend the mould life (Engelmann, Hayden *et al.* 2000). For the ejection system attention is paid to the wear between pins, sleeves and bores which they pass through, but not only these metallic interactions should be taken in account for the mould performance. The wear on the core mould must be reduced and for this the use of lubrication was an option, but now with the requirements of today standard of the ejection part the use of lubricants became inappropriate to reduce the ejection wear (Engelmann, Hayden *et al.* 2002).

Therefore it is important, when testing for friction, to know not only the mechanisms involved in the friction phenomenon and the average value of the friction force (or coefficient of friction), but also the time dependence and stability of the friction force over a range of contact conditions (Blau 2001).

2.4.2 Friction in injection moulding

Removing replicated parts from the mould is described as the demoulding stage. At this stage the replicated part is moved/removed from the mould. This

brings about a friction problem, and a particular and special contacting problem. Plastics parts are typically replicated above the glass transition temperature of their polymers. So, during the cooling stage of the replication process the part shrinks and is constrained by the mould cores. The mechanical properties of the polymeric part and the mould are quite different (by some orders of magnitude) (Crawford 1998) and for this the shrinkage coefficients of the polymeric part and the replication tool (mould) are different too (Pouzada, Ferreira *et al.* 2006; Delaney, Bissacco *et al.* 2012). This shrinkage causes stresses in the cross-section of the part and generates normal forces to the contacting surfaces that results in an additional problem for the demoulding. The force described results from the injection process itself and the cooling of the new polymeric part generated. After this injection process it is necessary to remove the part from the mould core and for this the tangential force required must overcome this effect (Pontes and Pouzada 2004).

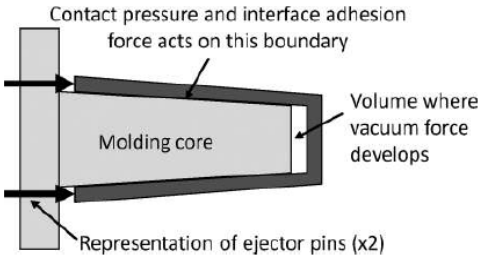

Figure 2.4: Demoulding forces for a cylindrical component (Delaney, Bissacco *et al.* 2012)

If atmospheric pressure does not exist between the part and the core mould during the demoulding action, a suction force will resist to the demoulding phase, thus increase the overall demoulding force required, as shown in Figure 2.4 (Delaney, Bissacco *et al.* 2012)

Factors that influence ejection friction

Economics imposes that the moulded parts are ejected as soon as they are dimensionally stable, in order to shorten cycle times (Ferreira, Neves *et al.*

2002). As ejection occurs while parts are at elevated temperatures, excessive or unbalanced demoulding forces may cause localized and gross deformation of the part, leading to part inefficiency (Bhagavatula, Michalski *et al.* 2004). The ejection system cannot fail during production, since this leads to the interruption of the injection process or to the damage of the mould (Araújo and Pouzada 2002).

Despite considerable knowledge regarding component and tool design, mould filling, tool fabrication and general processing requirements, part demoulding has often been neglected or given little importance on its effects on parts manufacturability (Delaney, Bissacco *et al.* 2012).

For an understanding the factors that influence the demoulding issues, and the mechanisms associated to the factors contributing to the demoulding force Delaney *et al.* made a review and classification of demoulding issues and proven solutions (Delaney, Bissacco *et al.* 2012). This work categorises the factors that influence demoulding force as being: the tool and part designs, normal force (the totality of shrinkage), relative tool/part material properties, surface topography, surfaces energies, electrostatic charge and the amount of moisture present. The factors discussed influence the demoulding force, and affect the coefficient of friction of the contacting pair. So the factors affecting this coefficient of friction must be targeted in any attempt to systematically reduce the overall demoulding force and the stress which will be acting on the components and replication tools. Menges *et al.* categorise these factors as being the result of the mould, moulding geometry, moulding material and processing conditions (Menges, Michaeli *et al.* 2001). Later on Pontes *et al.* studied the effect of holding pressure and the core surface temperature on the ejection force for various polymers (Pontes, Pouzada *et al.* 2005).

Despite considerable knowledge regarding component and tool design, tool filling, tool fabrication and general processing requirements, part demoulding

has often been neglected or given little importance on its effects on parts manufacturability (Delaney, Bissacco *et al.* 2012).

Consequences in product characteristics and performance

Demoulding is a common reason for process failure, often resulting in part or tool distortion and breakage, and also can affect the lifetime of the replication tool. These problems are concerned to the generation of new surfaces (parts) onto the replication surface (mould). The replication of small or micro-structured parts by injection moulding raises several challenges compared to macro-sized parts (Heckele and Schomburg 2004). The challenges for the structural strength of replication tools, specifically the microcores for high aspect ratio parts are already noted into the replication of microfeatures. When applying the ejection force by the ejection pins after the replication of the polymeric part onto this mould microfeatures, the development of tensile stress greater than the core tensile strength as show in (Hopkinson and Dickens 2000) albeit for the case of macroscopic parts produced using stereolithographic tooling. To successful demoulding without deformation or destruction of the parts with microstructures depends not only on the geometry and material used but also on the nature and position of the ejection force applied (Michaeli and Gartner 2006). The productivity in the injection moulding process requires the minimization of the cooling time at the cost of higher temperatures and poor mechanical properties of the moulded part (Ferreira, Neves *et al.* 2002). Internal stresses are caused by the thermomechanical process and with the demoulding force applied consequences will appear in the moulding part. The effect of the demoulding process results in some cases in the permanent deformation or distortion of the replicated part, regardless the demoulding force is applied to the parts that should be rigid enough to ensure no deformation in the part (Wang, Lee *et al.* 1996; Engelmann, Hayden *et al.* 2000; Ferreira, Neves *et al.* 2001). Unfortunately previous experiences from tool designers combined with the industrial experience of the mouldmakers

involving good felling and trial-and-error became preponderant in the options for the mould design. Such *ad-hoc* approaches can result in sub-optimal tool designs and increase both the product development cycle duration and the overall cost (Delaney, Bissacco *et al.* 2012). The demoulding problem is even more evident for micromouldings or parts with microfeatures. The demoulding of parts possessing dimensions or tolerances in the micrometre range needs a particular care, according to the difficulty of ejection (Heckele and Schomburg 2004). This phenomenon is accentuated for parts processing with high aspect ratios (Michaeli, Rogalla *et al.* 2000). Demoulding surface agents can be used, but this solution should be avoided in the case of medical or microfluidic applications parts, due to the possible contamination of the parts (Becker and Gärtner 2008). According to Michaeli and Gartner the concentrated demoulding forces provided by the traditional ejector pins are not suitable, because of the deformations or failure of the microparts (Michaeli and Gartner 2006) . A problem subsists with the mark of the ejector on the part. Mechanical ejector pins could be then an alternative solution (Wu and Liang 2005). According to Michaeli *et al.* new concepts were recently proposed for the demoulding techniques base on vacuum solutions, mechanical retraction systems of cavity or ultrasonic vibrations (Michaeli, Rogalla *et al.* 2000) . In addition, the surface roughness of the mould plays an important role during this phase. A new method has been developed by Yang *et al.* and involves decreasing the frictional coefficient of friction on the mould wall (Yang, Zhao *et al.* 2005). The material shrinkage has a major influence on the demoulding accuracy of the microstructured part. A precise control of the shrinkage by controlling the different processing phases can be a better solution for improving the demoulding (Giboz, Copponnex *et al.* 2007).

2.4.3 How to modify the friction properties

An extensive review of the effect of coatings in the contact mechanisms and surface design for generic processes was made by Holmberg *et al.* (Holmberg,

Matthews *et al.* 1998). During sliding, physical and chemical changes occur in accordance with the physical and chemical laws. The effects of the relative movement of the surfaces are friction, wear, temperature, sound and dynamic behaviour.

In the specific case of injection moulds the use of CrN coatings resulted in the reduction of frictional forces during ejection stages of a POM test ring. In the case of coatings of TiN or MoS_2 higher friction forces were developed with wider standard deviations (Dearnley 1999).

Charmeau *et al.* studied coatings for thermoplastics injection moulds to increase the lifespan of the mould before maintenance and decrease of the ejection force (Charmeau, Chailly *et al.* 2008). Polished surface and coatings processes were analysed. The coatings processes were PVD (Phase Vapour Deposition) and PACVD (Plasma Assisted Chemical Vapour Deposition) allowing thin coating manufacturing. The coatings investigated were Chromium Nitrium (CrN), Titanium Nitrium (TiN), Diamond like Carbon (DLC), glassy deposit (SiO_x) and Chromium. Two polymers were tested: a semi-crystalline poly(butylene terephthalate) (PBT) and a blend of copolymers of styrene acrylonitrile and acrylonitrile butadiene styrene (SAN/ABS). The analyses of the coatings in the ejection stage proved that their impact was polymer dependent. The ejection forces tends to increase for SAN/ABS and decrease for PBT.

Griffiths *et al.* (Griffiths, Dimov *et al.* 2007) studied the factors affecting the flow behaviour and paid a special attention to the interaction between the melt flow and the tool surface roughness. In another work (Griffiths, Dimov *et al.* 2008) they used design of experiments to study the demoulding of a microfluidics part as a function of a tool surface treatment and process parameters. The demoulding force was reduced and part quality improved with the use of the DLC surface treatment. The absence of a unique parameter level to optimize demoulding behaviour for the surface treatment and polymers

investigated was highlighted. Later they investigated the effect of two different surface treatments on the demoulding behaviour of parts with microfeatures (Griffiths, Dimov *et al.* 2010). In this research work on DLC the surface originated a reduced demoulding force for PC and ABS compared to the untreated surface.

Neto *et al.* presented experimental results using steel inserts with CVD diamond-coating over a CrN interlayer (Neto, Vaz *et al.* 2009) . To reduce the wall adhesion and simultaneously improve the mould heat extraction rates was their main objective. This preliminary work demonstrated the possibility of using CVD polycrystalline diamond to enhance plastic injection moulding and also highlights the importance of further studies to statistically evaluate the durability of the coating.

Also Cunha *et al.* showed that the surface treatment with titanium nitride (TiN) and chromium nitride (CrN) reduces the coefficient of friction (Cunha, Andritschky *et al.* 2002). The PVD nitride coatings have significantly better wear resistance than the substrate protected by traditional processes (heat treatment, nitriding the surface or hard chromium coating deposition).

Van Stappen *et al.* (Van Stappen, Vandierendonck *et al.* 2001) proposed to simulate the demoulding of the injection process in laboratory and correlated the results with surface energy measurements of the coated mould and of the plastics material. The main objective was helping in the decision of a proper coating for a certain kind of plastics. No correlation could be found between the demoulding behaviour of plastics *vs.* coated moulds and the measured surface energy values.

2.4.4 Optimization solutions to decrease ejection friction

On reviewing polymer-based microfabrication technologies Becker and Gartner identified some important features of replication tools (Becker and Gärtner 2008): (a) the geometrical replication depends upon the geometrical

accuracy of the master, (b) for successful demoulding no undercuts in the structure itself can be allowed, (c) the surface roughness of the master should be as low as possible for replicating structures and (d) a suitable interface chemistry between master and substrate has to be selected.

To ensure a good solution for the demoulding issues the principle that rules the better solutions assumes that the tool and the part designs can be optimized to maximise the likelihood of successfully demoulding. Well-known examples for injection moulded products are to add draft angles on all tool cores, to have a constant wall thickness throughout the part and to gate the part on the thickest region. The part deformation problems can be approached by increasing the structural rigidity of the part for successful demoulding in terms of design such as adding bosses/ribs where possible and the selection of optimum materials and processing parameters (Delaney, Bissacco *et al.* 2012).

Other less known solutions to part design which may be more applicable to micro-structured parts include sacrificial barriers. These are non-critical structures deliberately included in the part geometry to resist overall shrinkage in the vicinity of the microstructures. In the microhot-embossing context Worgull *et al.* used a frame to limit the in-process flow front (to reduce warpage and shrinkage) and create sacrificial features to take up the high contact stress during demoulding (Worgull, Heckele *et al.* 2005). A similar auxiliary structure as a thermal stress barrier in the form of an additional circular structure around the field of microstructure has been proposed by Guo *et al.* (Guo, Liu *et al.* 2007). The simulation results by finite element modelling predicted a significant reduction in the stress experienced by microstructures. One disadvantage of this approach is the additional space on the component to locate the sacrificial stress barrier.

Wang and co-workers studied an optimum ejector pins layout that distributed the overall ejection force among a series of ejector pins In these works different layouts, location, dimension, quantity and distribution of the ejector

pins were considered. The objective was to identify the balanced layout causing minimum stress and deformation to the product and developed a strategy of numerical optimization of the demoulding stage. The studies dealt with conventional demoulding concept of ejector pins to physically push off the component from the mould core. To predict the distribution of the ejection force among ejector pins a finite element thermoviscoelastic solidification analysis was performed. An assumption of uniformly friction distribution cannot be generalized and the balanced ejection is not simply balancing the ejector pins layout according the interface areas. The primary premise, according to Wang *et al.* (Wang, Kabanemi *et al.* 2000), is that the corners of the moulding will limit the shrinkage and thus minimise the contribution of warping to demoulding force. On the other hand the local stiffness of the part must be considered, so in reality the local contact pressure will be influenced by both the shrinkage and stiffness of the part.

Bataineh and Klamecki (Bataineh and Klamecki 2005)studied improvements to the ejector pins layout to predict local mould-part force. Experiments were made using ring and box-shaped parts to provide input of the coefficient of friction, material properties and total and local ejection forces, to the simulation process. Michaeli and Gartner proposed and trialled non-destructive methods to do the demoulding without ejector pins or plates (Michaeli and Gartner 2006). The method used was demoulding with ultrasonics. It was expected that with the utilization of ultrasonics the oscillation between the mould and the part would reduce the wall adherence this resulting in the reduction of the demoulding force, but the experimental results did not report this assumption.

Despite the improvement of the ejection system, the surface topography has been used as an indicator of the most dominant friction mechanisms. The principle of solution is that the replication tool surface has a topography which will minimise the overall demoulding force. In the context of minimizing the

overall time required to finish rapid tools Majewski and Hopkinson summarized the effects of tool surface roughness on part quality and demoulding force for parts injection moulded using laser sintered tools (Majewski and Hopkinson 2003). In this work it is suggested that the ejection force can be minimised through the use of very low surface roughness. However, Ferreira *et al.* (Ferreira, Neves *et al.* 2001) mentioned that very good polished surfaces (mirror-like) may facilitate the formation of a seal which prevents air entering the gap between the core and the part resulting in the local formation of vacuum forces that can make difficult to separate the part from the core. Finishing the core in the ejection direction air can enter the gap allowing atmospheric pressure to exist between the plastic and the steel core, eliminating the vacuum force. The existence of an optimum core surface roughness was reported by Sasaki *et al.* (Sasaki, Koga *et al.* 2000) with similar results observed by Pontes *et al.* (Pontes, Ferreira *et al.* 2004) and noted by Pouzada *et al.* (Pouzada, Ferreira *et al.* 2006). As the previous authors Kyuichiro (Kyuichiro 1995) verified in several pin-on-disk tests the same behaviour.

2.5 The mechanism of friction

In the early work on the discussion of the mechanism of friction Bowden put a simple question *"What is the cause of the resistance happening at the interface between solids during sliding?"*(Bowden 1952). At that time Bowden hoped that the discussion not becoming a humdrum topic.

In their classic textbook Bowden and Tabor identify two main contributions to friction (Bowden and Tabor 1986): the first one is connected to the adhesion between the contacting asperities, and the second to the asperities or bulk surface plastic deformation.

It is desirable to be able to isolate the contribution of each friction mechanism to the overall demoulding force (Delaney, Kennedy *et al.* 2010). The main

mechanisms in the normal sliding conditions encountered in engineering applications are the deformation and the adhesion components of the friction (Kim and Suh 1991). The deformation component of friction includes the ploughing of the surface by the hard surface (Kim and Suh 1993).

According to the adhesion and deformation model of friction (Bhushan 2002), the coefficient of friction can be presented as a sum of the adhesion component and the deformation component.

2.5.1 Ploughing

Kim and Suh (Kim and Suh 1991) described the mechanism of friction on three basic contributing factors. The frictional force is generated by asperity deformation, wear particles and adhesion. These developments suggested that the mechanical interactions at the sliding interface are the primary causes of friction between two surfaces.

Ploughing friction models assume that the dominant contribution to friction is the energy required to displace material ahead of a rigid protuberance moving along the surface. Such ploughing through plastic deformation will result in the formation of scratches across the surface of the replicated parts. But on the other hand the movement of the protuberance does not result in plastic deformation so there will be no scratching of the surface. This phenomenon, known as hysteresis, occurs due the subsequent recovery of the polymer after the indentation (Delaney, Bissacco *et al.* 2012). All the deformation that exists is elastic deformation and totally recovered. It is governed by the elastic or viscoelastic properties of the polymer, the relative velocity of the surfaces (the demoulding rate), and also the overall pressure distribution. Worgull *et al.* published results from simulated replication trials with the variation of the demoulding rates (Worgull, Kabanemi *et al.* 2008). The coefficient of static friction becomes substantially higher for the decrease of the demoulding rate.

The ploughing term associated to a conical asperity has been discussed by Tabor (Tabor 1981), who did not consider the mechanical properties of the contacting pair. In the Tabor model for sliding friction, the asperities (protuberances) of the harder surface are assumed to plough through the softer one. The ploughing resistance causes a force contributing to the frictional force. This contribution is referred to as the ploughing component of friction, the deformation term. A simple estimation for conical asperity of semi angle θ (Figure 2.5) gives the coefficient of friction due the ploughing term as:

$$\mu_d = \frac{2}{\pi}\cot\theta \tag{2.1}$$

The slope of surface asperities is less than 10°, that is, the semi angle $\theta > 80°$, and the coefficient μ_d should be about 0.05 and less. When elastic contact occurs, μ_d is often assumed to be negligibly small.

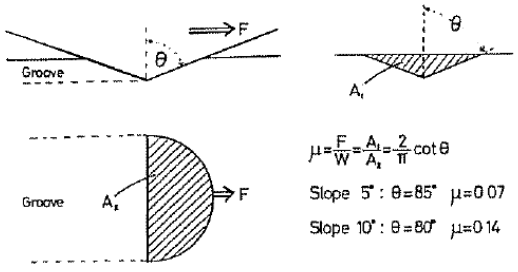

Figure 2.5: Ploughing term due to a conical asperity on a soft material (Tabor 1981)

During sliding the engineering surfaces (which are rough) are subjected to the so-called ploughing of the hard asperities into the softer mating surface. Hard particles, metal debris or other particles from the environment may also contribute to this deformation. With elastic deformation, that is if the penetration of asperities is small, the ploughing does not result in the formation of permanent tracks. If plastic deformation occurs, which is almost always the case with metals, grooves are left behind in the softer surface (Bowden and Leben 1939). Van Beek considers if the hardness of sliding surfaces differs by > 20% the roughness summits of the hard surface penetrate the softer material

(van Beek 2006). The Figure 2.6 shows the model used in the finite element code that considers a rigid sphere in contact with a less hard surface.

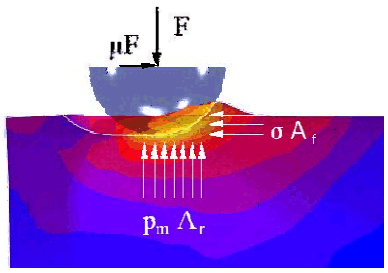

Figure 2.6: Model of ploughing friction (van Beek 2006)

To reduce friction due the ploughing low roughness should be achieved, this increasing the contacting radius and originating a larger area of contact (van Beek 2006).

2.5.2 Adhesion

Before refer the phenomenon of adhesion we must refer first the adsorption. It is an essential fact that the surface can be treated both as an ideal geometrical object with a highly peculiar topography and a physical object possessing a certain thickness and a specific mechanical behaviour. The atoms and molecules belonging to the surface have fewer "neighbors" than those in the bulk (van Beek 2006). This simple fact has consequences for the geometry and physics of a surface, so the interactions between its atoms and their neighbours vary, distorting the force field that penetrates to the depth of several interatomic distances (transitional layer). An excess of energy appears and the surface tension is a measure of a surface energy. Solids can be rated in the order of their surface tension into three groups; solids with high surface tension up to several Joules per square meter in vacuum (most of the metals and their oxides); solids with medium surface tension of the order of tenth fractions of Joule per square meter (e.g., ionic compounds) and solids with low surface tensions (most of the polymers).

Figure 2.7 shows schematically that the structure of the boundary layer is quite intricate. The mechanical behaviour of boundary layers accordingly demonstrates a rich spectrum of properties ranging from viscoelastic behaviour to perfectly elastic one (Myshkin and Petrokovets 2004).

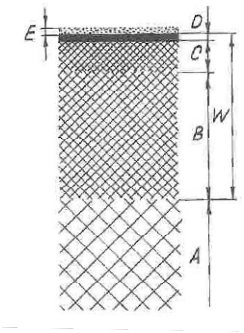

Figure 2.7: Surface layer structure: A – initial structure; B – region where supermolecular structure is fractured and oriented, as well as where the crystalline phase breaks down partly; C – strongly dispersed layer; D – low-molecular layer; E – gaseous phase; W – working layer (Myshkin and Petrokovets 2004)

Therefore the solid surface with the region adjacent to the bulk can be schematically represented as a laminated system comprising boundary (adsorbed) and the solid (bulk) phase of the basic material. Such representation is frequently convenient to analyse and simulate the surface effects in friction and wear (Myshkin and Petrokovets 2004).

When two very smoothly-finished and cleaned surfaces are pressed together, they may stick together through atomic or intermolecular forces. At this time should be made a distinction between cohesive forces, which occur between identical mating materials, and adhesive forces, which occurs between dissimilar mating materials (van Beek 2006).

For similar mating materials cohesive forces are easy to illustrate with gauge blocks (Figure 2.8).

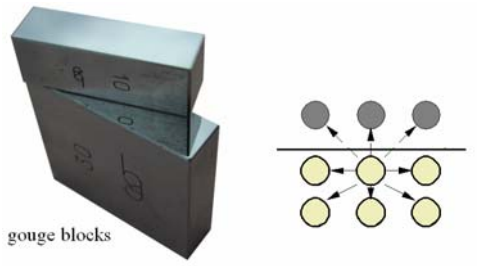

Figure 2.8: Atomic interaction at an interface as a cause of adhesion (van Beek 2006)

Gauge blocks are precisely manufactured blocks to calibrate micrometers and callipers. When the blocks are pressed together they remain attached. This phenomenon is explained by the very smooth super-finished surfaces that result in a large real contact area over which the atomic forces act.

For dissimilar mating materials the contact may create adhesive forces, this adhesive force is generally weaker than cohesive forces. Therefore the friction coefficient for two similar materials is normally higher than the friction coefficient for two dissimilar materials. As a general rule, contact between two similar materials must be avoided. This applies to metals, polymers and ceramic materials.

To help this explanation we must make a reference to materials compatibility. One factor determining the extent to which adhesive forces occur between different materials is their metallurgical compatibility (mutual solubility). The metallurgical compatibility is related to the surface energy of both materials γ_a and γ_b and the interface energy γ_{ab} in the contact between the materials. When two materials *a* and *b* come into contact, adhesive energy of $\Gamma_{ab}= \gamma_a+ \gamma_b- \gamma_{ab}$ is released. When two equal and smoothly finished materials are pressed together the surface energy is completely determined by the adhesive energy, $\gamma_{ab}=0$, $\Gamma_{ab}=\Gamma_{aa}= 2\gamma_a$. With two different materials (atom diameter, valency, packing, orientation) some interface energy remains, reducing the adhesive energy that is released. For most material combinations the interface energy lies between

$\gamma_{ab}=½(\gamma_{a+}\ \gamma_b)$, defined as metallurgical incompatible (poor mutual solubility) and $\gamma_{ab}=¼(\gamma_{a+}\ \gamma_b)$, defined as metallurgical compatible (van Beek 2006).

In the particular case of friction during demoulding in the injection moulding process, the adhesion term which is a surface effect, is a very difficult mechanism to isolate from the others (Ebnesajjad 2006). Delaney et al. (Delaney, Bissacco *et al.* 2012) have identified in the review the adhesion friction mechanisms and have categorized as consisting of thermodynamic/chemical adhesion, electrical/electrostatic adhesion and capillary attraction, as shown in Figure 2.9.

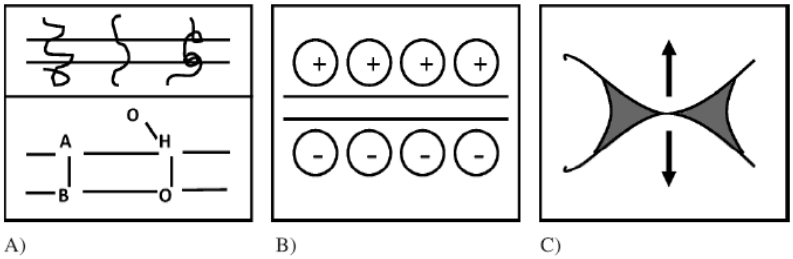

Figure 2.9: Adhesion mechanisms (A) thermodynamic/chemical/kinetic, (B) electrostatic, (C) capillary attraction (Delaney, Bissacco *et al.* 2012)

Some materials by diffusion or interfusion of chains may merge if the molecules of both materials are mobile and soluble in each other. For the case of stereolithography moulds Gonçalves *et al.* (Gonçalves, Salmoria *et al.* 2007) observed that polymers showed adhesion characteristics. The chemical affinity between the two stereolithography resins used and the moulding materials were evidenced by the friction experiments. The coefficient of static friction between the stereolithography blocks and the mouldings results not only from the roughness replication, but also from the adhesion between the stereolithography block and the thermoplastic. The latter effect is more important in the cases where chemical bonding and diffusion of the molten thermoplastic into the stereolithography block occurs. The degree of diffusion depends on the chemical affinity (or miscibility) between the materials, which

can be estimated from the Hildebrand solubility parameter. This parameter establishes a relationship with the polarity of the molecules which can be related to the chemical affinity of the materials. Generally, polymers with the same solubility parameter, and consequently the same cohesive energy density, tend to be miscible with each other or to show adhesive characteristics (Petrie 2000).

The use of the Hildebrand solubility parameter tables help to choose the best resin for a stereolithography moulding block if the thermoplastics to be injected is known in advance. The adhesion between the stereolithography resin for the moulding block and the material to be moulded can be assessed by a friction test made with samples overmoulded in testing blocks sterolithographed in the material similar to that used in the injection mould. This test informs not only on the effective friction properties but also on the likelihood of chemical adhesion between the thermoplastics and the stereolithography resin (Gonçalves, Salmoria *et al.* 2007).

The electrostatic adhesion arises from charge generation during contact. Some conducting materials from electrons transference could form a difference in electrical charge at the joint creating electrostatic attractive force and this force will be resistant to the separation (Delaney, Bissacco *et al.* 2012).

In case of lower values of roughness the gap between the contacting asperities can become filled with moisture resulting in the development of a meniscus force (capillary attraction). Adsorption of moisture at the narrow gap can lead to the formation of a liquid bridge resulting in surface tension. To Yoshikazu *et al.* (Yoshikazu, Kenji *et al.* 2001) the meniscus force is a major cause of the increment of the ejection force for smoother core moulds surfaces. An apparatus was used by Delaney *et al.* (Delaney, Kennedy *et al.* 2011) to predict the work of the adhesion for the demoulding force optimisation. In this research the definition of contact angle and wettability were used. It was

planned by the researchers that the model will be suitable for implementation in Finite Element Modelling.

Recently Chen and Hwang (Chen and Hwang 2013) developed an adhesion force tester to measure the adhesion force between the sample and tool surface during the injection moulding process.

2.6 Theories and friction models

Friction is a remarkable phenomenon. We have still much to learn about its nature. The history of friction is a very long story, dating back to the invention of the wheel, in order to reduce friction, and the discovery that one could produce fire from the heat generated by rubbing two sticks together, a positive use of high friction (Blau 1996). The contact between surfaces usually results in wear (Zambelli and Vincent 1998). Friction between contacting bodies is manifested in two ways. One way is as a force that must be overcome to initiate or sustains the motion. The other way is as the energy that is dissipated during relative motion. While friction and wear are distinct phenomena, they are also related. Wear mechanisms contribute to both aspects of friction, because wear processes require the application of force and energy consumption (Bayer 2002).

Figure 2.10 shows the transportation of an Egyptian colossus from a painting in the tomb of Tehuti-Hetep dated about 1800 BC. The colossus is fixed to a sledge and is pulled along by 172 men. One very interesting feature is the man on the front of the sledge who is apparently pouring a liquid on to the ground in front of the sledge, suggesting an early appreciation of the benefits of lubrication. It is estimated (Dowson 1998) that the colossus weighed approximately 60 tons (600 kN) and that, on average, each man could exert a pull of 800 N. For this in that epoch the people understood that could decrease the friction developed between the ground and the Egyptian colossus.

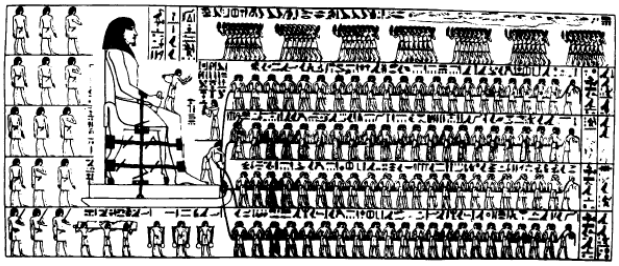

Figure 2.10: Transporting an Egyptian colossus (from D. Dowson, The History of Tribology, MEP, 2nd Edition, 1998, p.38)

Frictional behaviour has been the subject of systematic, documented studies and measurements for more than half a millennium Figure 2.11. One way to decrease this phenomenon is the use of lubrication, but this aspect will not be included in this discussion, because we are only interest in the direct contact between surfaces.

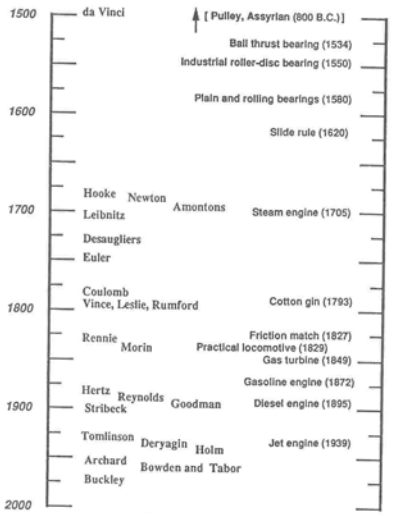

Figure 2.11: Timeline showing the correspondence between early work in friction research and the technology of the time (Blau 1996)

Friction is the resistance to motion during sliding or rolling that is experienced when the surfaces of two solid bodies move tangentially over another, Figure 2.12.

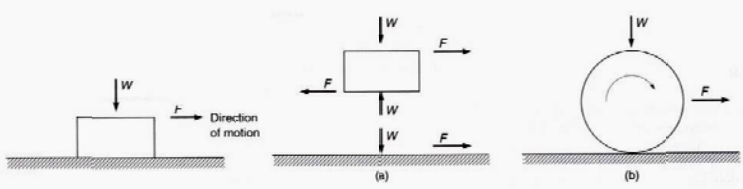

Figure 2.12: Schematic illustrations of (a) a body sliding on a surface with a free body diagram, and (b) a body rolling on a horizontal surface; W is the normal load (force) and F the friction force (Bhushan 2002)

The value of the tangential force that is required to initiate motion is the static friction force, F_{static} or F_s. it may take a few milliseconds before relative motion is initiate in the interface. The tangential force required to maintain relative motion is known as the kinetic (or dynamic) friction force, $F_{kinetic}$ or F_k. The static friction force is higher than the kinetic friction force, Figure 2.13.

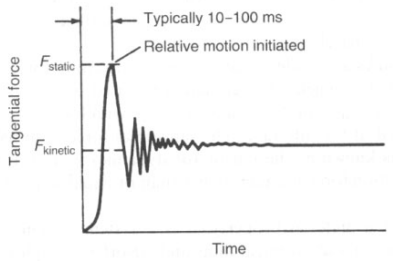

Figure 2.13: Tangential force as a function of time or displacement; F_{static} is the static friction force required to initiate motion an $F_{kinetic}$ is the kinetic friction force required to sustain motion. (Bhushan 2002)

There are three laws of dry friction (dry meaning that there is no lubrication of the interface):

1. The Friction Force (F) is directly proportional to the applied load (W)
2. The Friction Force (F) is independent of the apparent area of contact (A)
3. The Friction Force (F) is independent of the Sliding Velocity (V)

The first two laws arise from the studies of Leonardo da Vinci and Amontons, although the latter is actually credited with their formulation, as we know them today. These laws are widely applicable to the dry friction between interacting surfaces.

The first law gives rise to the definition of the coefficient of friction (μ) and the well-known equation

$$\mu = \frac{F}{W} \tag{2.2}$$

for F and W see Figure 2.12).

The second law is interesting, being counterintuitive with friction apparently independent of the area of contact. That is until one notes that it is the apparent area of contact that is referred to, not the real area of contact. The surfaces contact only at the peaks of asperities, the real area of contact being only a very small proportion of the total area of interaction between two surfaces, the apparent area of contact.

Friction will undoubtedly depend upon the real area of contact but it is feasible that it will remain unchanged with variations in apparent area of contact over a wide range of operating conditions. For example, if the apparent area of contact was reduced for a given load, then the real area of contact as a proportion of the apparent area of contact would increase but it may remain constant in absolute terms, resulting in the same friction force.

The third law was introduced by Coulomb in the 18th century. It has a much smaller range of applicability that the first two and should therefore be treated with caution when considering real engineering systems.

Friction is affected by many factors: material, environmental, interface condition, operating conditions. Some of those factors are difficult to assess and control. That is why friction becomes so complex to simulate in laboratory tests or to reproduce by theoretical modelling.

The friction force is the tangential force opposite to the movement, established in dry or in wet lubrication. Thus, friction is not a property of the materials alone, but a systemic reply as a function of the state of the surface and of the interfacial mean. Conceptually, the friction force is defined as the ratio of two forces acting, respectively, parallel and perpendicular to the interface between bodies under relative motion (Blau 2001) (see Figure 2.14).

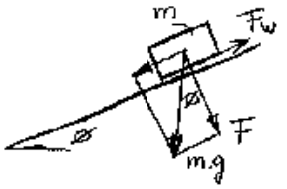

Figure 2.14: From the notes made by Leonardo Da Vinci (1452-1519)

The quantity known as the coefficient of friction has long been used in science and engineering and it is an empirical law of Coulomb friction. Most of the theoretical studies are based on this empirical law.

Suh *et al.* (Suh, Mosleh *et al.* 1994) presented friction as composed of three mechanisms: asperity deformation, adhesion and ploughing of the interface. The overall friction coefficient was then given by the weighed sum of these three components (Equation (2.3) and Figure 2.15).

$$\mu = \mu_d f_d + \mu_a f_a + \mu_p f_p \tag{2.3}$$

Starting with the suppositions of Suh *et al.*, Ferreira *et al.* (Ferreira, Laranjeira *et al.* 2003) presented a model for the coefficient of friction that has contributions of two components that was the ploughing and the deformation component. They conclude the roughness influence directly the coefficients of friction (static and kinetic). The theoretical model developed was sensible to changes in roughness but didn't respond to temperature variation.

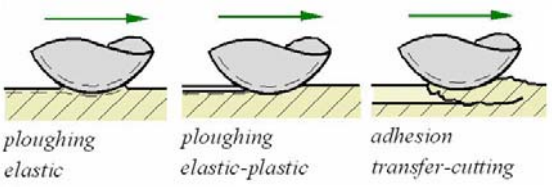

Figure 2.15: For sliding the asperity may result in elastic, elastic-plastic, and adhesion (van Beek 2006)

Warren and Krajcinovic (Warren and Krajcinovic 1996) presented a fractal model for the static coefficient of friction. In equation (2.4) the normal reaction is f_i and the shear force q_i, required to cause the i-th asperity to slip, is obtained using the Bowden and Tabor (Bowden and Tabor 1986) model for a narrow slider riding over a single pointed asperity. The local normal at the contact point is inclined at an angle α_i assuming the surface to be one-dimensional. The coefficient of friction component μ_a is attributed primarily to adhesion, and to a lesser extent to the underlying smaller scale roughness (Equation (2.4) and Figure 2.16).

$$\mu_i = \frac{q_i}{f_i} = \frac{\mu_a + \tan\alpha_i}{1 - \mu_a tan\,\alpha_i} = \mu_a + tan\,\alpha_i = \mu_a + \alpha_i \qquad (2.4)$$

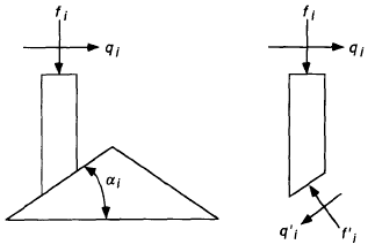

Figure 2.16: Bowden-Tabor model: narrow slider riding over a single pointed asperity (Warren and Krajcinovic 1996)

Sraffelini (Straffelini 2001) verified that for a metal pair of a tribological system, the average asperity junction is inversely proportional to the material yield pressure (p_Y) (Equation (2.5). The main aspect was to consider the

average shear strength of each junction (τ_m) as dependent on the effective work of adhesion. There exist a irreversible phenomena (plastic deformation) that occur during sliding.

$$\mu = \frac{\tau_m}{p_Y} \frac{1}{\sqrt{1 - 12\left(\tau_m / p_Y\right)^2}} \tag{2.5}$$

Benabdallah proposed a model that considers the coefficient of static friction (μ_s) dependent of the real area of contact (A_r) and of the normal load (F_n) (Benabdallah 2007). Assuming that the low range increase in normal load does not affect the number of asperities initially in contact, which in turn imply a power law relationship between A_R and F_n, the decrease of μ_s with F_n is justified by equation (2.6) where τ_0 and α are constants depending mainly on the material.

$$\mu = \frac{\tau_0}{F_n} A_r + \alpha \tag{2.6}$$

The design of the experimental apparatus (Figure 2.17) was based on the generation of an incremented centrifugal force that would progressively overcome the friction force between two bodies in static contact and loaded by a normal force. Each experiment consisted of placing the sample to be tested on a platform acting as counterface of the tribosystem. The system was then subjected to spinning thus generating increasing centrifugal force acting on the sample that would cause slippage. The detection of the critical moment at which initial relative motion takes place is of prime interest in this case because of its important impact on the accuracy of the measurement of the static coefficient of friction.

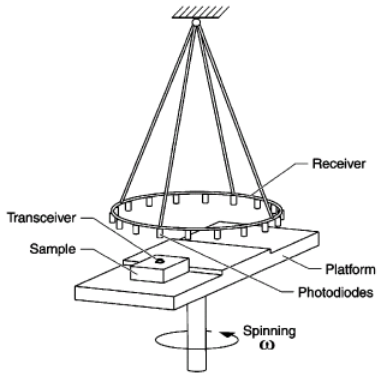

Figure 2.17: Schematic diagram of the testing apparatus (Benabdallah 2007)

The results suggest that assuming low range increase in normal load does not affect the number of asperities initially in contact, which in turn imply a power law relationship between A_r and F_n, the decrease of μ_s with F_n is justified by Equation (2.6). On the contrary, at relatively higher loads μ_s approaches a constant value due to the linear relationship of A_R with F_n that prevails in this condition. This also implies that at this stage, the interfacial shear strength of the micro-junctions becomes independent of the normal load.

Gao *et al.* (Gao, Luedtke *et al.* 2004) related that the coefficient of friction for no adhering surfaces has often been attributed to the work done against the externally applied load by the "top" surface as its asperities climb over the asperities of the "bottom" surface. The mean asperity slope gives the coefficient of friction of the Coulomb model. In contrast, the Bowden-Tabor and Greenwood-Williamson models consider the plastic or elastic deformations, respectively, of sheared asperities to derive Amonton's law. With regard to molecular-level mechanisms of frictional processes, the molecular dynamic simulations indicate that, while the above approaches may serve as useful phenomenological models, the spatial and temporal fluctuations revealed by the simulations are too large to be modelled in terms of semi static macroscopic-like particles moving past each other. Still in this paper, it is given an explanation of the Adhesion-Controlled and Load-Controlled Friction. In

previous experiments have shown that in general the friction force can be split up into separate and additive (external) load-dependent and (internal) adhesion-dependent contributions. Thus, for no adhering surfaces, the friction force is given by the Amonton's law, $F=\mu L$, independently of the contact are, while for adhering surfaces, there is an additional contribution that is proportional to the "real" molecular contact area (Figure 2.18). This contribution exists at zero and even negative loads so long as the surfaces remain in contact over a finite area. Strictly speaking, however, the adhesion contribution is not proportional to the area but to the number of interatomic or intermolecular bonds that are broken and reformed when the surfaces slide laterally past each other. The number of bonds is directly proportional to the contact area when the surfaces are perfectly smooth, when this area is referred to as the "real" contact area. For two perfectly flat, molecularly smooth surfaces, the "real" contact area is the same as the projected or "apparent" contact area. However, for rough surfaces, the real area of contact can be well below the apparent area (when the surfaces are hard) or well above it (when the surfaces are soft). These effects can give rise to adhesion and friction forces that can be orders of magnitude lower or higher than for molecularly smooth surfaces.

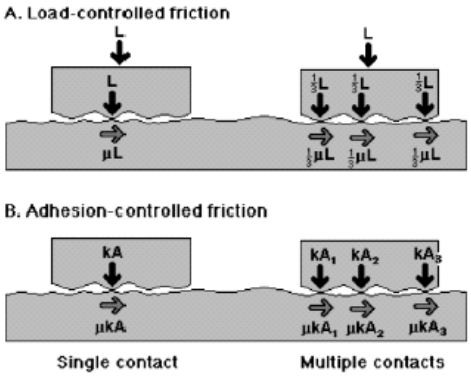

Figure 2.18: (A) Load-controlled friction and (B) Adhesion-controlled friction (Gao, Luedtke *et al.* 2004)

In Figure 2.18 can be observed the difference in the local distribution of the external total applied load or normal adhesive force between load-controlled no adhering surfaces (A) and adhesion-controlled surfaces (B). In the former case, the total friction force F is given either by F=μL for one contact point (left side) or by F=1/3μL+1/3μL+1/3μL=μL for three contact points (right side). Thus the load-controlled friction is always proportional to the applied load, independent of the number of contacts and of their geometry. In the case of adhering surfaces (B), the effective "internal" load is given by kA, where A is the real local contact area, which is proportional to the number of intermolecular bonds being made and broken across each single contact point. The total friction force is now given by F=μkA for one contact point (left side), and $F=\mu kA_1+\mu kA_2+\mu kA_3=\mu kA_{total}$ for three contact points (right side). Thus, for adhesion-controlled friction, the friction is proportional to the real contact area, at least when no additional external load is applied to the system.

2.7 Methods of characterising friction properties

Several types of standard tests were developed to do the characterization of friction properties (Blau 1992). The problem of these standards is that the conditions specified do not represent the true conditions present in the replication process. Without forget the recommendation of Blau (Blau 2001) that the friction tests results can be extremely repeatable and reproducible several groups have developed test devices and published details of friction measurements studies for specific processing conditions. James and Newell (James and Newell 1980) developed a friction test apparatus for polymeric wiper blades, Figure 2.19.

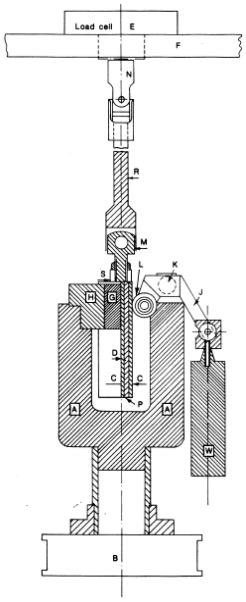

Figure 2.19: Illustration of the prototype equipment develop by James and Newell for polymers wiper blades (James and Newell 1980)

In these tests the normal load applied is not always directly proportionality to the friction resistance. Worgull *et al.* developed a system to do the characterization of friction applied to hot-embossing and injection moulding process (Worgull, Hétu *et al.* 2006; Worgull, Hétu *et al.* 2008).

Ferreira *et al.* developed a prototype apparatus (Figure 2.20) for testing thermoplastics in as-moulding conditions (Ferreira, Neves *et al.* 2001). The testing procedure included heating the specimens to the corresponding processing temperatures, applying a normal load (so that the specimen replicated the mould surface), cooling to ejection temperature and then pulling the specimen. The effect of the polishing direction, surface roughness and temperature on the coefficient of friction was studied. Results showed that the testing temperature and the surface roughness have a significant effect on the coefficient of friction for polycarbonate. For polypropylene, none of these parameters have a significant effect on the coefficient of friction, except possibly the interaction of polish direction and roughness. The coefficient of friction obtained for both polymers were higher than published values obtained by other authors.

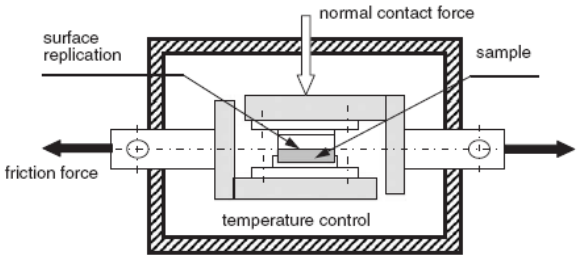

Figure 2.20: Illustration of the concept for the development of the prototype equipment (Ferreira, Neves *et al.* 2001)

Friction between the thermoplastic part and the injection mould core depends on the mechanical interaction between the two surfaces (shrinkage, mould roughness), but also on an adhesive component inherent to the properties of the two materials at the processing conditions (Kinsella 2004) and on the properties of the mating surfaces. The adhesive force is a result of atomic forces established between the contacting surfaces of the two materials.

Berger *et al.* (Berger, Friesenbichler *et al.* 2008) developed an apparatus to measure the demoulding forces (Berger, Friesenbichler *et al.* 2008). The

advantage of this apparatus is that the friction test is made inside of the mould cavity during the opening stage of the moulding cycle. The moulded part was injected under typical process conditions and during the opening stage it was possible measured the evolution of the friction force. The configuration of the moulded part is formed by a mould insert with a serrated surface (on the top) in order to fix the part while demoulding occurs and a flat surface (down) that is in contact with the surface which made the contacting friction pair (Figure 2.21).

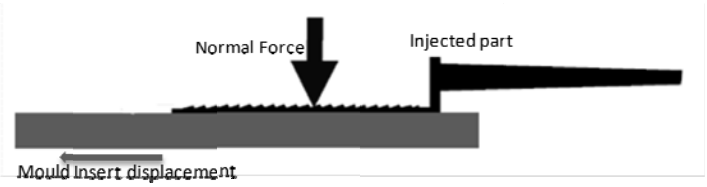

Figure 2.21: Friction test principles of the PCCL apparatus (Berger, Friesenbichler *et al.* 2008)

PP, PC, ABS, ABS/PC TPE and POM were tested using different plate shape, stainless steel cavity inserts with several conditions of surface finishing. The measured demoulding forces and coefficient of friction are strongly influenced by polymer, mold temperature, surface roughness and coating material, like TiN, CrN and TiAlN.

Delaney *et al.* (Delaney, Kennedy *et al.* 2011) reviews how this challenge of create a standardized equipment for a friction test during the demoulding in injection moulding has been addressed by other researchers and describes the development of an apparatus to measure friction under typical replication conditions. Experimental results of the thermal characterization of the device are reported.

2.8 Objective of the work

Having in view the current state of the art it appeared adequate to consider as main objectives of this research work the following topics:

i. Analysis of the factors that influence the ejection force in injection moulding;
ii. Analysis of the process of ejection of plastic parts in injection moulding;
iii. Methods for characterising the friction environment in the ejection of injection mouldings;
iv. Contributions to the development of a model that interprets the ejection of injection mouldings;
v. Experimental validation of the proposed way to predict the coefficient of static friction.

3. A MODEL FOR FRICTION IN INJECTION MOULDING

The content of this chapter was partially published as the research paper CORREIA, M.S.; MIRANDA, A.S.; OLIVEIRA, M.C.; CAPELA, C.; POUZADA, A.S. - Analysis of friction in the ejection of thermoplastic mouldings, Int. J. Adv. Manuf. Techn., Vol 59 (2012), pp. 977–986 DOI 10.1007/s00170-011-3573-2 published online 26 Aug 2011.

A copy of this paper is attached in APPENDIX 2 – PUBLICATIONS

3.1 Model for the demoulding process

Mathematical models for the ejection stage have been developed by several researchers. The guideline of these studies is based on the empirical law of Coulomb friction.

The model described in this chapter assumes a full replication process, where the polymeric surface is an impression of the mould surface.

In the polymeric injection mould process the moulding part shrinks onto cores. For sleeves or box-shaped parts, the release force F_R was given by Menges and Mohren (Menges, Michaeli *et al.* 2001) as:

$$F_R=\mu \times P_A \times A_C \tag{3.1}$$

where μ is the coefficient of static friction P_A is the average contact pressure and A_C the area of contact.

The influencing factors relevant to the ejection of injection mouldings must be considered. These include the moulding shrinkage, the mechanical properties of the contacting materials and how the coefficient of friction depends on all the other parameters (Figure 3.1).

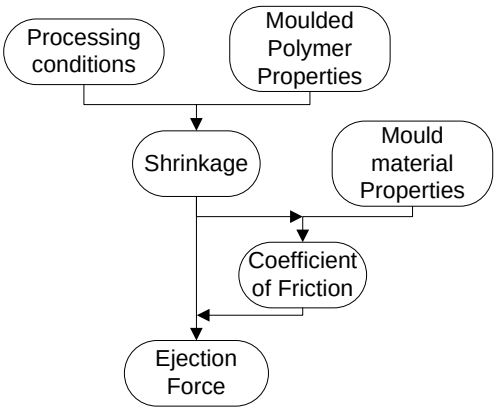

Figure 3.1: Factors relevant to ejection in injection moulding

Simulation tools were used to quantify the value of contact pressure or by direct measurements with a sensor in the mould or by part measurements followed by calculations. In the case of cylindrical cores the pressure can be obtained if the shrinkage at ejection temperature is known as shown by Pontes *et al.* (Pontes, Pouzada *et al.* 2005). After a cylindrical part demoulding the relative change in the circumference perimeter can be used to obtain the tensile strain in the part cross section when the part is still on the core. Multiplying the elastic modulus by this tensile strain, by the contacting area and by the coefficient of friction gives an estimation of the required force for the demoulding operation. The equation that describes the demoulding process in this case is:

$$F_R = \mu \times E(T) \times \Delta d_r \times t \times 2\pi L \qquad (3.2)$$

where $E(T)$ is the elastic modulus of the thermoplastics material at the demoulding temperature, L is the length of the part in contact with the mould core, Δd_r the relative decrease in part diameter and t is the thickness.

Pontes *et al.* (Pontes, Pouzada *et al.* 2005), for the case of tubular mouldings and Titomanlio and Jansen (Jansen and Titomanlio 1996; Titomanlio and Jansen 1996) for the case of injection moulded plates, used the same approach for the design of a thermomechanical model to predict the shrinkage and ejection.

For the case of plastics thin-wall injected parts Haragas *et al.* (Haragas, Tudose *et al.* 2008) developed calculations methods for the demoulding force. The demoulding force can be calculated according to proposed methods if the material and the geometric dimensions of the injected part are known.

Rectangular mouldings, due to corner effects, in contrast with tubular (circular) moulding do not have a constant pressure on all surfaces. For this the demoulding force can vary along the side walls of moulding boxes as indicate in Figure 3.2. The moulding corners are a restriction to shrinking and with this minimize the warpage of the box in those points. On the other hand not only the shrinkage influences the contact pressure but even the local stiffness of the moulding box has an interesting contribution on the friction force developed (Delaney, Bissacco *et al.* 2012).

To measure the contact pressure is a complex issue the measurement is made within the mould. Pressure change occurs during the replication and their variation due to the localized geometrical variations part. Experimental study developed by Kurt *et al.* (Kurt, Saban Kamber *et al.* 2009) indicates that the cavity pressure and mould temperature are the dominant factors determining the quality of the final product in plastic injection moulding.

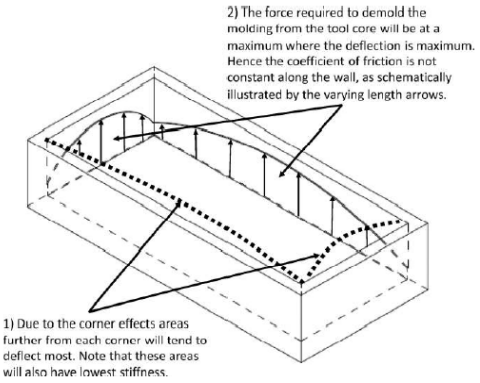

Figure 3.2: Corner effects on the demoulding force (Wang, Kabanemi *et al.* 2000; Delaney, Bissacco *et al.* 2012)

For non-conventional moulds such as those in stereolithography materials that are used for small series of production some adhesion problems were reported by Gonçalves *et al.* (Gonçalves, Salmoria *et al.* 2007). This kind of additive production using the layer-by-layer mould generation results in a bad surface finish. The characteristics of the laser beam that generates the surfaces usually can be identified in the roughness stair-step profile of the mould cavity. So during the demoulding phase the deformation mechanism is dominant. Due to the full replication of the mould surface on the moulding part there is an interlocking between them. Pham and Colton (Pham and Colton 2002) based on the previous work of Colton *et al.* (Colton, Crawford *et al.* 2001) developed a model to quantify the demoulding force for parts on stereolithography moulds. The mould insert cavities had four different shapes: boss, box, triangular and hexagonal. The model was based on the thermal shrinkage and the stair-step roughness profile of the mould surface which creates an overlap between the part and the mould making demoulding more difficult. The force component due to the stair profile was theorized to be the force necessary to deform the part and mould elastically to overcome the overlap. The coefficient of friction applied is increased to an equivalent coefficient of friction which incorporate the effect of increase deformation needed for the mould and

moulding to deform sufficiently to slide over each other. These layered structures of stereolithographic tools may be compared to the period profile of mould surface produced by micro milling (Delaney, Bissacco *et al.* 2010). In this work it was extended the application of the Colton *et al.* model (Colton, Crawford *et al.* 2001) to predict the demoulding forces for regular periodic surfaces based on the understanding of the process parameters of turned surfaces used in the machining process. The development of accurate models for the demoulding forces requires knowledge of the dominant interfacial contributions for the friction and knowledge of the size scale at which the dominant contributions operate (Delaney, Kennedy *et al.* 2010).

Pontes *et al.* (Pontes, Pouzada *et al.* 2005) presented a thermo-mechanical model to predict ejection force. This model assumed that polymers change from purely viscous to purely elastic below a transition point. In addition the existence of a suitable value for the static coefficient of friction was assumed.

The coefficient of friction is conceptually defined as the ratio of the demoulding force (tangential to the surface) and the contacting force (normal to the surface). This is a constant characteristic related to the material pair in contact and to the properties of the contacting surfaces. Problems often arise when engineers attempt to use tabulated coefficients of friction to solve specific problems in mechanical design or failure analysis (Blau 2001). The systems-dependence of frictional behaviour is sometimes ignored, leading to misapplication of published data.

The model described in equation (3.1) has been applied to both macro and micro parts. The shrinkage of the moulding part is the responsible for the contact pressure generated and the adhesion force is always ignored. In this context the shrinkage term relates to the total strain, which as reported by Jansen and Titomanlio (Jansen and Titomanlio 1996), may be the sum of the thermal strain (shrinkage due to temperature), hydrostatic strain (due to the compressibility of the material), crystallization strain (for crystalline materials)

and reaction strain (for thermoset materials) as applicable. But if a part size decreases the assumption that the adhesive force is negligible becomes questionable (Delaney, Bissacco *et al.* 2012).

The discussion to-date has been related to parts in injection moulds. But similar problems appear in other replication processes such as hot embossing. Guo and co-workers proposed that the contact pressure results from the combination of thermal stress and adhesive forces, then used empirical formulas to calculate the actual adhesion forces terms of the contact geometry and the surface energy of adhesion (Guo, Liu *et al.* 2007; Guo, Liu *et al.* 2007). In this way it was possible to predict the demoulding forces for microstructures applying a value for the coefficient of friction.

In the case of the demoulding of ultraviolet nanoimprint lithography Amirsadeghi *et al.* assumed that before demoulding happens quasi-static equilibrium conditions exist (Amirsadeghi, Lee *et al.* 2011). Demoulding is the process to overcome all the chemical and mechanical interactions at the probe/resist interface that have been formed by the process.

3.2 Surface texture

Most surfaces have regular and irregular spacing's that tend to form a pattern or texture on the surface. This surface texture is generated by the mechanical process of finishing the part. In the case of metallic injection moulds the machining or the finishing process itself has the greatest impact on the geometry of the surface. A major factor is the action of the cutting tool on the material. Elements such as tool shape, speed, feed, and cutting fluid can be varied to affect the surface topography. Other factors affecting the surface are the instability of the cutting tool due to chatter or unbalance in the grinding wheel, and errors in the machine tool.

The reason to measure the surface topography is try to predict the performance of the component. As an example, a bearing surface requires a level of surface

texture that allows lubricant to be retained in small pockets and at the same time allows the bearing to slide with a minimum of friction. If the surface is too rough, wear can quickly develop; however, if the surface is too smooth, inadequate lubrication and seizure might occur.

The other reason to measure a surface is to control the manufacturing process. By measuring the surface topography during processing, an operator can detect changes in the surface finish and adjust the manufacturing process to ensure that the process remains in the allowed range (Cotell, Sprague *et al.* 1994).

Each finished part shows deviations from its geometrically ideal shapes (Sander 1991). Besides deviations of size – i.e. deviations from prescribed nominal values – the surface irregularities have to be assessed: deviations of form and position; waviness; roughness and lay. Deviations of form and position are referred to as large-scale irregularities; waviness, roughness and lay are called small-scale irregularities (Figure 3.3).

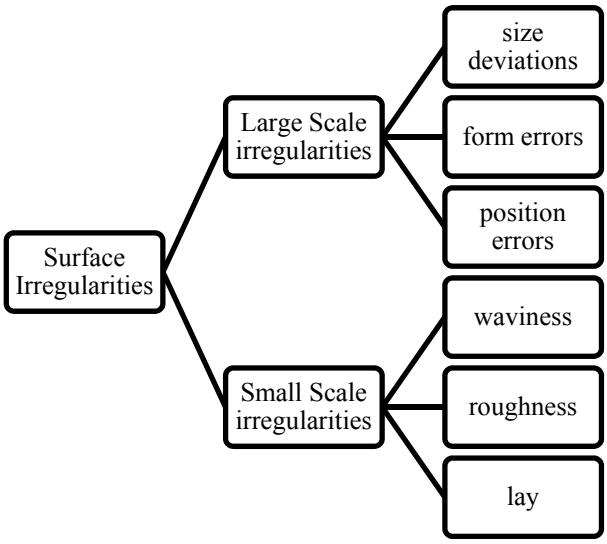

Figure 3.3: Surface irregularities classification, adapted from Sander (Sander 1991)

The surface or topography may have three distinct attributes: waviness, roughness and lay. Waviness may be considered undulations on a surface with a relatively low frequency or long wavelength, up to the order of millimetres.

This type of irregularity are often produced by vibration in the machining process (Blau 1992).

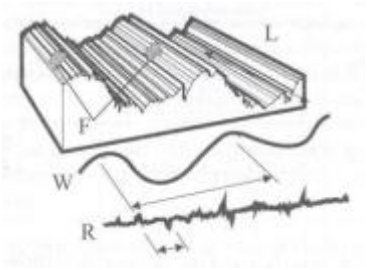

L – Lay

F – Flaw

W – Waviness spacing

R – Roughness

Figure 3.4: Surface topography illustration of the roughness, waviness, and general form of a surface analysis. Adapted from (Cotell, Sprague *et al.* 1994; Teixeira 2001)

Roughness is high frequency or short wavelength irregularities on a surface. Lay is the well-defined orientation of surface pattern. Although somewhat arbitrarily defined, these attributes allow us to build a modular structure of a surface. Surface texture or topography is mainly formed by roughness superimposed on an underlying waviness. If the combined roughness and waviness has a well-defined pattern, the surface is said to possess lay. It is important to distinguish between surface texture and the general shape or form of the surface. It is easy to mistakenly classify errors in shape, when the actual component is compared with the design, as surface texture or topography. This is not the case, such deviations are form errors.

Form is the general shape of the surface neglecting surface texture and *form error* is a deviation of the general shape from the intended form of the surface. The classification of form deviation is shown in Table 3.1.

For the metallic probes used in this work it was necessary to do the surface characterization which requires the understanding of the roughness profile. The term *roughness* refers to the fine irregularities (peaks and valleys) produced on a surface by the forming process (Figure 3.4).

Table 3.1: Classification system for form deviation according to DIN 4761.

Form Deviation	**Examples of type of deviations**	**Examples of causes**
Class 1: Shape deviation 	Deviations from straightness, flatness, roundness, etc.	Faults in machine tool guide ways, deflection of machine or work piece, incorrect clamping of work piece, hardening distortion, wear
Class 2: Waviness 	Undulations	Eccentric clamping, deviations in the geometry or running of a cutter, vibration of the machine tool or tool chatter
Class 3: Roughness 	Periodic	Form of tool cutting edge, feed or infeed of tool
Class 4: Roughness 	Score marks, flaking, protuberances	Chip formation process, deformation of material during blasting
The class 1 to 4 form deviations represented above are usually superimposed on the actual surface. Example: 		

A simple way of analysing deviations from the nominal surface is by assessment the surface with the stylus. The recorded image will look like the one demonstrated in the Figure 3.5. The evaluation length (*ln*) for assessing roughness measurement is standardised according to ISO 4288. For every roughness measurement, roughness values are calculated over five adjacent sampling lengths (*lr*-cut-off) and then averaged.

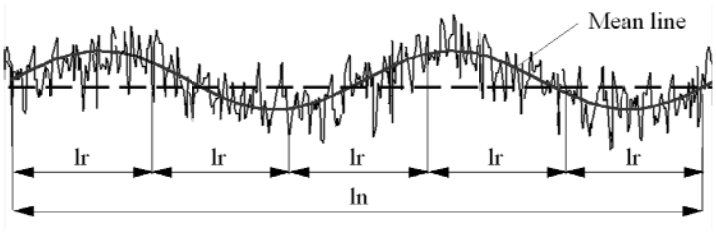

Figure 3.5: Surface texture (van Beek 2006)

3.3 Roughness parameters

The surface could be described by several roughness parameters. The major problem is to choose which are the more adequate to define the generated real surface. Surface roughness parameters are usually categorised in three groups according to its functionality. These groups are defined as amplitude parameters, spacing parameters and hybrid parameters. An extensive review of these parameters was made by Gadelmawla *et al.* (Gadelmawla, Koura *et al.* 2002).

The arithmetic average height parameter (*Ra*) is the first roughness parameter that was developed and it remains the most common. It is the average deviation of the profile from a mean line or the average distance from the profile to the mean line over the length of the assessment. *Ra* is used for detecting general variations in the overall profile height and when it changes, it usually means that something in the process has changed. Because *Ra* is an average, localized individual defects in the surface do not greatly influence the results, therefore this is not useful in detecting defects.

The spacing parameter *S* (Figure 3.6) is defined as the average spacing of adjacent local peaks of the profile measured along the assessment length. The local peak is defined as the highest part of the profile measured between two adjacent minima and is only measured if the vertical distance is greater than or equal to 10% of the *Rt* (Figure 3.7) of the profile.

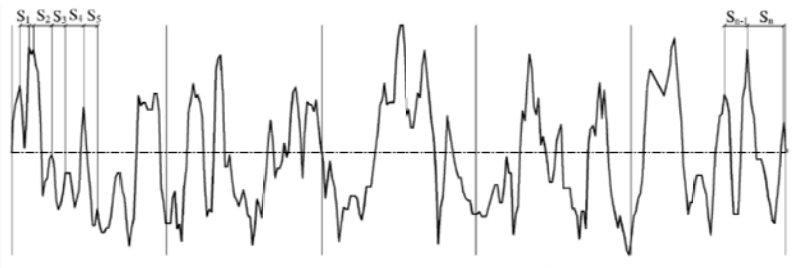

Figure 3.6: Mean spacing of adjacent peaks (*S*) (Gadelmawla, Koura *et al.* 2002)

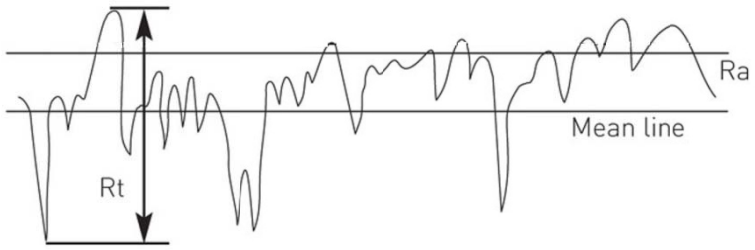

Figure 3.7: Definition of the R_a and R_t roughness parameter

Some confusion can be made between the parameters *S* and *Sm*. The *Sm* parameter (Figure 3.8) is defined as the mean spacing between profile peaks measured on the mean line. The profile peak is the highest point of the profile between upwards and downwards crossing the mean line. The difference between the two mean spacing parameters, *S* and *Sm*, is that the first parameter is measured at the highest peaks of the profile, whilst the second parameter is measured at the intersection of the profile with the mean line.

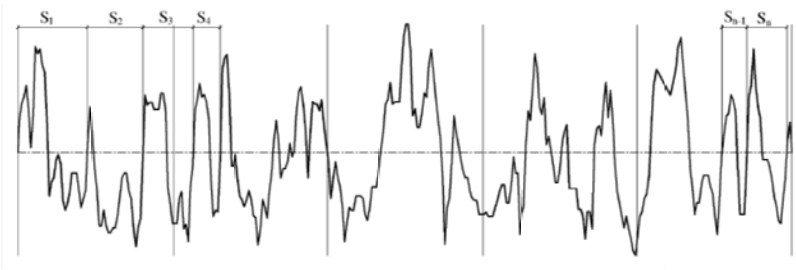

Figure 3.8: Mean spacing at mean line (*Sm*) (Gadelmawla, Koura *et al.* 2002)

The peak count, *Pc*, expressed as the number of peaks per unit length, is computed from the number of peaks counted in the evaluation length (five evaluation segments, Figure 3.9). The number of peak/valley pairs per unit length extending outside a "deadband" centred on the mean line. The width of a peak/valley pair is defined by the distance between crossings of the dead band region. For all practical purposes, a peak would be registered if a continuous trace starts below the mean line, goes above it, and then below it.

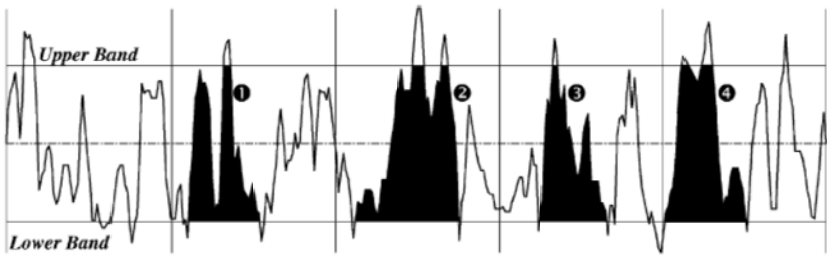

Figure 3.9: Peak count (*Pc*) parameter within a selected band (Gadelmawla, Koura *et al.* 2002)

Due to the way the metal surfaces were generated by EDM, the roughness is homogeneous whatever the measuring direction used. Surface roughness measurements were made to assess the number of peaks, $(P_c)_s$, existing in an evaluation area (A_E) in mm^2. The number of peaks, N_p, per unit area was obtained using the equation:

$$N_P = (P_C)_s / A_E \tag{3.3}$$

Different manufacturing processes produce different surface profiles and because of this it is necessary to make a correct choice of the parameters used to describe the surface.

3.4 Friction based on geometrical aspects

The mechanical interlocking during the replication process and subsequent damage during the demoulding stage will depend upon the surface irregularities on the mould and the tendency of the replicating material to fill or replicate these irregularities. This principle of solution relates to how the part and tool material selections can be optimized to prevent the replicating material from becoming mechanically entangled with and being subsequently damaged by the replicating tool (Delaney, Bissacco *et al.* 2012).

Suh *et al.* discussed the fundamentals of friction phenomena (Suh, Mosleh *et al.* 1994). The friction space concept for these researches is a geometric illustration of the coefficient of friction as a function of three mechanisms: asperity deformation, adhesion and ploughing. In order to obtain the lowest coefficient of friction in dry sliding, the mechanical components of friction must be minimized. These authors believe that if the ploughing and deformation components of friction are eliminated, the coefficient of friction would be extremely small under normal sliding conditions. In order to minimize the mechanical effects Kim and Suh (Kim and Suh 1993) investigated the frictional behaviour of lightly loaded, extremely smooth, hard materials with the goal of obtaining purely elastic contact at the interface. They conclude that fracture and plastic deformation could not be avoided completely. Ferreira *et al.* (Ferreira, Laranjeira *et al.* 2003) used Suh *et al.* (Suh, Mosleh *et al.* 1994) interpretation and the expressions for the coefficient of static friction by Suh (Suh 1986) for the ploughing and the deformation components.

The model developed in this chapter is the interpretation of the demoulding mechanism in injection moulding. This was made through a mixed approach (theoretical, numerical and experimental) following previous works by Suh *et al.* (Suh, Mosleh *et al.* 1994) and Ferreira *et al.* (Ferreira, Laranjeira *et al.* 2003). This interpretative analysis considers the three contributors for the friction force: ploughing (F_{plough}), deformation (F_{deform}) and adhesion ($F_{adhesion}$) as described in equation (3.4).

$$F_{friction}=F_{plough}+F_{deform}+F_{adhesion} \quad (3.4)$$

Roughness is the major variable in the friction force developed during the ejection stage, since it influences directly the ploughing and deformation components of friction in the contact between the steel hard mould and the soft plastic materials.

The ploughing models assume that the dominant contribution to friction is the energy required to displace material ahead of a rigid protuberance or protuberances moving along a surface (Blau 1996). Tabor discussed the ploughing term associated to a conical asperity (Tabor 1981).

To simulate the contact during the ejection stage of injection moulding process, the hard tool surface (metallic mould) was represented by an array of conical asperities. The indentation of the hard asperity on the soft surface (polymeric part) was characterized by the indentation radius, r, and the indentation depth, d, as shown in Figure 3.10. In this figure, the two elementary forces, normal force (f_{normal}) and friction force ($f_{friction}$), involved in the contact mechanism of one single asperity are also shown.

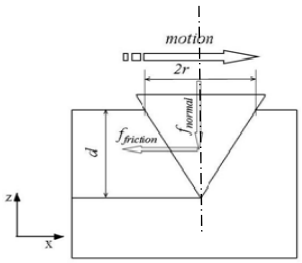

Figure 3.10: Conical asperity geometry and elementary forces

The reason for the consideration of the total indentation was presented in the beginning of this chapter, when reference to the total replication of the metallic surface was made. An analytical model his proposed based on this experimental evidence and geometrical considerations are made on the contacting surface based on the roughness parameters and material properties. It is noted that the material properties must be reviewed under realistic conditions which will exist at the demoulding interface. The relative mould and moulding material properties together with the processing conditions (ejection temperature) will affect the tendency of ploughing friction to occur and will also affect the friction component.

In this study roughness parameters were used to describe the surfaces in contact. An amplitude parameter, the arithmetic average height (*Ra*), and two roughness spacing parameters (*S* and *Pc*). In Figure 3.11, the mean line is defined. Considering *Ra* as the arithmetical mean roughness and *S* the local mean peak spacing, each asperity is geometrically defined in terms of the height:

$$d=4Ra \tag{3.5}$$

and the cone radius:

$$2r=S \tag{3.6}$$

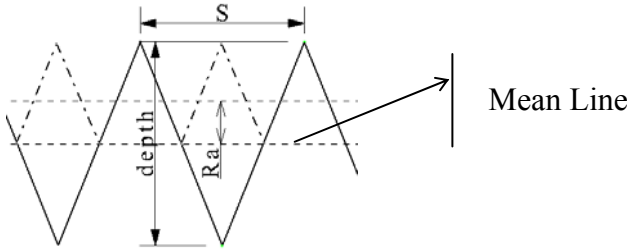

Figure 3.11: Asperity model

Therefore, the cross-sectional area (A_z) of a triangular indentation formed by the conical asperity is:

$$A_Z=2\times S\times Ra \tag{3.7}$$

The ploughed groove results from the plastic deformation associated to the yield stress of the polymeric material, σ_y. The resistance of each asperity to the relative motion, or elementary ploughing force, f_{plough}, is the product of the surface pressure, S_0, by the cross-sectional area, A_z. Upon yielding, it can be considered that the pressure is equivalent to the compressive yield stress, which is very dependent on temperature. Thus, the elementary ploughing force is:

$$f_{plough}=A_Z\times\sigma_y \tag{3.8}$$

For the whole apparent contacting surface, assuming that S is the mean spacing of profile irregularities, the ploughing force (F_{plough}) is the sum of all the elementary forces acting on each asperity. The product of f_{plough} (equation (3.8)) by the number of peaks per square millimetre (N_P, defined in equation (3.3)) results in equation (3.9) which defines the maximum value for the specific resistance force per unit area of relative sliding motion that should be expected if the engagement of the asperities is maintained:

$$\frac{F_{plough}}{A}=2\times N_p\times S\times R_a\times\sigma_y \tag{3.9}$$

This can result from the ploughing mechanism that causes abrasion of the polymeric material as shown in Figure 3.12.

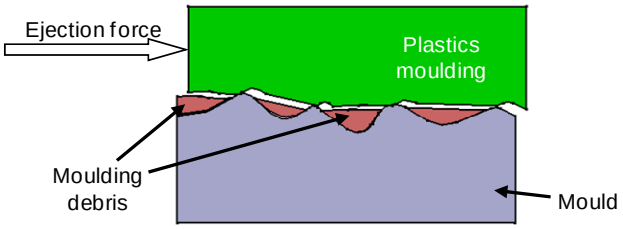

Figure 3.12: Abrasion of the polymeric material

It should be noted that, almost without exception, ploughing is accompanied by adhesion and, under certain conditions, the ploughing may result in microcutting, that is, additional work is carried out and the friction is increased (Myshkin, Petrokovets *et al.* 2005).

3.5 Numerical model

The assessment of the elementary forces associated to friction in the ejection process can be done using the finite element method. In this numerical simulation a representative volume element under homogeneous boundary conditions was considered. This element includes the contact geometry with the surface profile. If the model considers only deformations applied in the normal direction, the computational homogenization procedure yields a homogenized contact law for the contact pressure. To derive a friction law the model must also take into account the sliding or tangential motion. For the numerical simulation of the micro-mechanical model it is necessary to define a general contact law for the contact forces in the normal and tangential directions. The friction law results either from a constitutive relation describing the deformation in the contact area and/or the elastic-plastic response of the solid, which is related to ploughing and deformation. The numerical simulation of this type of micro-structure allows computing the normal and tangential contact forces on the rough surfaces, which only occur in some parts of the micro-asperities, as depicted in Figure 3.13. The sum of these forces allows to determine the resultant force on the entire contact surface (Wriggers 2006).

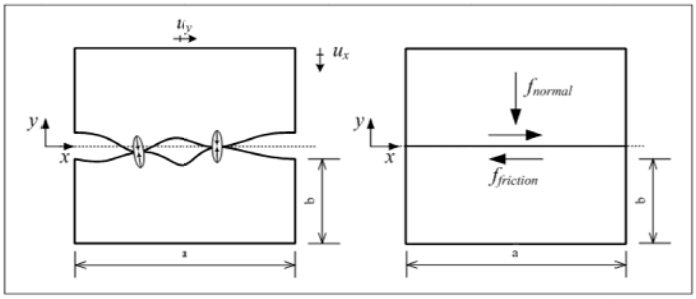

Figure 3.13: Micro-asperities relative motion and resultant homogenized forces

The homogenization procedure involved the following steps: (i) discretization of the representative volume element, taking into account the roughness characteristics; (ii) application of a homogeneous deformation pattern to the boundary of the blocks, in the normal and tangential directions. As a first step a normal displacement is applied until the prescribed normal force is reached. After that, the relative displacement is incrementally applied in the tangential direction, keeping the normal displacement fixed.

In the present case the adopted finite element model had only one elementary asperity in order to compare the elementary force with that determined with the previous model, Equation (3.8). Considering the very different mechanical properties of the mould and the moulded polymer, the elementary asperity is considered as rigid and modelled with Bézier surfaces. According to Zhang *et al* and Wriggers (Zhang, Hodgson *et al.* 2003; Wriggers 2006), the deformable body dimensions, should be selected based on the roughness parameters, *Ra* and *S*. The selected dimensions must guarantee that the sample is large enough to avoid the interference of the boundary conditions in the numerical simulation results.

Since the injection process always involves surface replication, it was assumed that the polymeric part topography will be exactly the same as the mould. The replication occurs as a result of the applied normal contact force. Therefore a stress field is induced in the polymeric part in this first deformation stage. In

this simulation the indentation step was taken into account before the evaluation of the deformation stage.

The simulations were performed with the in-house finite element DD3IMP code (Deep-Drawing 3D Implicit code), specifically developed to simulate sheet metal forming processes (Menezes and Teodosiu 2000). The Signorini condition is used to model the unilateral contact conditions and the friction contact problem between the tool and the deformable body was modelled with the Coulomb's classical law, adopting an evolutional law that takes into account the effect of the local pressure on the local coefficient of friction. The contact search algorithm is based on a master-slave approach, being the master the rigid tool and the slave the deformable body. The contact with friction is considered by an augmented Lagrangian approach (Oliveira, Alves *et al.* 2003).

It should be mentioned that to derive a friction law it is required to perform the numerical simulation for different normal contact forces and sliding distances. The numerical simulation of only one elementary asperity is considered in this study to estimate the two friction force components (ploughing and deformation), following the approach suggested by Wriggers (Wriggers 2006). Numerical simulations were actually performed with a null coefficient of friction for the different elementary asperities analysed in this study, as Jeon and Bramley did considering several asperities (Jeon and Bramley 2007). Each numerical experiment still takes some time, due to the problem dimension (Wriggers 2006). Also, it is necessary to consider different geometries to obtain a statistical representative distribution of the micro-geometries. However, the objective in this work was to gain some insight into the behaviour of the micro-asperities of the contact interface.

This numerical model allows estimating the two components (ploughing and deformation) of the friction force as shown by the equation:

$$f_{num}=f_{plough}+f_{deform} \quad (3.10)$$

The elementary numerical force was multiplied by the number of peaks to obtain the global numerical force per unit area (as in section 3.4):

$$\frac{F_{num}}{A} = N_p \times (f_{plough} + f_{deform}) \quad (3.11)$$

This numerical force it is the global value of the sum of the two components relative to the ploughing and the deformation components.

3.6 Mixed-approach model for the assessment of the demoulding force components

Equation (3.4) describes the total friction force during the demoulding stage and Figure 3.14 describes the mixed-approach methodology to calculate the value of the demoulding force. The total force is the sum of ploughing component (F_{plough}, obtained by the analytical model), the value of the deformation component (F_{deform}, calculated as the difference between the results of the numerical simulation and of the ploughing analytical model) and the adhesion force component (inferred from the experimental results).

The value for the deformation component is based on the numerical simulation results and the ploughing analytical model according to equation (3.12).

$$F_{deform}=F_{num}-F_{plough} \quad (3.12)$$

Finally the adhesion component is inferred by the experimental results (F_{exp}) and the numerical simulation (F_{num}) result according to equation (3.13).

$$F_{adhesion}=F_{exp}-F_{num} \quad (3.13)$$

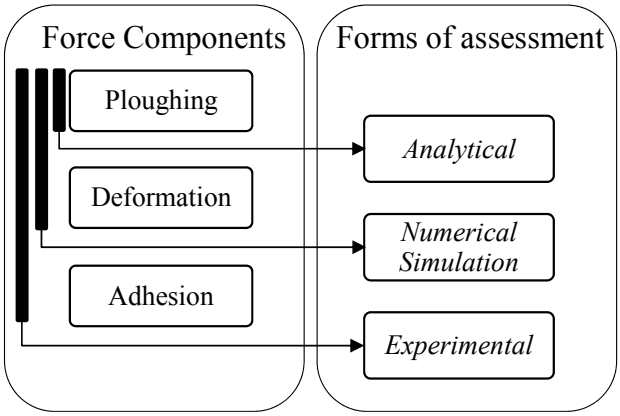

Figure 3.14: The mixed-approach model

3.7 Final remarks

The ejection force of injection moulded thermoplastics depends on the contact conditions at the moment of ejection. During the injection of the melt replication of the polymer part onto the mould surface takes place. The demoulding process follows this initial replication process. The demoulding friction process could be separated in three different mechanisms: ploughing, deformation and adhesion. It can be difficult, experimentally, to isolate and quantify the exact contributions of each component for the global friction force.

To understand the contribution of each mechanism involved in friction during the ejection stage a mixed approach was established: analytical simulation of the ploughing friction, numerical simulation of the ploughing and deformation component, and assessment of the adhesion component based on the previous calculations and or experimental results.

4. EXPERIMENTAL WORK

This chapter describes the materials, the processing and characterization techniques and the equipments used in this work. Furthermore, the test methods, the friction tests and the simulation analyses are also detailed herein.

4.1 Materials

The steel AISI H13 common used for injection moulds dies for thermoplastics materials was used for the metallic probe in the experiments in University of Minho. The experiments done in the Polymer Competence Centre of Leoben were with grades from Böhler the M340 and M333.

Three polymers were used in this research: a polypropylene, a polycarbonate and a PC/ABS.

4.1.1 Mould materials

The metallic probe material used in the experiments in the Mouldfriction of University of Minho was an AISI H13 1.2344 tool steel, Ramada Orvar 2M (F. Ramada, Portugal). The data sheet of this material is included in APPENDIX 1 – MATERIALS.

For the experiments in the instrumented mould in the PCCL two mould steel grades for injection moulds from Böhler were chosen. The M340 is a resistant corrosion steel with good wear resistance too and the M333 which has a better ability of hand finish methods (polish) used for plastic products which require

an outstanding surface finish. The data sheets of these materials are included in APPENDIX 1 – MATERIALS.

4.1.2 Polymers

A polypropylene homopolymer, Domolen 1100 N of Melt-Flow Rate (MFR) 12 g / 10min (230 ℃ / 2.16 kg) (DOME Polypropylene, The Netherlands) was used to mould the plastics test pieces.

A polycarbonate PANLITE L-1225 Z100 manufactured by Teijin Kasei America Inc. (Teijin Chemicals) with low viscosity (Melt-Volumetric Rate MVR 11 cm^3/10 min (300 ºC/1.2 kg)) and good UV resistance was used. It is typically used in automotive applications, general purpose, lenses, transparent or translucent parts.

The PC/ABS RonfalinC130 natural with MVR of 20 cm^3 / 10 min (260ºC/5 kg) is a polymer with heat resistance, impact resistance, reinforcement, UV resistance, flame retardancy and chemical resistance.

The datasheets of these materials are included in APPENDIX 1 – MATERIALS.

Some of the polymers properties are described in Table 4.1.

Table 4.1: Properties of the polymers

Property	**PP**	**PC**	**PC/ABS**
	DOMOLEN 1100N	PANLITE L-1225 Z100	RONFALIN C130 natural
Density [kg/m^3]	910	1200	1150
Tensile modulus of elasticity [MPa]	1550	2400	2400
Shear modulus [MPa]	800	---	---
MFR [g/10 min.]	12	11	
Mould Shrinkage [%]		0.6	0.5

4.2 Processing

4.2.1 Injection moulds

It was used a Krauss-Maffei KM60-210A injection moulding machine of the University of Minho to produce the samples for the friction tests. In this mould it is possible to inject two samples with the same geometry but with different injection point as shown in Figure 4.1.

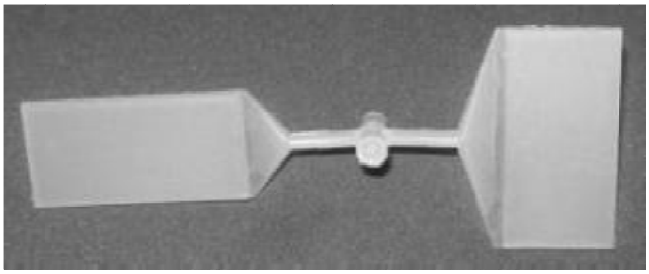

Figure 4.1: Samples with runner system

In the Polymer Competence Centre of Leoben (PCCL) the tests were performed on a fully-electric injection moulding machine Battenfeld 1000/200CDK-SE with an additional hydraulic unit.

4.2.2 Injection moulding

As shown in Figure 4.1, rectangular plates of 62×31×2 [mm^3] were moulded using the Krauss Maffei KM-60 210 injection moulding machine of 600 kN clamping force (Krauss Maffei, Germany). These rectangular plates are used in the Mouldfriction tests. From these injection mouldings parts, small blocks were cut with 5×6×2 [mm^3] for mechanical characterization by dynamic mechanical analysis (DMA), 50×10×4 [mm^3] for the determination of the elastic modulus in compression, and 10×10×4 [mm^3] for the strength evaluation.

4.3 Characterisation tests

The mechanical characterization of the materials is necessary to get input data for the simulation software.

4.3.1 Mechanical testing

The mechanical properties of the injection moulded parts were determined in tension and in compression using a universal testing machine Zwick Z100 (Zwick, Germany) with controlled temperature environment chamber. The compression tests were performed according to the ISO 604 standard.

For this mechanical characterization parallelepiped (50×10×4 [mm^3]) samples were used for determination of the elastic modulus and (10×10×4 [mm^3]) samples for the yield strength tests. For the determination of the Young modulus and yield strength and the temperature characterization, the tests were made at 23 ºC, 50 ºC, 65 ºC and 80 ºC. To do the determination of the Young Modulus the velocity used in the test was 1 mm/min and 50 mm/min for the yield strength.

The variation of the elastic modulus of the polymeric material with the temperature was also assessed with a DMA Triton model Tritec 2000 (Triton Technology, United Kingdom), following to the DIN53457 standard. The evaluation of the mechanical properties was done in the range of temperature from 22 ºC to 120 ºC using a heating ramp rate of 5 ºC/min.

4.3.2 Topography characterization – Roughness

The roughness of the steel surfaces was measured with a profilometer Perthometer M2 (Mahr, Germany), Figure 4.2. The cut-off length was selected according to the DIN 4768 standard.

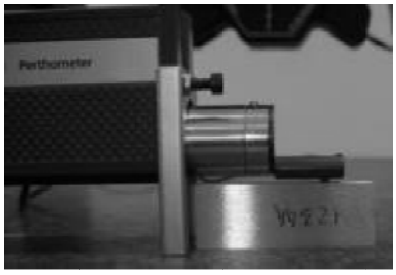

Figure 4.2: Metallic probe roughness characterisation

In Figure 4.3 it is shown an example of the parameters that are possible to obtain with the Perthometer M2 when measuring the roughness of one of the steel probe used in this research in the Mouldfriction equipment.

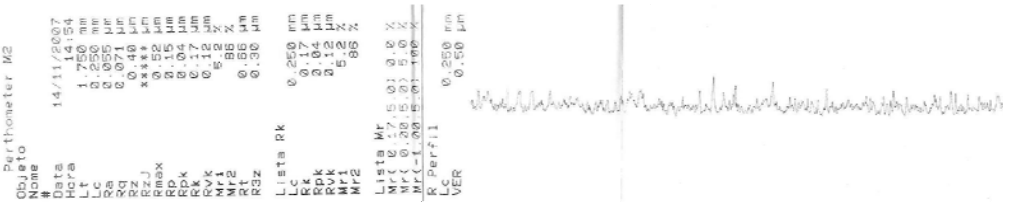

Figure 4.3: Parameters calculated with Perthometer M2 for the metallic probe with Ra=0.052 µm

In the Polymer Competence Centre of Leoben it was used a system topography surface measurement Confocal Microscope FRT MicroProf (FRT, Germany). This is a 3D optical measuring system for computer-supported 3D contour and surface roughness measurements. The measuring system is a non-destructive, non-contact measurement system suitable for all surface types and is used to measure small and micro-components for research, development or failure analysis purposes. The advantages of the MicroProf optical 3D measurement system are the high resolution and the high measurement speed.

4.3.3 Surface analysis

The objective of the use of microscope Zeiss MC 80 (Carl Zeiss, New York) was to show the experimental evidence of the main mechanism during friction.

In Figure 4.4 it is shown the surface aspect of polypropylene in the replication test of the metallic probe. The replication in this example was made at 150 ºC during 120 s with contact pressure of 650 kPa on a moulding surface with Ra=0.5 µm.

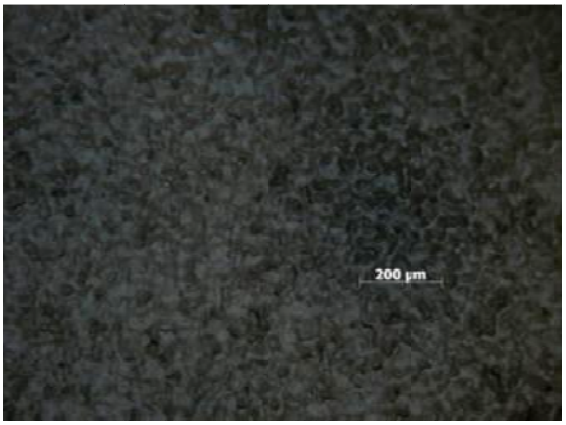

Figure 4.4: Replication with Ra=0.55 µm, contact pressure of 650 kPa at 150 ºC

4.4 Friction testing

4.4.1 Friction testing - Mouldfriction

The friction tests were carried out using the Mouldfriction prototype equipment described in Pouzada *et al.* (Pouzada, Ferreira et al. 2006). This equipment was fitted on an universal testing machine Instron 4505 (Instron Corp., USA), with a load cell of 1 kN (Figure 4.5). The tests were done using a crosshead displacement rate of 10 mm/min.

Figure 4.5: Universal testing machine Instron 4505 with the Mouldfriction equipment.

The Mouldfriction prototype is able to study the effect of different parameters (temperature, roughness and contact pressure) on the coefficient of friction during the ejection of plastic parts from injection moulds. A scheme of the friction test is shown in Figure 4.6.

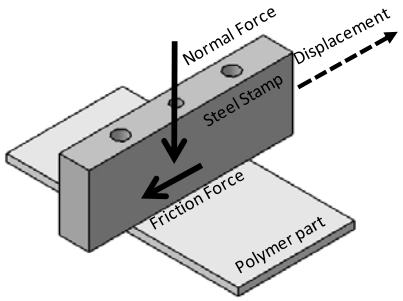

Figure 4.6: Scheme of the steel probe and the polymeric part in the friction test

The friction tests were carried out following the method proposed by Pouzada *et al.* (Pouzada, Ferreira *et al.* 2006). In a first stage, the steel probe was heated up to 150 °C. Then, the probe was pressed against the polymeric part at the recommended contact pressure and this is maintained until the end of the process. After 120 s of contact, the applied pressure guaranties the replication of the metallic surface on the polymeric part is obtained. After this 120 s period, the system was cooled down until the required test temperature, which corresponds to the one used in the ejection stage. The system is maintained at

this temperature for 120 s. Then the relative displacement was started with a velocity of 10 mm/min until a total displacement of 4 mm is achieved.

The selected values for the contact pressure are the usual to guarantee the replication on the polymeric part. The testing temperature is within the common range of ejection temperatures for these materials. In Figure 4.7 is plotted an experimental curve for polypropylene in the Mouldfriction prototype with the tested conditions identified.

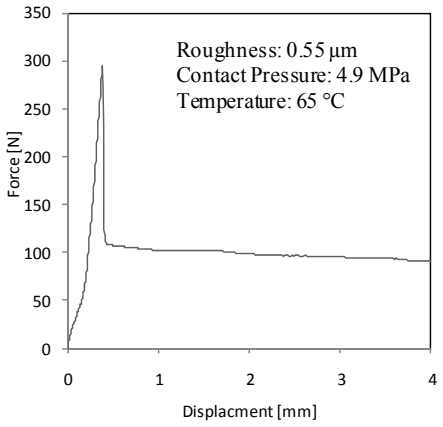

Figure 4.7: Friction force evolution for polypropylene in the Mouldfriction tests

The trace of the force in the Mouldfriction apparatus enables identifying the static friction force and the dynamic friction force. At the first stage there is an increase of the friction force to a maximum value correspondent to the static friction force. Only after achieving this value, the displacement between the two surfaces correspondents to the contacting pair begins. After starting the displacement between the surfaces the force decreases to a value that is the dynamic friction force. In the case of the ejection of polymeric parts from the moulds cores the static friction force is the important as it may cause problems in ejection or distortion or damage of the mouldings.

The normal load is a function of the pressure exerted by the pneumatic cylinder of the Mouldfriction device. The calibration of the normal force in function of

the pressure done by the pneumatic cylinder was calibrated as described by Sabino-Netto (Sabino-Netto 2008). A load cell of 5 kN was used for the calibration. Several tests were done (Figure 4.8) by varying the pneumatic pressure from 250 to 700 kPa.

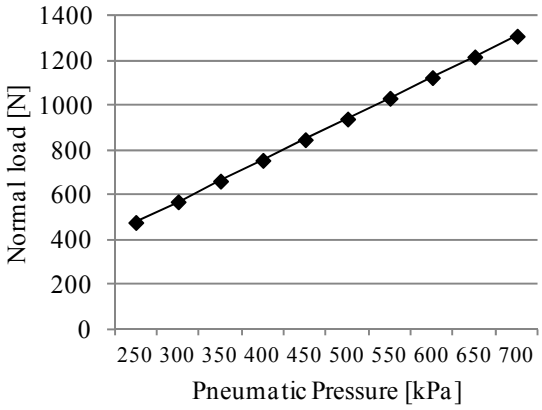

Figure 4.8: Normal load (force) calibration of the pneumatic cylinder

With the experimental data it was possible to obtain the linear fitting equation for the calibration of the pressure, as in Equation (4.1).

$$F_{normal}=1.85 \times P_{cylinder} + 14.43 \text{ [N]} \quad (4.1)$$

The coefficient of static friction (Equation (4.2))is calculated as the ratio between the maximum value of the force in Figure 4.7, (static friction force, $F_{friction}$), and the normal force calculated with Equation (4.1).

$$\mu = \frac{F_{friction}}{F_{normal}} \quad (4.2)$$

4.4.2 PCCL instrumented mould

The measurement apparatus at PCCL, Polymer Competence Centre of Leoben, for demoulding forces is based on a two-plate injection mould. The advantage of this apparatus is that the friction test is made inside of the mould cavity during the opening stage of the moulding cycle. The moulded part is injected

under typical process conditions and during the opening stage it is possible to measure the evolution of the friction force. The configuration of the moulded part is formed by a mould insert with a serrated surface (on the top) in order to fix the part while demoulding occurs and a flat surface (down) that is in contact with the surface which made the contacting friction pair. A vertically driven hydraulic piston moves the mould insert and is fixed horizontally to the moving half mould. The bottom side of the moulded part is formed by the plate-shaped, changeable mould insert, which is the metal specimen for the friction test.

Test procedure occur following conventional injection moulding process, the moulded part is injected, compressed and cooled. An additional loading force is applied during the cooling stage to make the shrinkage compensation Figure 4.9-A). This guaranties that during the test the area of contacting surfaces remains the same until the end of testing process.

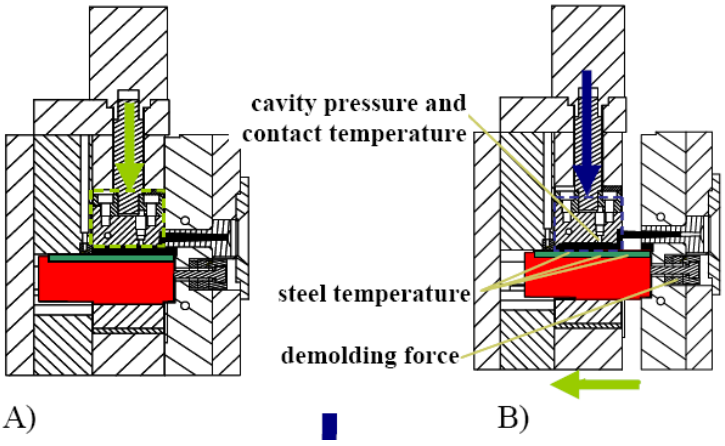

Figure 4.9: A: compensation of different shrinkage in holding pressure phase, B: apparatus while demoulding force measurement (Berger, Friesenbichler *et al.* 2008)

After the cooling stage the horizontal wedge is pulled out and a vertical force pushes down the moulded part Figure 4.9-B) with the desired vertical force value for the testing procedure. The demoulding length is 30 mm. The monitoring of the evolution of friction force is resumed in Figure 4.10.

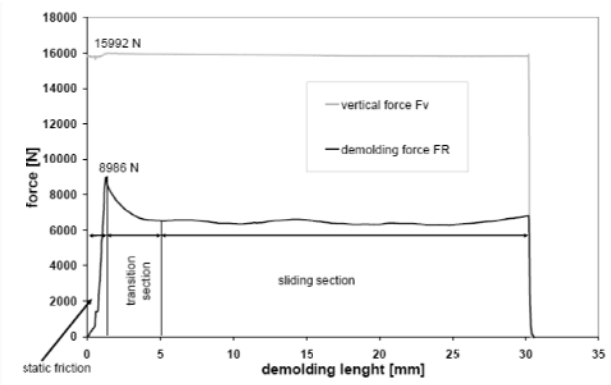

Figure 4.10: Monitoring of vertical force and resulting demoulding force FR as a function of demoulding length for ABS/PC. Mold insert: Böhler M333 Isoplast plastic mold steel (Berger, Friesenbichler *et al.* 2008)

4.5 Simulation

The DD3IMP in-house code, of CEMUC, Centro de Engenharia Mecânica da Universidade de Coimbra, was used to perform the numerical simulations. This code has been continuously developed to simulate processes involving large deformations and rotations. It allows taking into account the strong non-linearities related with the large deformations and rotations, the elastoplastic material mechanical behaviour and the evolutive contact with friction conditions (Menezes and Teodosiu 2000; Oliveira, Alves *et al.* 2008). In spite of being originally developed for sheet metal forming processes (*e.g.* (Padmanabhan, Oliveira *et al.* 2008)) it is used in many different research fields, as fracture mechanics (*e.g.* (Antunes and Rodrigues 2008)), thin-films mechanical characterization (*e.g.* (Antunes, Fernandes *et al.* 2008), analysis of local (Pereira, Oliveira *et al.* 2010) and global contact conditions (Oliveira, Alves *et al.* 2011).

In the FEM simulations with DD3IMP, the elastic behaviour of the deformable body is considered isotropic. Thus, it is only necessary to define the Young's modulus and the Poisson coefficient. Regarding the plastic behaviour, this was also considered as isotropic, described by the von Mises yield criterion and a

Swift-type hardening law. The material parameters necessary to describe the hardening are the yield stress (Y_0) and the hardening coefficient (n), such that:

$$Y = K(\varepsilon_0 + \bar{\varepsilon}^{\mathrm{p}})^{\mathrm{n}} \quad (4.3)$$

where Y is the flow stress, $\bar{\varepsilon}^p$ is the equivalent plastic strain and K and ε_0 are material parameters, such that $Y_0 = K\varepsilon_0^n$.

The material under analysis was considered as elastic perfectly plastic. Therefore, the hardening coefficient was assumed has being always 0.001. The Young's modulus values and the Swift law material parameters (Y_0 and K), for each temperature, were determined based on the experimental materials characterization tests.

The finite element model adopted corresponds to a 2D analysis of the contact conditions between the solid and the asperity. The solid is modelled as a rectangle with dimensions *a* for the length and *b* for the thickness, as shown in Figure 4.11. Nevertheless, this deformable body is discretized with 3D solid finite elements. Therefore, the 2D finite element model considers plane strain conditions along the *Oy* direction, for which a dimension of 100 μm was selected. Thus, the forces evaluated by the model will correspond to values measured for a height of 100 μm. This strategy was adopted to allow a comparison with the analytical model already introduced, although it is known that a real micro-geometry is always a two-dimensional surface (Wriggers 2006).

As previously mentioned, the dimensions *a* and *b* must be selected based on the on the roughness parameters, *Ra* and *S* (Zhang, Hodgson *et al.* 2003; Wriggers 2006). These dimensions must be large enough to avoid the interference of the boundary conditions in the estimative of the forces by the numerical simulation. According to Zhang *et al* and Wriggers (Zhang, Hodgson *et al.* 2003; Wriggers 2006), the boundary conditions that should be adopted correspond to assume that the bottom surface of the deformable body is fixed

while the outer vertical surfaces present null displacement in the *Ox* direction (see Figure 4.11).

The manufacturing industrial process generates certain roughness values. Thus the choice of manufacturing process must take into account the surface finish that will be obtained. In the case of EDM process the *Ra* values may range from 0.4 to 25 μm and in the case of surfaces with a polished finish can range from 0.0125 to 0.2 μm (TESA 2012). In industrial practice it is usual (to plastic parts without a specific finishing requirement and that components do not have high aesthetic requirements) the mould surface roughness is between 0.2~0.8 μm (SINO 2011). In the experimental tests performed during this work, the maximum value of the roughness (*Ra*) is near 2 μm. For this value of *Ra* the maximum height of the roughness profile is around 4 μm. Therefore, the dimensions of the rectangle used in numerical model (see Figure 4.11) were selected as *a*=230 μm, *b*=60 μm. For this dimensions it was verified that there is no interference of the boundary conditions on the contact forces distribution.

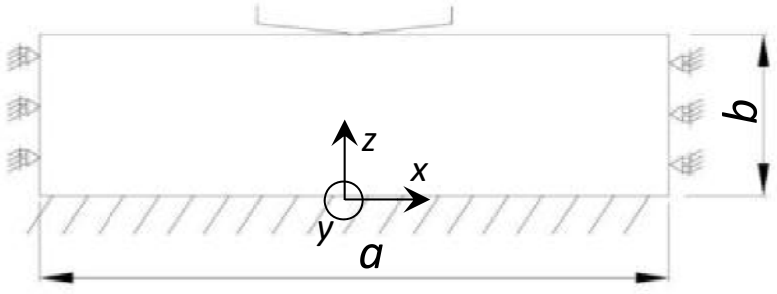

Figure 4.11: Finite element model showing the global coordinate system, the asperity geometry, the deformable body dimensions and the boundary conditions

In the present study the solid was discretized with a traditional trilinear eight-node hexahedral finite element associated with a selective reduced integration scheme (Hughes 1980). This type of solid elements is known to present more accurate results for a nearly square geometry. Also, to assure an accurate description of the contact evolution and, consequently, of the overall contact

force evolution, the finite element size in the contact area must correspond to a turning angle per element lower than 10° ((Li, Carden *et al.* 2002; Padmanabhan, Oliveira *et al.* 2007)). Thus, the finite element size is dictated by the smallest radius of curvature of the asperity (see Figure 4.11). In this study, taking into account this parameter for the different asperities analysed, the finite element size adopted for the contact surface was 0.5 μm. However, in order to guarantee a good compromise between computational efficiency and results accuracy, it is impossible to model the deformable body with a uniform mesh of 0.5 μm. The model considers a structured, non-uniform finite element discretization of the deformable body in the *Oz* direction, as shown in Figure 4.12. The discretization was performed guaranteeing that near the contact surface the elements have a square geometry, with a finite element size of 0.5 μm, as shown in the detail presented in Figure 4.12.

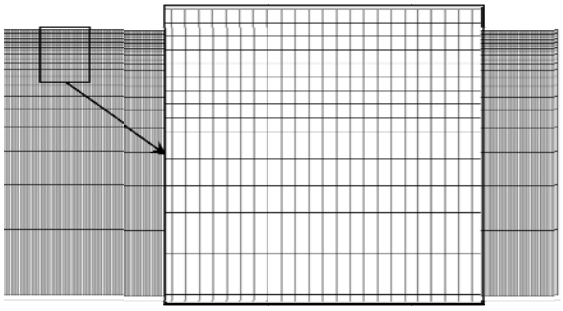

Figure 4.12: Finite element non-structured mesh in the *Oz* direction showing the detail of the top surface, for which an approximately square geometry of the finite elements was adopted.

Regarding the coefficient of friction, the simulations were performed assuming an evolutional law for this parameter as suggested by Magny (Magny 2002). The adopted evolutional law takes into account the effect of local contact pressure on the local coefficient of friction:

$$\mu = B - (B - A)\exp\left(-mp^{n}\right) \tag{4.4}$$

where A, B, m and n are parameters of the best fit of the Voce-type law to the observed dependence of the coefficient of friction on the contact pressure, p Figure 4.13.

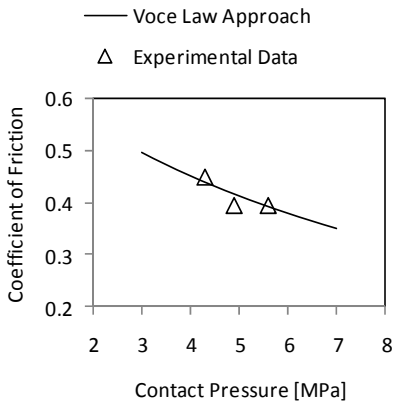

Figure 4.13: Variation of coefficient of friction with contact pressure

It must be noted that the Voce-type law has four parameters and that only three experimental results were available. Thus, the parameters were identified by best fitting and considering saturation behaviour for high contact pressure values, in order to minimize numerical problems.

5. RESULTS AND DISCUSSION

The experimental results of this research work are reviewed and analysed in this chapter.

5.1 Materials characterization

The data results of these tests were used in the model development and to examine their behaviour in friction.

5.1.1 Mechanical properties

Compressive tests and Dynamic Mechanical Analysis (DMA) were performed for all the polymeric materials in this research work. For the compressive tests in the polymeric materials four testing temperatures were used. The chosen values for the testing temperature were the standard room temperature of 23 ºC and three others corresponding to the demoulding temperature.

Polypropylene

The results of the compression tests on PP (Domolen 1100N) are summarised in Figure 5.1. The DMA analyses were performed in the temperature range from 23 °C to 160 °C. The elastic modulus as well as the compressive strength data and the evolution of the elastic modulus with temperature obtained from DMA analyses are summarized in Figure 5.2. These data confirm a good

adjustment between the elastic modulus obtained by DMA analysis and conventional compression testing.

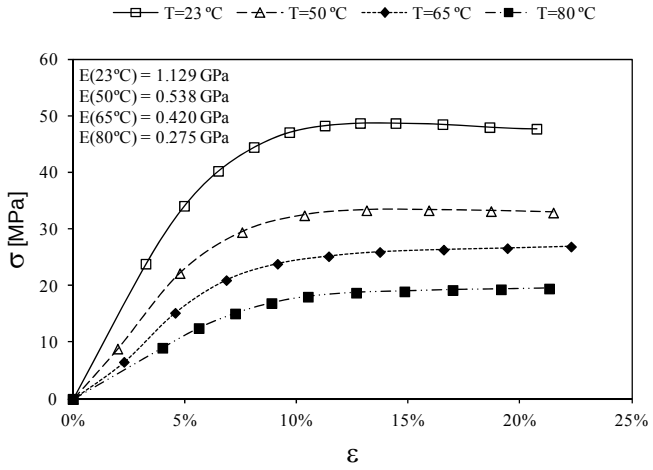

Figure 5.1: PP (Domolen 1100N) compressive test evaluation

In fact with the DMA analysis was possible to confirm the results of the compressive tests for the Young modulus to the different values of temperature.

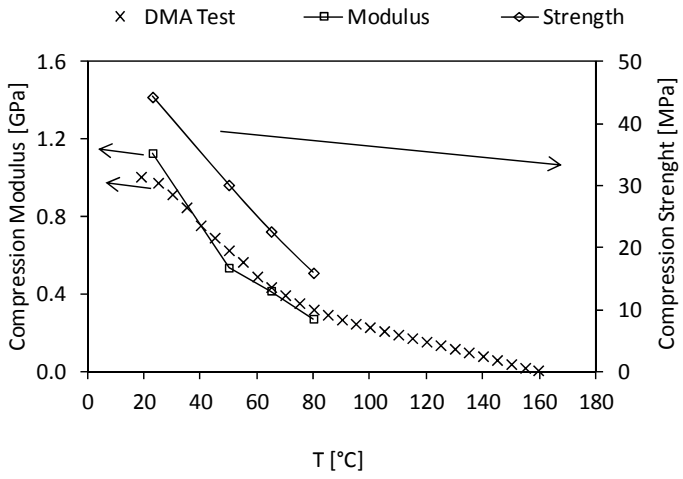

Figure 5.2: Mechanical properties of PP (Domolen 1100N) determined using compressive tests and DMA analysis

Polycarbonate

The same evaluation was made of PC Panlite L-1225 Z100 and the results are exposed in the Figure 5.3 and Figure 5.4. The glass transitions temperature determined for the PC material was 154°C.

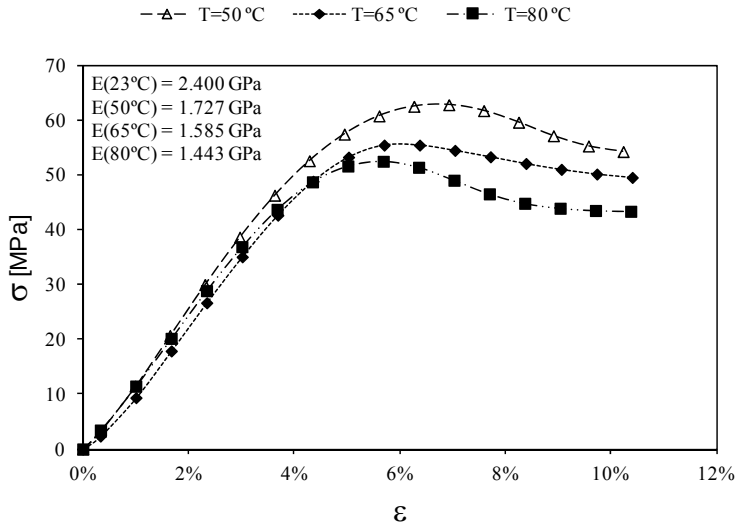

Figure 5.3: PC (PANLITE L-1225 Z100) compressive test evaluation

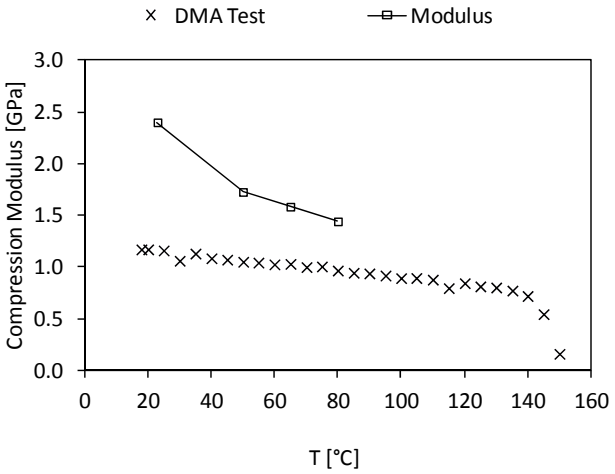

Figure 5.4: Mechanical properties of PC PANLITE L-1225 Z100 determined using compressive tests and DMA analysis

The results for PC/ABS Ronfalin C130 are shown in Figure 5.5 and Figure 5.6

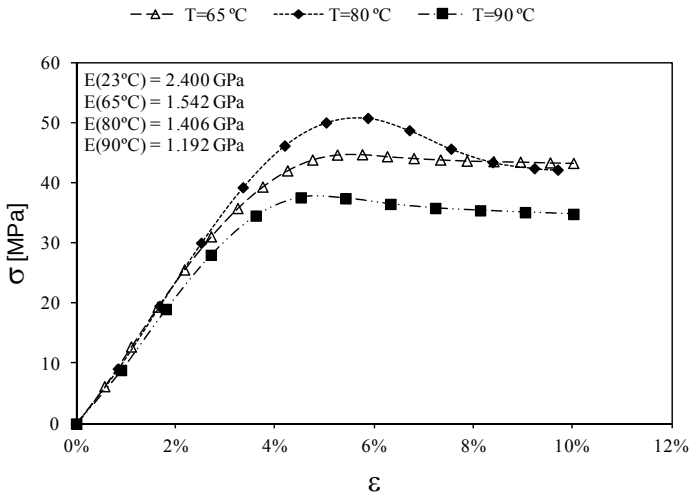

Figure 5.5: PC/ABS (Ronfalin C130) compressive test evaluation

The blend PC/ABS has two glass transitions: 110 °C for ABS and 146 °C for PC.

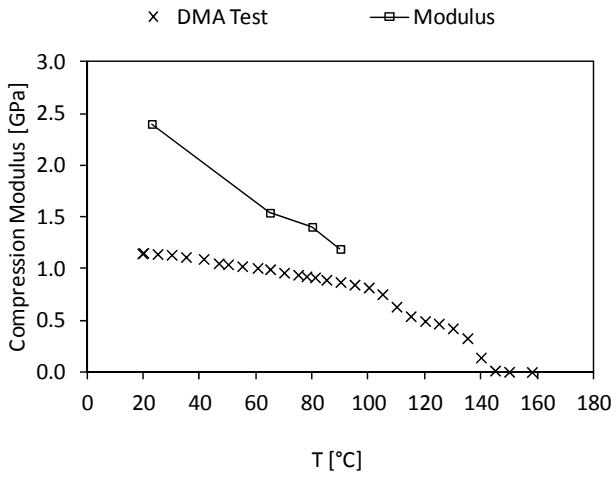

Figure 5.6: Mechanical properties of PC/ABS (Ronfalin C130) determined using compressive tests and DMA analysis

5.1.2 Roughness

The roughness characterization in the four metallic probes was carried out with a Perthometer M2 which is a profilometer with a stylus. The measurements of the roughness were made according to the DIN 4768 standard. The surface measurements were done in the direction of sliding in the friction tests.

These tests were confirmed with the confocal microscope FRT MicroProf. This is a non-contact measurement device and was possible to confirm the data acquired with the Perthometer. With the FRT MicroProf it is possible to complement through surface area analysis the tests carried out with the profilometer that assesses the linear variation of the roughness only. With these tests in terms of area it was possible to verify the homogeneous character of the contact surface roughness.

The manufacturing process that generated the surfaces is quite stable ensuring uniformity of the surface roughness. The FRT MicroProf acquired the surface points and with the Matlab software it was possible to get an idea of the roughness distribution over the evaluated area. It is possible to verify this conclusion in the Figure 5.7 for $R_a = 0.55\ \mu m$ and Figure 5.8 for $R_a = 1.95\ \mu m$.

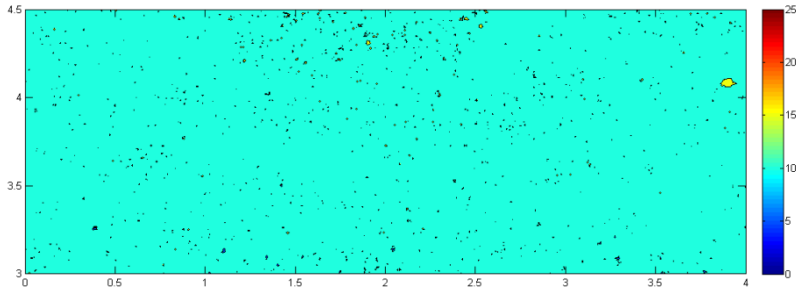

Figure 5.7: Evaluation of the surface roughness for the metal probe with Matlab software for $R_a = 0.55\ \mu m$

The whole area of analysis of 5.6×5.6 [mm^2] is shown in Figure 5.8.

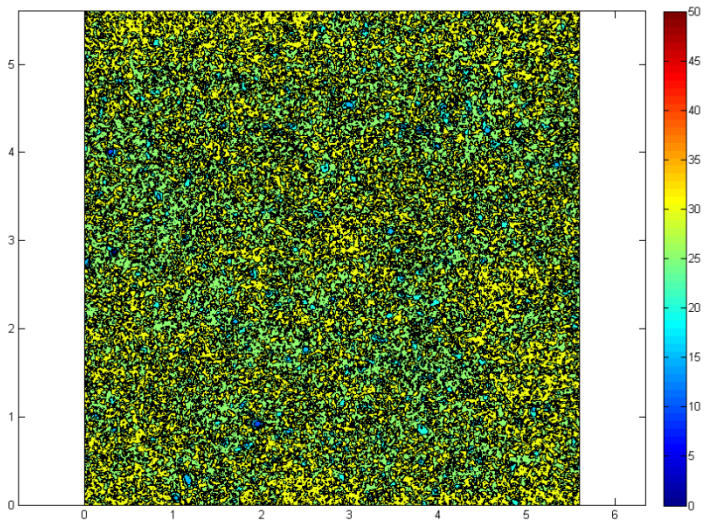

Figure 5.8: Evaluation of the surface roughness for the metal probe with Matlab software for $R_a = 1.95\ \mu m$

The roughness values parameters of the metallic probes used are described in Table 5.1. In this table it is also shown the number of peaks per unit area (N_P) for the two highest values of roughness that are used in the model described in Chapter 3.

Table 5.1: Roughness of the metallic probes

$\boldsymbol{R_a}$	$\boldsymbol{R_{max}}$	S	$\boldsymbol{N_P}$
$[\mu m]$	$[\mu m]$	$[\mu m]$	$[Number\ of\ peaks/mm^2]$
0.04	0.76	283.6	---
0.05	0.71	79.6	---
0.55	5.84	61.4	248
1.95	17.28	71.4	279

5.2 Measurement of the friction force

Two different methods were used to evaluate the behaviour during friction in demoulding conditions.

5.2.1 Mouldfriction test

The experiments to evaluate the variation of the friction force were made with the Mouldfriction prototype apparatus. For the various surface roughness conditions the temperature and contact pressure were varied. Four steel probes and three conditions of temperature and contact pressure were used.

Effect of temperature

For the polypropylene Domolen 1100 N three test temperatures were used: 50, 60 and 85 °C. These temperatures are typical ejection temperatures for this material. The evolution of the friction force in PP could be observed in Figure 5.9 for Ra of $0.04\,\mu m$, Figure 5.10 for $Ra = 0.55\,\mu m$ and Figure 5.11 for $Ra = 1.95\,\mu m$. Due to the conclusions drawn from the mechanical characterization tests carried out on polymers, it was expected that with increasing the test temperature the polymer becomes softer, making it easier to slip and thus making the friction force smaller. To the smallest values of roughness this is not so evident. In Figure 5.9 in the transition from 50 to 65 °C it is possible to verify the behaviour expected. With the increasing of the testing temperature a stabilization of the friction force generated between the metallic part and the polypropylene occurs.

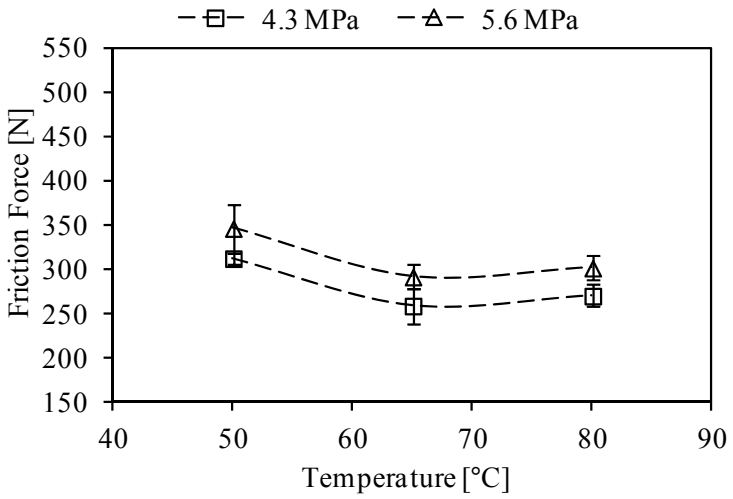

Figure 5.9: PP friction force dependence on temperature for $R_a = 0.04\ \mu m$

In Figure 5.10, the case of $R_a = 0.55\ \mu m$, for each contact pressure there is no noticeable variation with the test temperature.

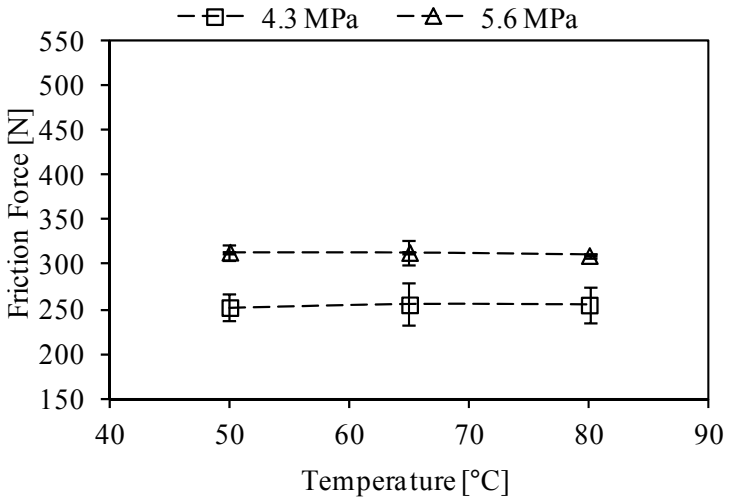

Figure 5.10: PP friction force dependence on temperature for $R_a = 0.55\ \mu m$

The initial expectation of the force reducing with the increasing temperature is only verified in the case corresponding to Figure 5.11. For this high roughness value the increase of testing temperature result in the decrease of friction force.

Therefore it seems that there is an important roughness effect on the friction force behaviour. Only with the increase of the polymer plastic deformation the expected effect of the temperature is evident.

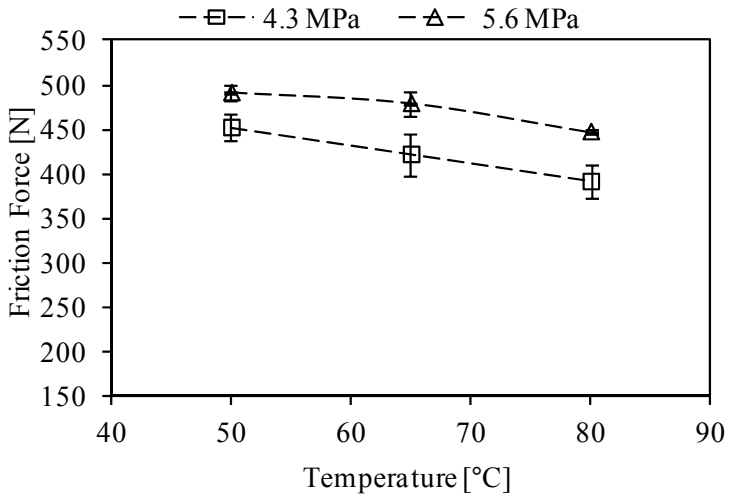

Figure 5.11: PP friction force dependence on temperature for $R_a = 1.95\ \mu m$

From this amount of information on the evolution trend of the friction force it was made the fitting of the experimental points were done with a second-degree polynomial equation. The local derivative (slope) was determined at each experimental data point. Table 5.2 shows the local slope of the friction force evolution in the previous curves.

Table 5.2: Local slope [*N/°C*]for the friction force with temperature variation for PP

	Ra =0.04 µm		*Ra* =0.05 µm		*Ra* =0.55 µm		*Ra* =1.95 µm	
T [°C]	4.3 MPa	5.6 MPa	4.3 MPa	5.6 MPa	4.3 MPa	5.6 MPa	4.3 MPa	5.6 MPa
50	-5.71	-5.79	-4.14	0.32	0.32	0.07	-2.01	-0.14
65	-1.40	-1.48	-1.38	-1.46	0.09	-0.13	-2.02	-1.45
80	2.90	2.82	1.38	-3.24	-0.13	-0.33	-2.04	-2.77

For all the analysed cases there is little influence of temperature on the friction force. Regarding the tendency of the local slope there is a trend of negative growth (for high contact pressures and higher roughness) representing a drop of the mechanical properties of the polymer and with this a decrease of the

demoulding friction force. The negative slope is justified by the decrease of the mechanical properties of PP with the increasing test temperature. For the case of $R_a = 0.55\ \mu m$ the variation of the friction force becomes negligible. In the others cases a small temperature dependency occurs.

Equilibrium between the ejection temperature and the mechanical properties of the polymeric part must be guaranteed. A bad choice of this relationship could lead to a deformation or distortion of the component. In fact one of the most important conditions to discuss is temperature, this ensures a decrease of the time of the moulding cycle. A good choice also guarantees the minimum development of the friction force during the ejection time. The best option for the production run is a maximum ejection temperature, a minimum cycle time and a minimum friction force during the ejection of the part.

Effect of pressure

The normal load is a function of the pressure exerted by the pneumatic cylinder. The pneumatic cylinder pushes the metallic probe against the polymer part. In the observations the contacting pressure done by the pneumatic cylinder on the contacting surfaces is considered. In the Figure 5.12 (for $R_a = 0.04\ \mu m$) there is an increase of the friction force with increasing contact pressure until 4.9 MPa and then a stabilization. For this case of the lowest roughness the increase of the contacting pressure results in the maximum effect of the roughness, and for this material and surface conditions, for values higher than 4.9 MPa a stabilization of friction force occurs.

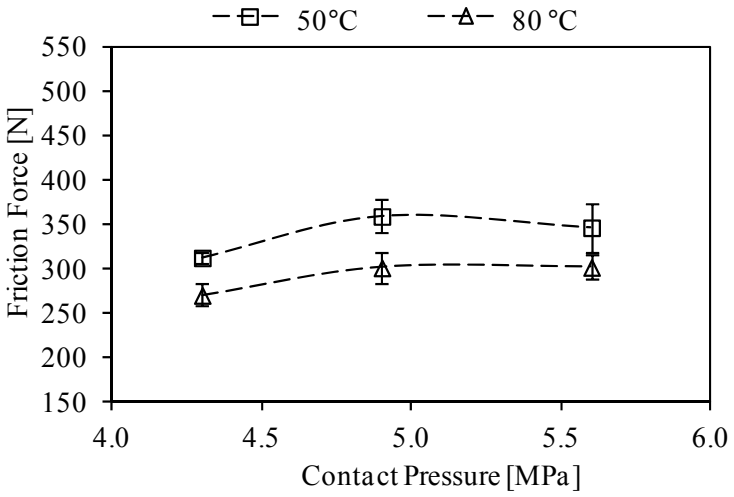

Figure 5.12: PP friction force dependence on the contact pressure for $R_a = 0.04\ \mu m$

This more pronounced effect of the contact pressure with higher roughness was expected. For these cases there is an increase in friction force with the contact pressure. The increase of the contact pressure results a linear increase of the friction force (Figure 5.13).

With the increase of the roughness there is a more evident dependence of the friction force on the contact pressure (Figure 5.14) especially for the highest temperatures.

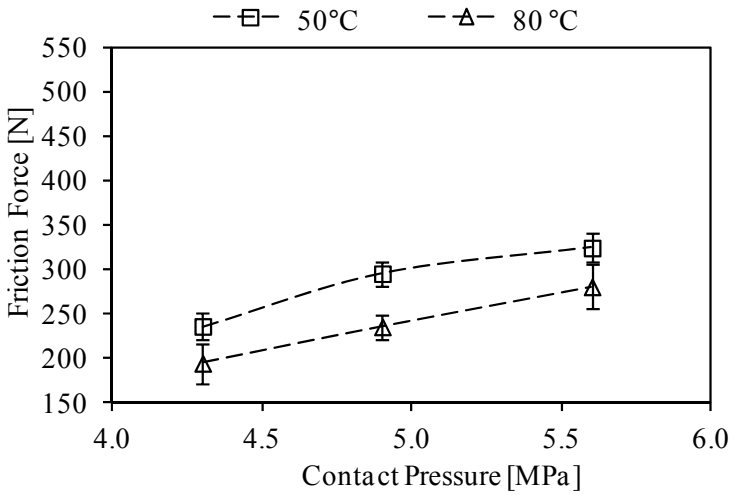

Figure 5.13: PP friction force dependence on contact pressure for $R_a = 0.05\ \mu m$

In that the effect in friction force for the lowest value of temperature is concerned (Figure 5.14) the increase of the contact pressure leads to a slight increase of the friction force. For the highest temperature the friction force has a linear increase variation with the contacting pressure.

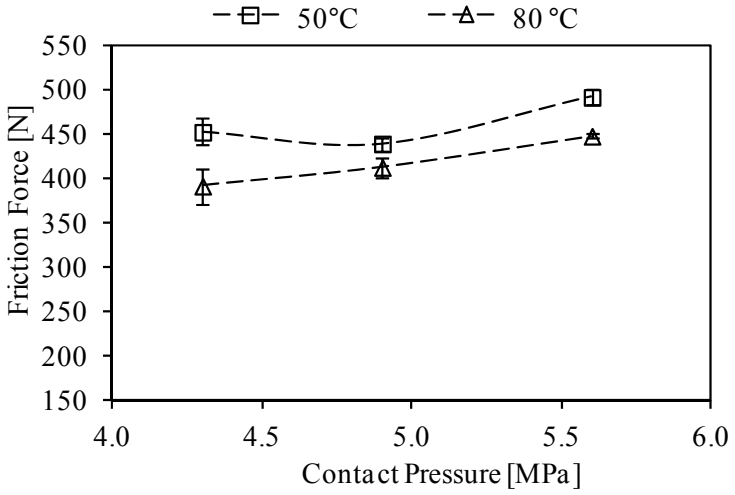

Figure 5.14: PP friction force dependence on contact pressure for $R_a = 1.95\ \mu m$

As it was done for the temperature, the local derivative (slope) was determined in each experimental data point for the contacting pressure.

In Table 5.3 it is possible to verify the variation of the local slope for the different conditions of contact pressure.

Table 5.3: Local slope [*N/MPa*]for the friction force with contact pressure variation for PP

	Ra =0.04 μm		*Ra* =0.05 μm		*Ra* =0.55 μm		*Ra* =1.95 μm	
Contact Pressure [MPa]	T=50ºC	T=80°C	T=50ºC	T=80°C	T=50ºC	T=80°C	T=50ºC	T=80°C
4.3	121.85	75.12	125.16	70.26	103.07	59.20	-66.63	28.04
4.9	33.44	28.06	72.16	66.40	51.80	43.80	22.64	41.97
5.6	-69.72	-26.84	10.33	61.89	-8.01	25.82	126.80	58.23

Generally, it was expected this frictional force to increase with the increasing contact pressure. This behaviour of the friction force is a result of the more intimate contact caused by the contact pressure. But for the first three values of roughness there is a decrease in the local slope with the increasing contact pressure. This means that by increasing the contact pressure the increase of frictional force is less evident; in some cases (*Ra*=0.04 μm and *Ra*=0.55 μm with T=50 ºC) there is a stabilization or even change trend. This frictional behaviour may be explained by the lower stiffness of PP at this temperature. It was also verified in the finite element analysis that these conditions lead to a null frictional force due to the deformation which occurs only in the elastic regime. For the case of higher roughness the trend is to increase the local slope calculated with the polynomial approach. The effect of the mechanical interlocking is the dominant process for these higher values of roughness.

Effect of roughness

The starting point in the analyses and discussion of the roughness effect should be the review of the mechanism in which is divided the contribution for the friction force. The dominant mechanisms involved in friction are ploughing, deformation and adhesion. The two first mechanisms referred to are mostly mechanical effects. These mechanisms result in the volume of material that can be ploughed and deformed during the initial moment of displacement resulting

in the static friction force. The relative contribution of adhesion in the frictional force has a variation that is dependent on the value of the roughness of the surfaces and on the material. In the experimental data, the effect of roughness is similar to other authors' data ((Sasaki, Koga *et al.* 2000; Kinsella, Lilly *et al.* 2005; Berger, Friesenbichler *et al.* 2008)). Observing Figure 5.15, and Figure 5.16, it is possible to confirm a minimum value of the friction force for $Ra \approx 0.5\ \mu m$. To lowest values of roughness there exists an increase of the friction force. For PP this is the point where the adhesion effect becomes more preponderant in friction.

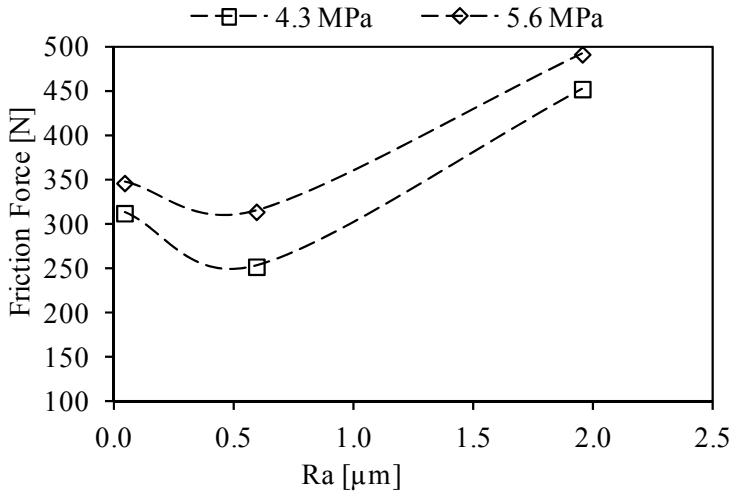

Figure 5.15: PP friction force dependence on roughness for T=50 °C

Adhesion exists in all contacting conditions, but the relative effect of this mechanism becomes more relevant for lowest values of roughness. For highest values of roughness the "mechanical" effects (interlocking) of ploughing and deformation are dominant in the friction force developed in the contacting surfaces. For all contact pressures, at different testing temperatures, the increase of friction force with the reduction of surface roughness was observed.

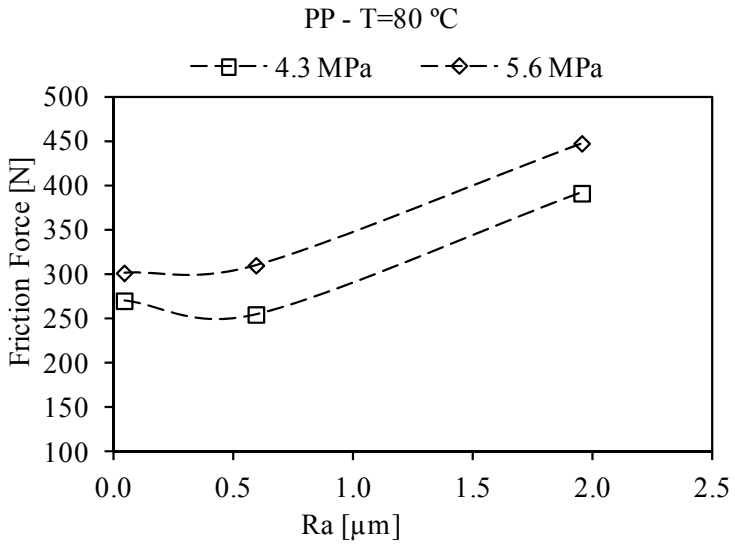

Figure 5.16: PP friction force dependence on roughness for T=80 °C

For the roughness variation the fitting of the experimental data were done by a second-degree polynomial. The local derivative of these equations was calculated for each roughness experimental data, the slope results are resumed in Table 5.4.

Table 5.4: Local slope [*N/µm*] for the friction force with roughness variation for the PP

	T=50 ºC		T=65 ºC		T=80 ºC	
Ra [µm]	4.3 MPa	5.6 MPa	4.3 MPa	5.6 MPa	4.3 MPa	5.6 MPa
0.04	-183.43	-113.26	-44.32	16.19	-64.77	-9.01
0.05	-180.74	-111.28	-42.96	17.04	-63.43	-8.11
0.55	-46.46	-12.31	24.83	59.93	3.65	36.54
1.95	329.52	264.83	214.65	180.02	191.48	161.56

In this Table 5.4 it can be observed what happens to the slope of the polynomial approach curves: for the variation of frictional force with the roughness there exists a local minimum in the range of tested roughnesses, to the exception of temperature of 65 °C and the higher contact pressure in which occurs a decrease in slope with decreasing the surface roughness. For all other temperatures and roughness lower than 0.55 µm the tendency is to increase the

frictional force with decreasing the surface roughness. For these values of roughness the preponderance of adhesion effect overrides the effect of the deformation of the polymeric material.

Effect of moulding materials

The results for an amorphous polycarbonate PANLITE L-1225 Z100 and a PC/ABS Ronfalin C130 blend are presented and discussed in this section.

The test temperatures where defined according to the usual ejection temperature for each material, according to Table 5.5.

Table 5.5: Mouldfriction testing temperatures

Material	Test **temperature** [°C]		
PP – DOMOLEN 1100 N	50	65	80
PC – PANLITE L-1225 Z100	50	65	80
PC/ABS – RonfalinC130	65	80	90

Three surface conditions (roughness) were evaluated with varying contact pressure and temperature.

The increase of the friction force with the increase of the test temperature was evident for all surface roughness conditions. Figure 5.17 shows this variation for $R_a = 0.55\,\mu m$. The same behaviour was verified by Wang *et al.* (Wang, Kabanemi *et al.* 2000). PC exhibits a strong temperature dependence. With the increase of temperature and the approximation of T_g it occurs an increase of the friction force.

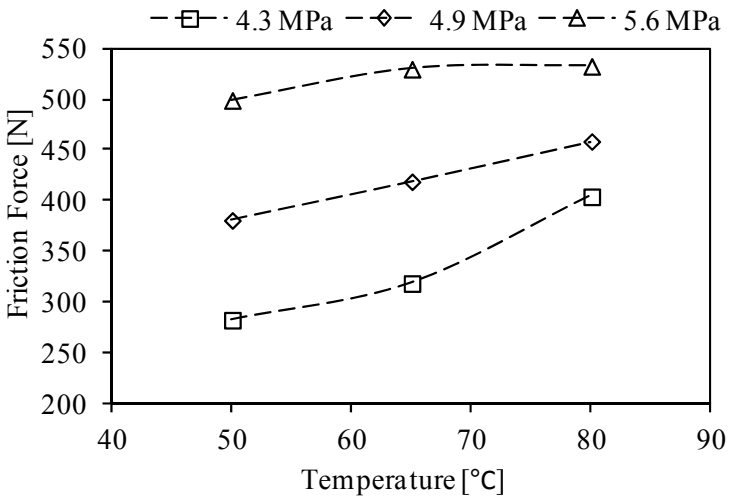

Figure 5.17: PC friction force dependence on the temperature for $R_a = 0.55\ \mu m$

Concerning the variation of the contact pressure (Figure 5.18 shows the case of $R_a = 0.55\ \mu m$) the same behaviour for PC was observed by other authors (Berger, Friesenbichler *et al.* 2008). The increase of the contacting pressure results in the increment of the friction force, for all cases of roughness and temperature. Those authors suggested that the chemical composition and the morphology of mating surfaces are influencing the friction.

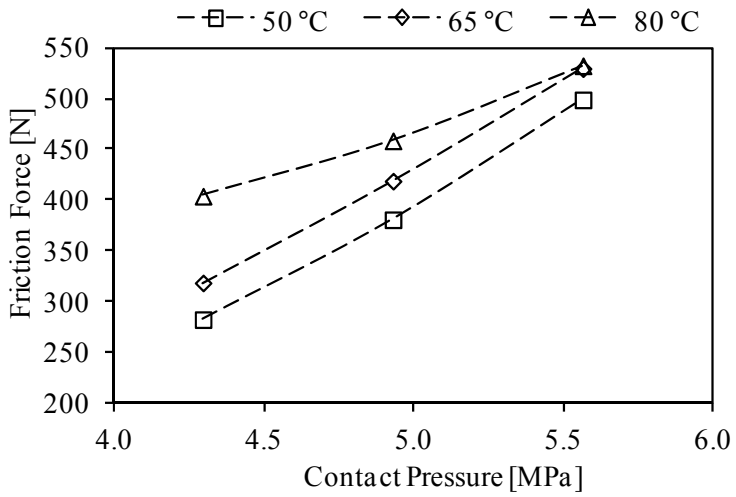

Figure 5.18: PC friction force dependence on the contact pressure for $R_a = 0.55\ \mu m$

In the analysis of the behaviour of PC with the roughness variation (Figure 5.19 and Figure 5.20) it was observed the same behaviour observed in the previous tests with PP. The minimum of friction force was achieved around the roughness value of 0.5 μm. At the lower values of the roughness there occurs an increment of the friction force developed between the steel part and the polycarbonate. This is not so evident for the cases of contact pressure of 5.6 MPa. For this contacting pressure the variation is almost linear.

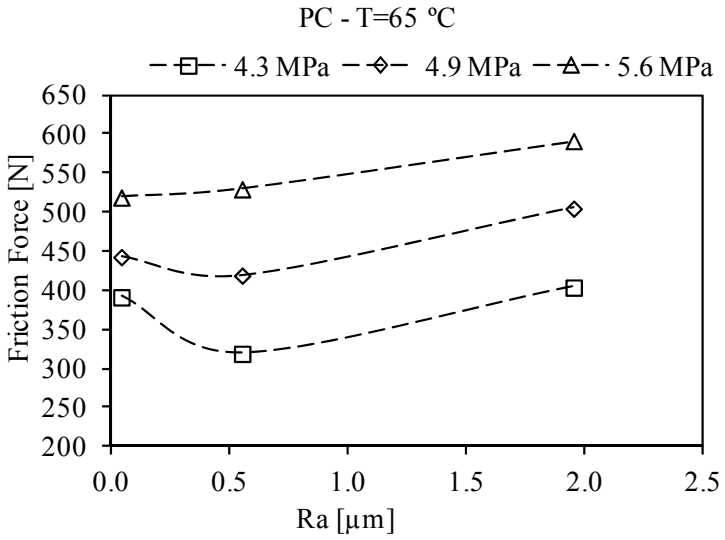

Figure 5.19: PC friction force dependence on the temperature for T=65 °C

For all the temperatures studied only for the case of higher contact pressure there is no increase in the friction force with the decrease of the surface roughness.

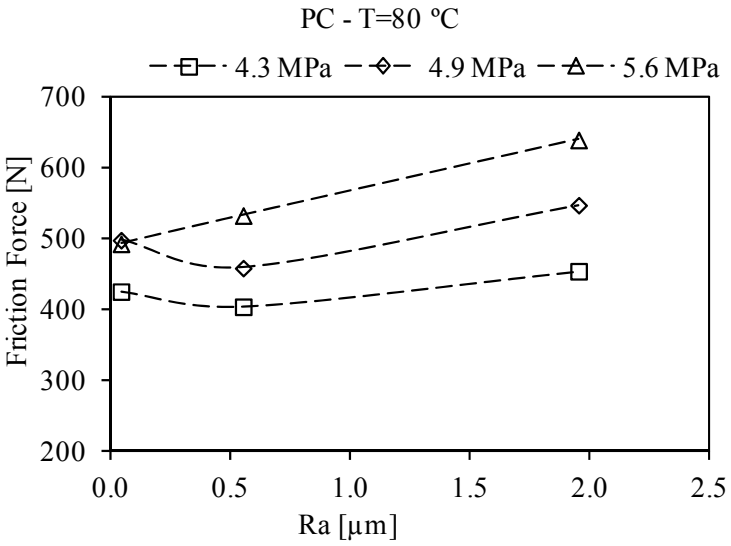

Figure 5.20: PC friction force behaviour with roughness variation for T=80 °C

For the PC the fitting of the experimental data were also done by a second-degree polynomial. The local derivative of these equations was calculated for

each temperature (Table 5.6), contact pressure (Table 5.7) and roughness (Table 5.8) experimental data. For the case of PC only three roughness surfaces were analysed.

Table 5.6: Local slope [*N/°C*] for the friction force with temperature variation for the PC

	Ra =0.04 μm			*Ra* =0.55 μm			*Ra* =1.95 μm		
T [°C]	4.3 MPa	4.9 MPa	5.6 MPa	4.3 MPa	4.9 MPa	5.6 MPa	4.3 MPa	4.9 MPa	5.6 MPa
50	2.05	-1.15	3.85	0.76	2.48	2.98	-1.95	0.97	1.48
65	2.20	2.07	0.12	4.05	2.59	1.12	1.59	2.20	2.60
80	2.35	5.28	-3.61	7.34	2.70	-0.74	5.13	3.43	3.71

The temperature has different effects depending on the contact pressure and the roughness. Thus in Table 5.6 it can be seen that for the highest roughness the friction force increases more when the test temperatures are higher. In the case of two lowest roughness values, for the highest contact pressure, the tendency is to stabilize the frictional force as the test temperature increases. Here it seems that the effect of elasticity of PC has an important role in this aspect, although numerical simulations have not been performed for this material.

In the analysis of the local slope for the contact pressure variation (Table 5.7) is verified that for the smaller roughness the tendency is to stabilize the frictional force with the exception of temperature, but for T=65 ºC there is an more pronounced increase with the rising contact pressure. At the tested average roughness the frictional force always increases but this increase is more important with larger contact pressures. As for the highest value of surface roughness and T=50 ºC a gradual increase in the frictional force occurs. With the temperature increase the frictional force modifies the variation to a behaviour close to the linear variation at T=80 ºC.

Table 5.7: Local slope [*N/MPa*] for the friction force with contact pressure variation for the PC

	Ra =0.04 μm			*Ra* =0.55 μm			*Ra* =1.95 μm		
Contact Pressure [MPa]	T=50 °C	T=65 °C	T=80 °C	T=50 °C	T=65 °C	T=80 °C	T=50 °C	T=65 °C	T=80 °C
4.3	138.19	61.75	173.95	139.32	149.68	70.74	113.35	170.39	147.48
4.9	104.04	98.88	58.52	168.85	165.34	99.67	121.25	148.92	145.54
5.6	64.20	142.21	-76.15	203.30	183.60	133.42	130.47	123.86	143.28

In Table 5.8 it is observed the effect roughness on the friction force. Also in these cases there is a minimum value of the frictional force as the surface roughness varies to the exception of the contact pressure of 5.6 MPa. This minimum corresponds to the inflection of the behaviour of the frictional force. So to lower values of roughness the friction force increases due to the phenomenon of adhesion. For higher surface roughness values the deformation effects become predominant and the frictional force increases.

Table 5.8: Local slope [*N/μm*] for the friction force with roughness variation for the PC

	T=50 °C			T=65 °C			T=80 °C		
Ra [μm]	4.3 MPa	4.9 MPa	5.6 MPa	4.3 MPa	4.9 MPa	5.6 MPa	4.3 MPa	4.9 MPa	5.6 MPa
0.04	-213.60	-196.04	12.06	-196.04	-75.22	14.57	-62.43	-114.25	78.37
0.55	-86.39	-87.88	25.58	-87.88	-17.72	27.00	-21.10	-39.48	77.31
1.95	262.83	209.04	62.70	209.04	140.15	61.14	92.38	165.76	74.40

For PC/ABS several tests were carried out with the same metallic probes used for the previous materials.

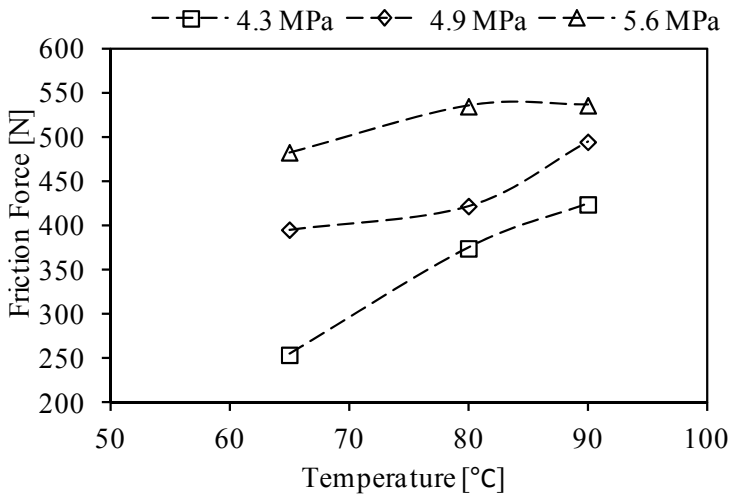

Figure 5.21: PC/ABS friction force dependence on temperature for $R_a = 0.55\ \mu m$

With the temperature variation the PC/ABS showed the same behaviour of PC. Higher values of test temperature increase the friction force, as in Figure 5.21. It should also be noted that for the highest contact pressure a stabilization of the frictional force occurs at the higher temperatures.

With the contact pressure growing (Figure 5.22) the developed friction forces are higher.

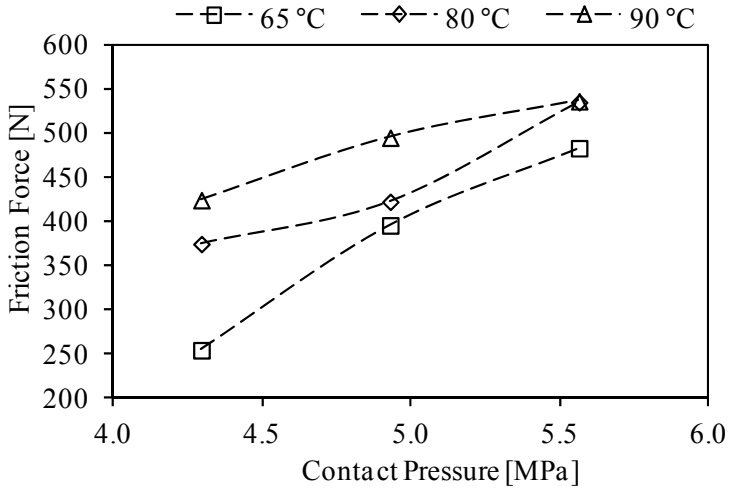

Figure 5.22: PC/ABS friction force dependence on contact pressure for $R_a = 0.55\ \mu m$

In the roughness effect analyses for the blend PC/ABS the friction force behaviour is similar (Figure 5.23) to the previous cases to the exception of the tests at 90 °C (Figure 5.24).

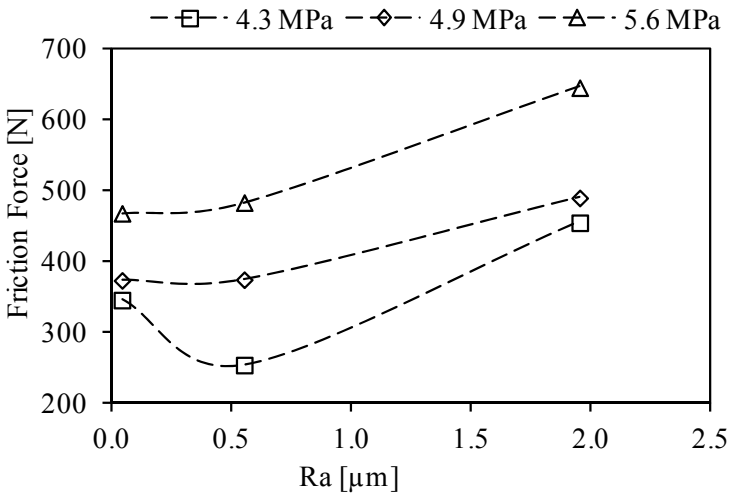

Figure 5.23: PC/ABS friction force dependence on roughness for T=65 °C

For the smallest values of roughness tested, the increasing of the friction force is not verified. The lower mechanical strength and stiffness results in a decrease of the frictional force.

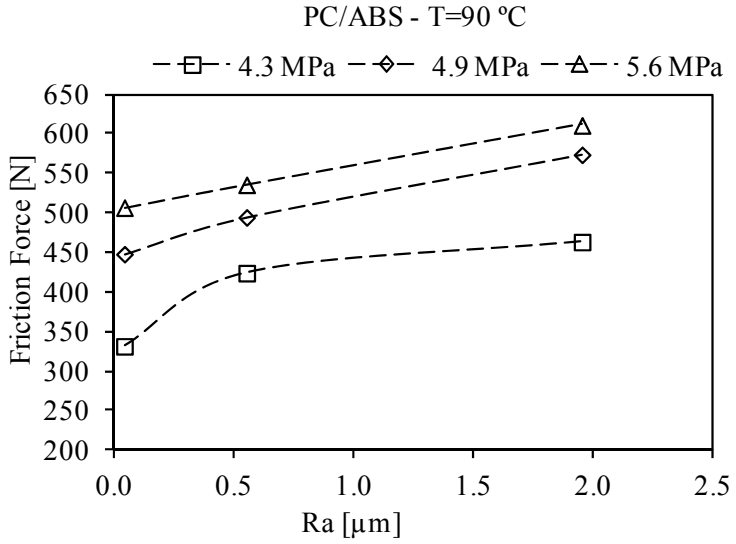

Figure 5.24: PC/ABS friction force dependence on roughness for T=90 °C

In Table 5.9 the slope of the polynomial approximation of the friction force with temperature variation is calculated. It is found that in general terms there is a decrease of the slope of the polynomial approximation with increasing the temperature. For higher temperatures, near 110 °C corresponding to the T_g of ABS, it occurs a considerable drop in the mechanical properties and this is the reason for the decrease in the friction force for higher values of temperature.

Table 5.9: Local slope [*N/°C*] for the friction force with temperature variation for the PC/ABS

	Ra =0.04 µm			*Ra* =0.55 µm			*Ra* =1.95 µm		
T [°C]	4.3 MPa	4.9 MPa	5.6 MPa	4.3 MPa	4.9 MPa	5.6 MPa	4.3 MPa	4.9 MPa	5.6 MPa
65	5.47	8.36	12.95	9.82	-1.50	5.47	5.27	8.50	-5.41
80	-1.79	1.56	-0.71	6.18	5.06	1.45	-0.63	0.94	-0.51
90	-6.63	-2.97	-9.82	3.74	9.43	-1.23	-4.55	-4.11	2.76

On evaluating the case of the variation of frictional force with the contact pressure (Table 5.10) it was observed that for the lowest value of the roughness and lower test temperatures there is an increase of the slope of the friction force for higher contact pressures, while for the highest test temperature the behaviour is the opposite. The change in the mechanical behaviour of ABS as

the glass transition temperature approaches changes the way how the frictional force responds.

Table 5.10: Local slope [*N/MPa*] for the friction force with contact pressure variation for the PC/ABS

	Ra =0.04 µm			*Ra* =0.55 µm			*Ra* =1.95 µm		
Contact Pressure [MPa]	T=65 °C	T=80 °C	T=90 °C	T=65 °C	T=80 °C	T=90 °C	T=65 °C	T=80 °C	T=90 °C
4.3	15.29	111.21	228.53	264.21	25.00	133.85	54.35	228.04	230.51
4.9	92.39	145.07	142.48	183.83	121.64	90.15	145.17	93.52	121.49
5.6	182.34	184.56	42.09	90.05	234.39	39.17	251.13	-63.42	-5.70

In Table 5.11 the friction force behaviour of the PC/ABS blend is analysed. The variation of the friction force with the roughness is similar to the other materials tested. The existence of a local minimum for the friction force is detected in almost all cases. It revealed the importance of the adhesion at lower values of roughness.

Table 5.11: Local slope [*N/µm*] for the friction force with roughness variation for the PC/ABS

	T=65 °C			T=80 °C			T=90 °C		
Ra [µm]	4.3 MPa	4.9 MPa	5.6 MPa	4.3 MPa	4.9 MPa	5.6 MPa	4.3 MPa	4.9 MPa	5.6 MPa
0.04	-264.99	-19.43	6.71	-19.43	-113.93	-74.28	222.53	100.42	57.21
0.55	-93.05	23.35	52.50	23.35	-15.48	-23.37	140.60	81.94	55.73
1.95	378.91	140.79	178.21	140.79	254.77	116.37	-84.32	31.21	51.69

The comprehensive analysis of what occurs to the three polymeric materials (Table 5.12) shows that the influence of the temperature is not the dominant factor in the behaviour of the friction force and is more pronounced for PC and even more for PC/ABS. The effect of the contact pressure is more evident in PC, and this effect is more important in the friction force behaviour than the temperature. The roughness is more influent in the case of PP than the other materials being this impact more significant for the higher temperatures. So the most important factor that affects the friction force in all materials tested is the roughness.

Table 5.12: Variables affecting the moulding materials

Material	Temperature	Contact pressure	Roughness
PP	↑	↑ ↑	↑ ↑ ↑ ↑ ↑
PC	↑ ↑	↑ ↑ ↑	↑ ↑ ↑ ↑
PC/ABS	↑ ↑ ↑	↑ ↑	↑ ↑ ↑ ↑

5.2.2 PCCL instrumented mould

To understand the friction process and to measure the interaction force between the moulding part and the mould some systems have been developed. The Polymer Competence Centre in Leoben (PCCL) has an in-mould system which is able to measure the friction force developed between the injected part and the mould. The measurement of the friction force is made during the opening of the mould. In this system the polymer is injected over a metal probe, similarly to a normal injection process. After the cooling stage and when the desirable temperature is reached (ejection temperature) the mould opens. During the mould opening it is measured the friction force between the moulding and the probe.

The objective of these tests was to get results from other system used to measure the ejection friction. For this purpose two materials were tested with the PCCL instrumented mould and with the Mouldfriction prototype.

The materials tested in the PCCL instrumented mould were the PC PANLITE L-1225 Z100 and the PC/ABS Ronfalin C130. The tested conditions are summarised in Table 5.13.

Table 5.13: Testing conditions in the PCCL

Contact pressure [MPa]	Testing temperature [°C]	Probe Roughness - R_a [µm]
4.3	65	0.03
4.9	80	0.33
5.6	90	

Considering the evident difference between the two testing methods to measure the friction force, tests were made to compare the evolution of the friction force for the same materials. The values measured of the contacting pressure between the two test methods showed a small difference, with a maximum of 2 % (0.08 MPa).

As shown in Figure 5.25, the increase of the temperature results in the decrease of friction forces. Although the results obtained in this case follow the trend that was expected initially, there is an opposite behaviour comparing with the observed in the Mouldfriction tests for PC. These results confirm the mechanical characterization tests carried out on this material.

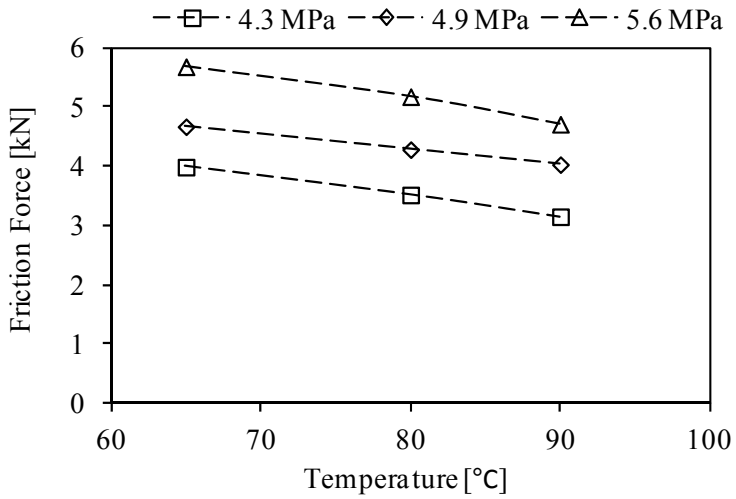

Figure 5.25: PC friction force dependence on temperature for $R_a = 0.33\ \mu m$

The friction force variation with the contacting pressure (Figure 5.26) was analysed and the behaviour was found to be the same of other similar tests in the Mouldfriction prototype.

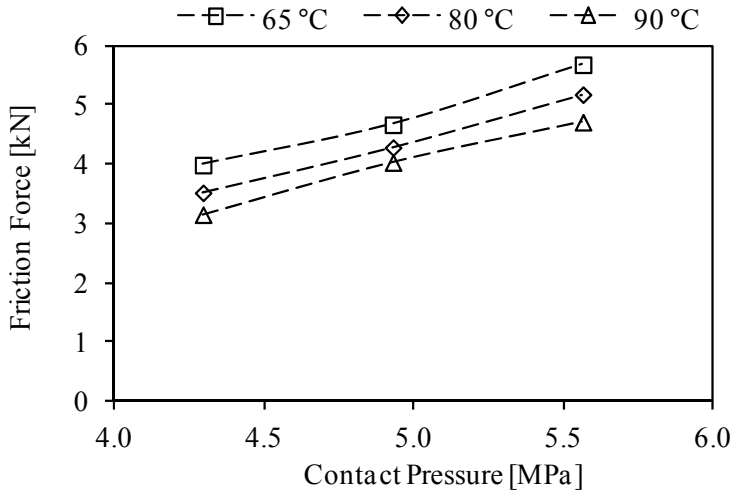

Figure 5.26: PC friction force dependence on the contact pressure for $R_a = 0.33\ \mu m$

Figure 5.27 shows the variation of the friction force with the roughness for the testing temperature of 90 °C. In the other tests for 65 and 80 °C the results

showed a similar friction force variation. In the experiments done with the PCCL instrumented mould, it was only possible to do tests with two surface roughness conditions. The highest roughness value tested 0.33 μm seems to be in the roughness values were the adhesion becomes more preponderant and for lower values of roughness an increase of friction force occurs.

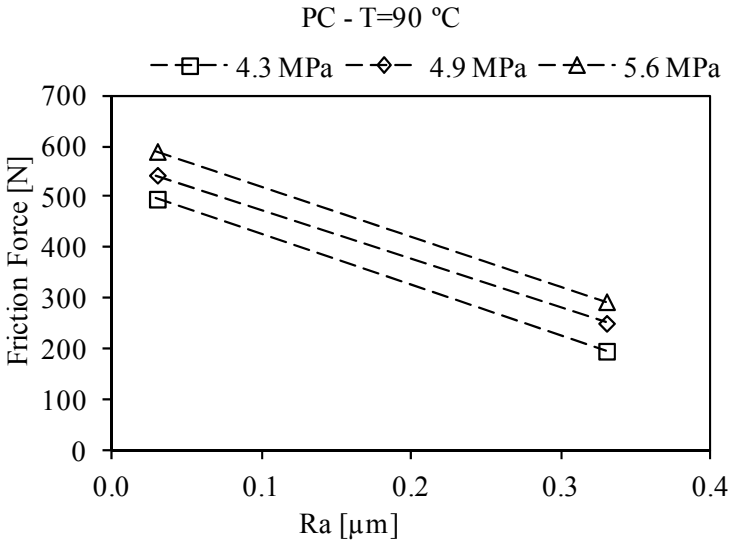

Figure 5.27: PC friction force dependence on roughness for T=90 °C

For the case of the PC/ABS blend only the 0.33 μm roughness was tested. This material has a friction force behaviour that is not influenced by the temperature variation. For all cases of contact pressure the variation of the friction force is negligible (Figure 5.28).

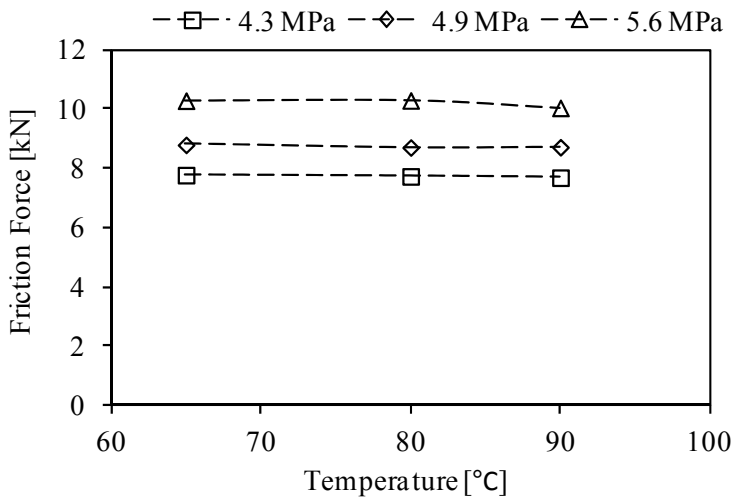

Figure 5.28: PC/ABS friction force dependence on the temperature for $R_a = 0.33\ \mu m$

It is not evident any difference between the three tested temperatures for each contact pressure, (Figure 5.29). The increment of contact pressure resulted in an increase of friction force which is not affected by temperature variation.

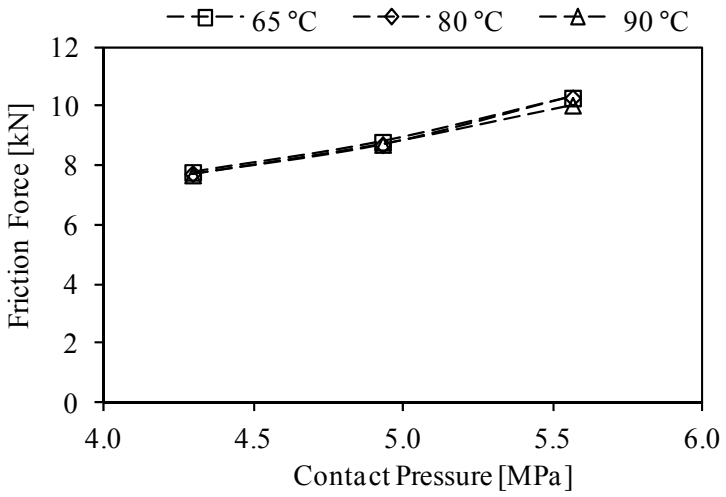

Figure 5.29: PC/ABS friction force dependence on the contact pressure for $R_a = 0.33\ \mu m$

5.3 Calculating the coefficient of friction

The area of the contacting surface between the moulding and the mould in the PCCL system is 50×70 $[mm^2]$ and in the Mouldfriction prototype is 7×31.25 $[mm^2]$. There is a large difference (sixteen times) between the two contacting surfaces as shown in Figure 5.30.

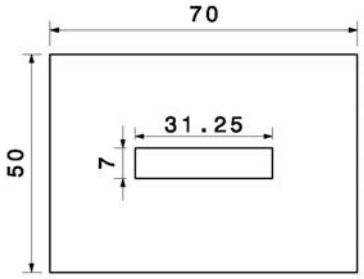

Figure 5.30: Contacting areas ratio (dimensions in millimetres)

To compare the two systems, in terms of friction force, the metal probes must be made of the same material and with the same surface finishing. Only if the surface roughness (and the machining method) were the same it was possible to

create a relationship between this two contacting areas, but this was not the case in the previous results.

To calculate the coefficient of friction based on the Da Vinci equation (4.2), it is necessary to know the two forces that are used in the equation.

The value of the normal force (F_{normal}) is based on the contact pressure and the friction force ($F_{friction}$) the maximum value of the force evolution during sliding of the two surfaces, and corresponds to the static friction force.

It is necessary to determine the value of the coefficient of static friction in the particular contacting tribological system. In this system the measurement of contacting conditions such as: temperature, surface condition (roughness), contacting area, contact pressure (normal force), leads to the experimental determination of the friction force.

This is the method used to determine this coefficient and accepted by all. But one of these variables (area) is difficult to get with precision. The main reason is that is not possible to know the effective contacting area. The contacting area used was considered to be the apparent contacting area, which is the geometrical plane of the surface. In fact the contacting area in this tribological system is bigger than the apparent contact area used for the determination of the normal force. The explanation of this is the assumed total replication of the mould in the moulding surface. The effect of replication of the roughness surface during the injection of the part ensures that the effective contacting area is bigger than the apparent one. The definition of the contacting conditions in the moment of the demoulding process is very important for the precise determination of the coefficient of friction. This parameter is influenced by temperature, roughness, contact pressure, the materials in contact and the contacting area (equation (5.1)).

$$\mu(T, R_a, p, Materials, Area) = \frac{F_{friction}}{F_{normal}} \tag{5.1}$$

The calculation of the coefficient of friction based on the equation (5.1) was made. The results for PC are shown in the Figure 5.31, Figure 5.32 and Figure 5.33. In the calculations the value used for the contacting area was the apparent contact area.

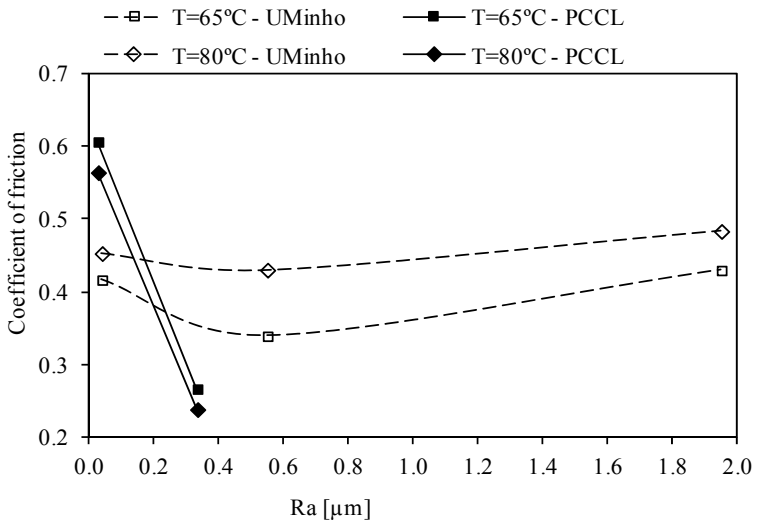

Figure 5.31: Coefficient of friction for PC at 4.3 MPa with roughness variation

For PC it was possible to perform a set of similar tests in the two test systems but with the limitation of only two roughness values in the tests made with the PCCL system. For the comparison of results between the two methods the values of the coefficient of friction are slightly different but show the same trend with the change of roughness. The coefficient of friction results for the same conditions of temperature and contact pressure exhibit an opposite variation. In the PCCL system with the increase of the test temperature the coefficient of friction decreases whereas in the case of Mouldfriction system the evolution is the opposite.

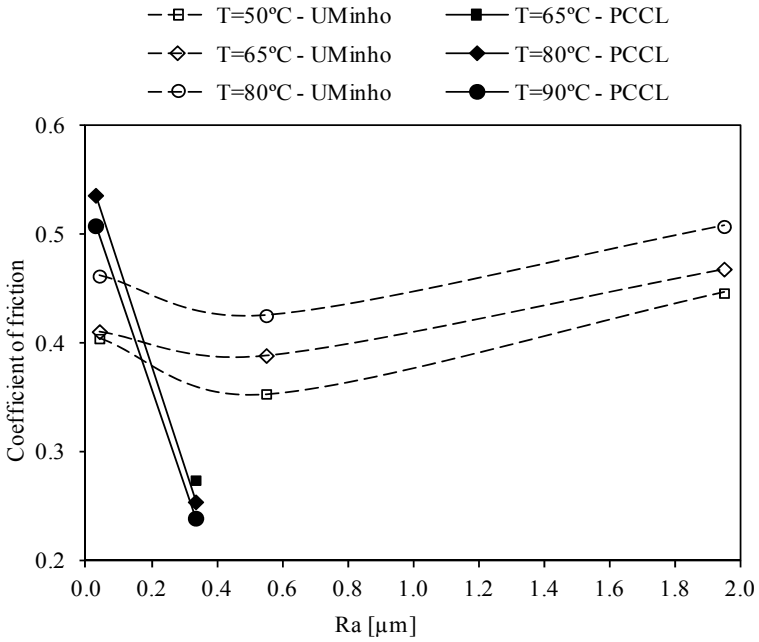

Figure 5.32: Coefficient of friction for PC at 4.9 MPa with roughness variation

The way and time of the contact pressure application is somewhat different. In the case of Mouldfriction system the contact pressure is kept constant during the entire process. In the case of the PCCL system the contact pressure is performed after cooling to the test temperature and the objective is to compensate the shrinkage of the polymer during the solidification process.

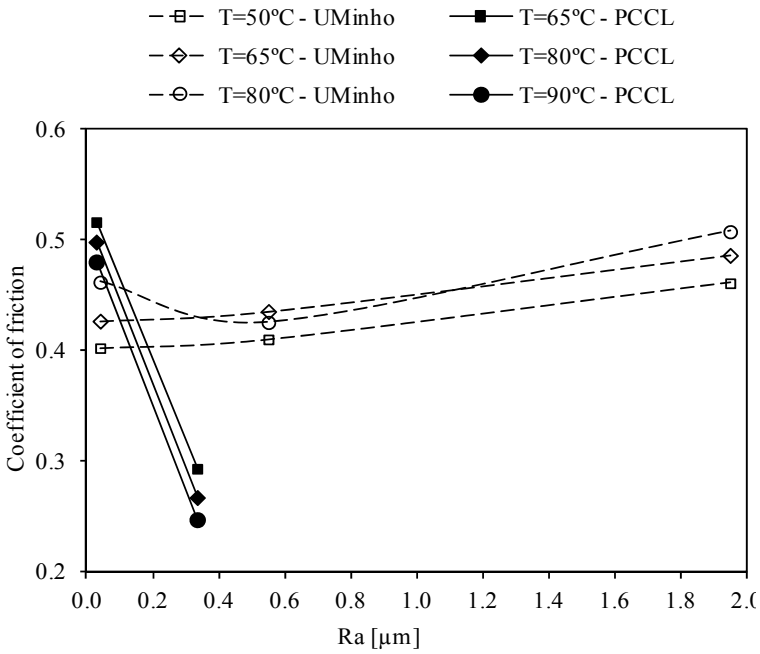

Figure 5.33: Coefficient of friction for PC at 5.6 MPa with roughness variation

Other tests were carried out in the same roughness range with the PCCL instrumented mould. The same behaviour for PC was reported by Berger *et al.* (Berger, Friesenbichler *et al.* 2008).

5.4 Analysis of the friction process

In the injection moulding the friction developed in the demoulding is a complex process. The friction that occurs in this situation is very peculiar. First of all the way the surface is formed. The polymer surface (moulding) is generated against the metal part (mould). The objective is obtaining a replica of the mould part onto the moulding part. The polymer is injected into the impression in molten state. The moulding part is obtained by replication of the impression in the mould, both at the macro scale for the overall geometry and at the microscale for the roughness. At this microscale vision it is possible to observe the replication of the texture of the metallic surface. This replication appears to be caused by the shrinkage of the moulding onto the mould part.

With the solidification occurring against the surface of the mould part and the shrinkage the roughness and other details of the mould surface are pasted to the moulding part. The third and last step is getting off the moulding part from the mould, the demoulding operation.

After the injection stage, in which the polymer goes through a complex thermomechamical process, the part must be removed from the mould. The replication and shrinkage of the part causes an interlocking between the moulding part and the mould core. When the moulding part is pushed out in the demoulding operation the moulding is deformed and ploughed by the harder surface of the metal core. The replicated moulding must perform the functions desired by the end user and the tool must produce these parts repeatedly according to the quantity and quality required. The design of the part and the mould has a significant impact on the successful demoulding stage.

Experimental observations of the polymeric surface during the friction tests made on the Mouldfriction prototype were carried out by light microscopy. Pictures were made to reveal the replication of the steel probe on the polymeric part (Figure 5.34). The observation of this picture ensures that there is a homogeneous distribution of the roughness. This replication of the metallic surface on the polymeric part was already confirmed by Ferreira *et al.* (Ferreira, Costa *et al.* 2004). In Figure 5.35 it is shown the surface aspect of the moulding surface after the friction test. Comparing Figure 5.34 and Figure 5.35 it is not evident that the plastic deformation plays an important role in the development of the friction force during the friction test.

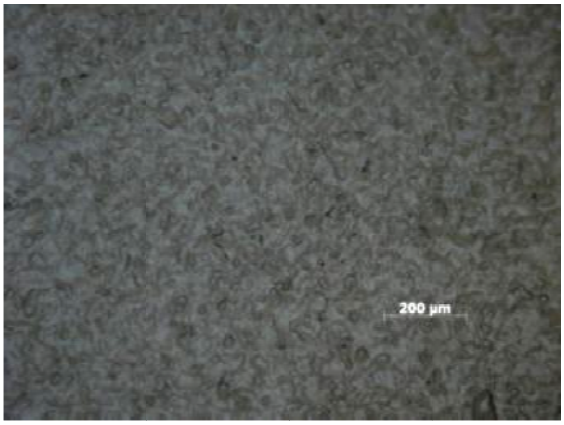

Figure 5.34: Polymeric part surface after replication of the steel probe with Ra=0.55 µm

After the friction tests only the plastic deformation is visualized. Scratches in the surface produced by the asperities are not as evident as expected. The reason for this erase of the experimental evidence was the displacement by 4 mm of the metallic probe over the polymeric surface during the friction test. During this relative displacement other asperities slide over the scratches done by the previous asperities. The last asperity erases the experimental evidence of starting process of development of friction.

Figure 5.35: Polymeric part surface after friction test with 4 mm displacement

As it was not been possible to prove the scratching in the surface it has been taken another approach to do this experimental validation. New tests were

performed. The first one was done according to the friction test proceeding, but the test was stopped when the friction force decreased 10 % of the maximum value of friction force measured. This was to considerer the beginning of the sliding friction process. The demoulding, in fact, occurs when this maximum value is achieved. After this the moulding gets released from the mould part. The observation of polymeric surface of this test can be made in Figure 5.36.

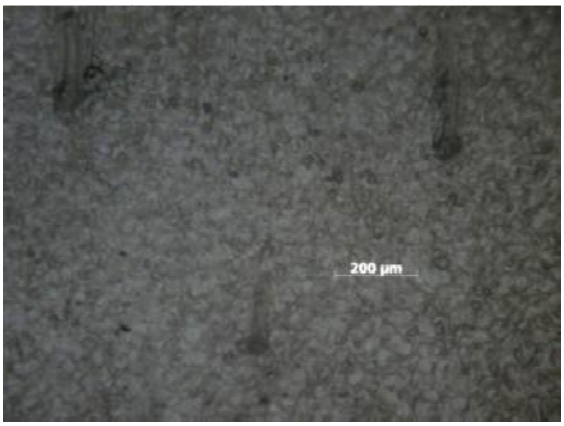

Figure 5.36: Moulding surface before the sliding friction process

In this Figure 5.36 is possible to observe the starting process of friction. To understand what happens during the development of friction a displacement length in the friction test was imposed. The marks (scratches) started to appear in the beginning of the sliding process, and grew with the friction process development (Figure 5.37).

Figure 5.37: Moulding surface after friction test with 0.5 mm displacement

In this new approach the evidence of scratching was observed and this was the main reason for using the roughness to do the parameterization of the theoretical surface in contact. Some researchers demonstrated that for low values of roughness there is an increase in the friction force, this being due to the higher relative contribution of adhesion to the friction force (Sasaki, Koga *et al.* 2000; Pouzada, Ferreira *et al.* 2006). This adhesion component becomes more relevant to the friction force with decreasing surface roughness. It is not possible to predict the contribution of the mechanism of adhesion to the friction force based only on the mechanical model presented that is based on the mould surface roughness and the mechanical properties of the materials.

The microscopic mechanisms involved in friction are the mechanical interactions of surface asperities, the ploughing of the harder surface on the softer surface and the deformation and/or fracture of surface layers. So, it is possible to identify the mechanisms that are responsible for this particular frictional process. Based on this experimental evidence the model has been developed (Chapter 3). It is now explained how the model was used.

5.5 Application of the prediction model to PP

5.5.1 Input data

In the FEM simulations with the DD3IMP code, the geometry of the elementary asperities was defined based on the measured roughness variables, described in Section 3.5 and presented in Table 5.14. The mechanical properties and the coefficient of friction determined experimentally were used as input. Some of the experimental data in Figure 5.2 are tabulated in Table 5.15.

Table 5.14: Conditions used for the numerical simulation

Surface roughness [μm]		Contact Pressure [MPa]	Temperature [ºC]
S	Ra		
283.6	0.04		
79.6	0.05	4.3	50
61.4	0.55	4.9	65
71.4	1.95	5.6	80

The slave deformable body was discretized with a high-density mesh (Figure 4.12), which considers plane strain conditions. This strategy was adopted to allow a comparison with the analytical model already introduced, although it is known that a real micro-geometry is always a two-dimensional surface (Wriggers 2006).

Table 5.15: Experimental data used in the simulation

Temperature [ºC]	Young modulus [GPa]	Strength in compression [MPa]
23	1.129	44.3
50	0.538	30.1
65	0.420	22.6
80	0.275	16.0

The base of the slave body considering the polymer part (moulding) was fixed and the mould part (roughness asperity) was considered rigid because of the high difference in the mechanical properties of the two parts (mould and moulding).

As it was difficult to do the construction in the numerical model of the two contacting surfaces according the roughness geometry, the simulation was divided in two distinct steps. The first was the indentation stage; in this phase the asperity was pushed against the moulding part by a distance equivalent to the roughness considered. The second phase was the sliding through the moulding surface; in this stage the vertical displacement during sliding was not allowed.

5.5.2 Numerical simulation of ploughing and deformation

In Figure 5.38 it can be observed the evolution of the indentation force for the two highest values of roughness, *Ra*. The maximum force corresponds to a displacement equal to four times the *Ra* value.

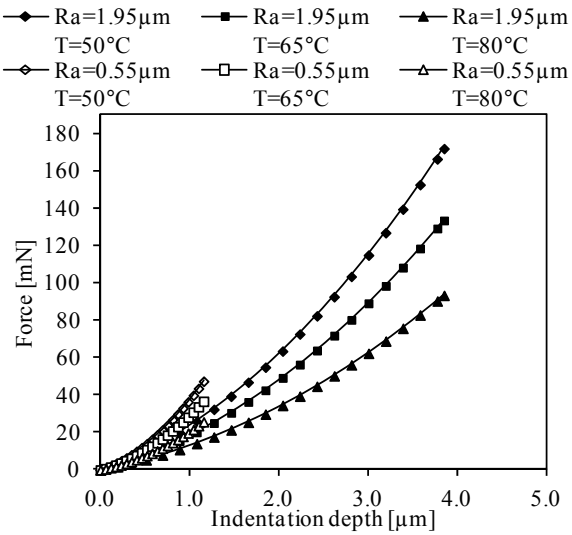

Figure 5.38: Variation of the indentation force with test temperature

At the end of the indentation stage and only for the surface with the highest roughness, an irreversible deformation of the polymer was observed (Figure 5.39 a)). For the lower values of roughness the polymer kept in the elastic regime at the end of the indentation process.

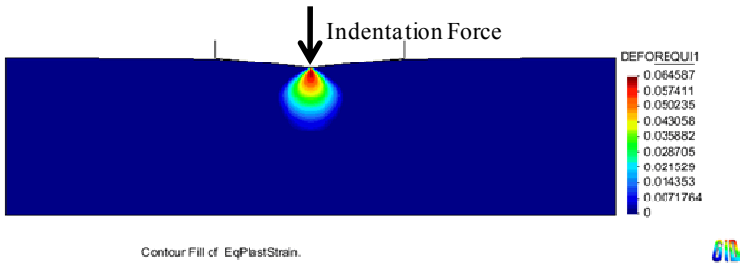

a) Indentation stage

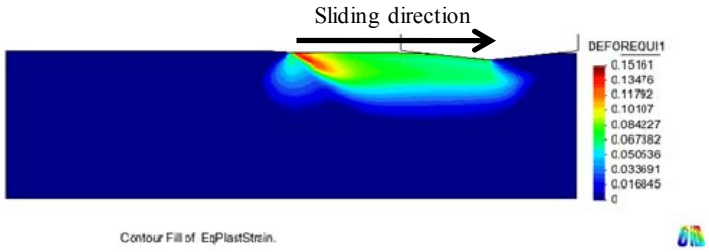

b) Displacement stage

Figure 5.39: Equivalent plastic strain for 65 ºC and Ra=1.95 µm

The frictional force increases at greater roughness values because a bigger plastic deformation is required to initiate the relative displacement of the surfaces.

The Figure 5.40 shows the simulation of the friction force evolution during the displacement stage, as predicted by the numerical simulation. As it would be expected the increase in roughness results in an increase of the friction force.

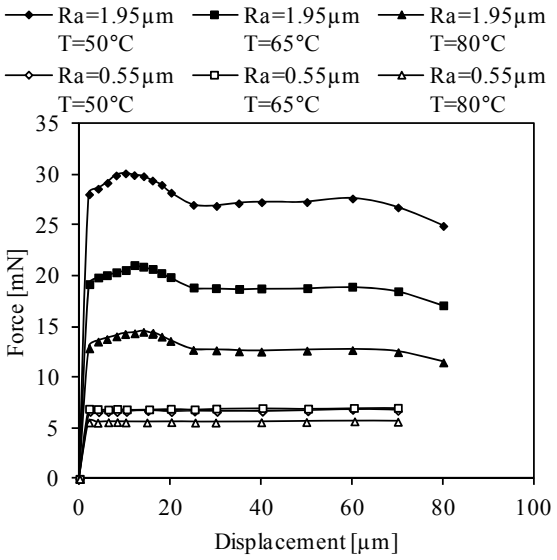

Figure 5.40: Evolution of friction force during the displacement stage

5.5.3 Analytical prediction of ploughing

The analytical model was used to determine the value of the friction force that corresponds to the mechanism of ploughing, which results from the mechanical interaction of the metallic surface on the polymeric part.

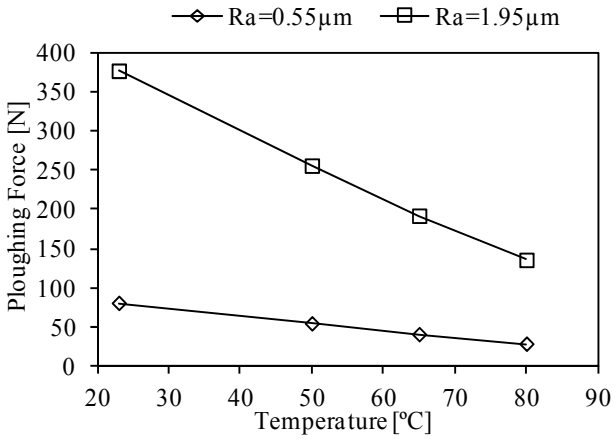

Figure 5.41: Analytical ploughing force model evolution with temperature variation

Figure 5.41 shows the evolution of the ploughing force (equation (3.9)) for the two surfaces with the highest values of roughness. Because the analytical model for the ploughing force is based on roughness parameters and mechanical properties the behaviour of this mechanism has a linear variation with temperature, according the mechanical properties evaluated in the characterization tests for the PP. For the two lower values of roughness the ploughing force value is negligible as observed in the numerical model.

5.5.4 The adhesion component

For the injection moulding process, there is currently no scientifically-validated approach that can quantitatively measure adhesion force accurately (Chen and Hwang 2013). Unfortunately, the adhesion force in the injection mould process is responsible for the damage of moulding parts or even moulds mechanisms such like the ejection pins. For this in industrial practice a number of issues were identified has responsible for the reduction of quality of the surfaces of moulding products. Serious adhesion makes it difficult to release the sample from the mould cavity, and results in deformation or cracking on the surface of finished parts after demoulding. The usually approaches to reducing adhesion force are: adding mould release agents into the polymer (may cause unstable product quality or poor mechanical properties), application of release agent on the cavity surface (only effective for few shots, and may appear flow marks on the surface moulding part), improve the ejection system (when the moulding geometry part is complex tool design may become complicated) and mould surface handling (surface polish or surface treatments).

As other authors have mentioned (Chen and Hwang 2013) no model is still available for the adhesion component of friction; thus, by now only some conclusions or tendencies will be mentioned. For the materials tested (PP, PC and a PC/ABS blend) around $R_a = 0.5\ \mu m$ there exists a minimum for global friction. The increasing role of the adhesion contribution for average roughness

lower than 0.5 μm can be evidenced (for the case of PP) by subtracting the ploughing and deformation contribution from the experimental data, as shown in Figure 5.42. In this figure the estimated contribution of each term is also depicted. It is possible to confirm the importance of the adhesion component especially at low values of roughness. When the average roughness increases the deformation and ploughing components are preponderant and the adhesion contribution becomes residual.

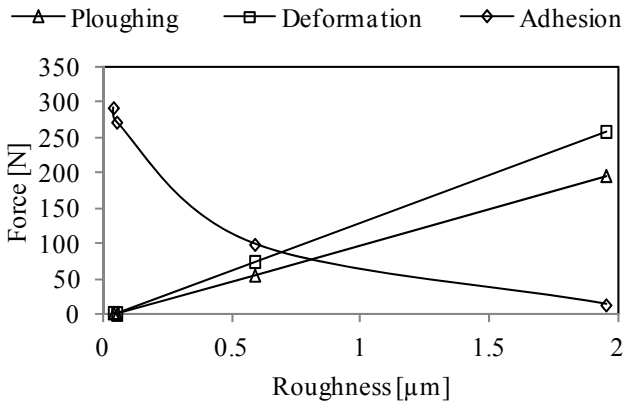

Figure 5.42: Friction force components contribution (P=4.9 MPa and T=65 °C) for the PP

5.6 Can friction in demoulding be predicted?

Typically 80 % of the moulds market is in applications for the automotive industries. Therefore a polymeric part for automotive applications has a wide roughness range. These variety of surface roughness goes from $R_a = 0.01\ \mu m$ to $R_a = 0.02\ \mu m$ in the case of mirror optical polish finish for lenses, from $R_a = 0.03\ \mu m$ to $R_a = 0.05\ \mu m$ in case of mirror polish finish for transparent parts, around $R_a \approx 0.5\ \mu m$ to buttons for air-conditioning or buttons for automotive radio and $R_a \approx 1.9\ \mu m$ for speakers radio parts.

Based on the experimental and the previous numerical results, equations (3.9) and (3.11) were applied to estimate the ejection force for PP Domolen 1100N.

The experimental data for the cases of $R_a = 0.5\ \mu m$ in Figure 5.43 and Figure 5.44 were compared with results of the analytical model and of the numerical simulation. For the lowest value of roughness the friction model and the simulation could not describe the actual tribological process. In fact, when the mould surfaces are very smooth $(R_a = 0.05\ \mu m)$ the polymer deforms only elastically as it was observed in the numerical simulations.

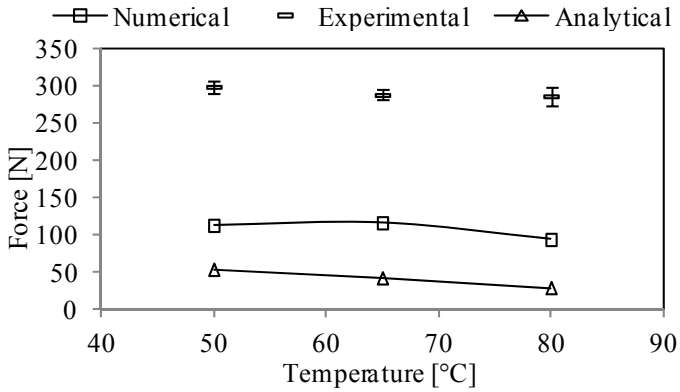

Figure 5.43: Analytical and numerical modelling versus experimental data for $R_a = 0.55\ \mu m$

The adhesion component was not considered in any of the two theoretical models, and this may help to justify the large difference between experimental data and the models.

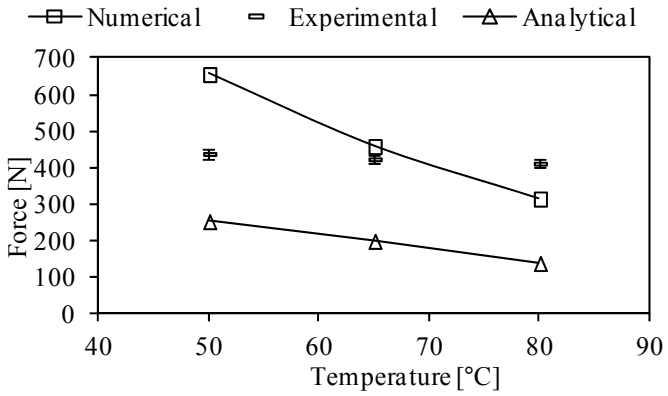

Figure 5.44: Analytical and numerical modelling versus experimental data for $R_a = 1.95\ \mu m$

The model was used to perform the numerical simulation of the contribution of components of deformation and ploughing to the frictional force. In Table 5.16 is exposed the error value associated to each simulation performed. It is noted that only for one case which has a pair of values T=65 °C and Ra=1.95 μm the error is acceptable. Therefore it is verified that only in this case the relation of temperature and pressure the value of the frictional force is somewhat dependent component of the adhesion process.

Table 5.16: Percentage error in the model approach

Ra [μm]	T=50 °C	T=65 °C	T=80 °C
0.55	62.1%	59.5%	67.0%
1.95	33.1%	7.6%	23.5%

The coefficient of friction worked out from the experimental data shows an increase in the lower region of the surface roughness (Figure 5.45). This increase of the coefficient of friction is due to increased adhesion which results from the more intimate contact (higher pressure) and non-permanent deformation when the roughness amplitude is small.

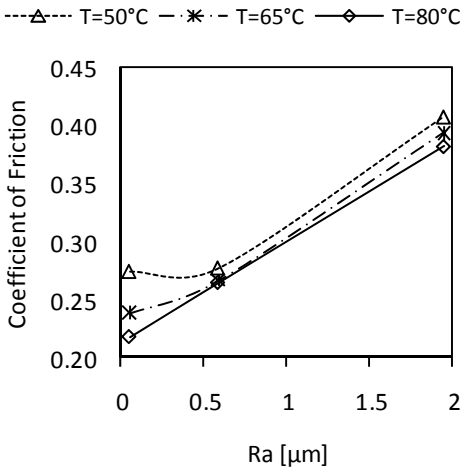

Figure 5.45: Experimental coefficient of friction as a function of roughness and temperature. Contact pressure of 4.9 MPa for PP

A full method to predict the ejection force in injection moulding should include the three terms referred to in Equation (3.4). In this study it was possible to establish an analytical model for the ploughing term and account for ploughing and deformation by numerical simulation. When the surface roughness *Ra* is much higher than 1 µm this approach allowed estimating the contribution of the ploughing and deformation terms of the ejection force with acceptable precision. In the case of smoother surfaces large deviations were observed which may be attributed to the non-consideration of the contribution of adhesion which may be more relevant under such conditions.

CONCLUSIONS

This study aimed at identifying the factors that influence the ejection in injection mouldings, and contributing to the establishment of a model for the interpretation of the mechanisms involved in the friction issues associated to the demoulding of plastics parts. The former include the mechanical properties of the contacting materials and how the friction force depends on temperature, contact pressure and roughness, and the later a multi-disciplinary way of interpreting the mechanisms that characterise the friction process.

The main conclusions of the work are:

Analysis of the factors that influence the ejection force in injection moulding

i. In injection moulding the ejection of the moulded part involves a tribological process where on top of the usual sliding process there is the contribution of the replication of the plastics part on the moulding surface. In this specific tribological situation there is physical interlocking of the two surfaces especially when the roughness is high;

ii. Experimental tests highlighted the influence of roughness, temperature and contact pressure on the friction force upon demoulding of three commercial polymeric materials – polypropylene (PP), polycarbonate (PC) and a PC/ABS blend - against a metallic surface;

iii. It was shown the relevance of knowing the value of the roughness of the moulding surface as this value has the leading influence on the demoulding process of plastics parts;

iv. The knowledge of the mechanical properties of the polymers, namely the Young's modulus and the ultimate compression stress, especially in the cases of the semi-crystalline materials (as PP) and the polymer blends (as PC/ABS), is necessary due to their strong dependence on the temperature in the demoulding temperature range.

Analysis of the process of ejection of plastic parts in injection moulding

v. The governing mechanisms involved in this specific frictional process are the mechanical interactions of surface asperities, determining the ploughing of the surface and the deformation of the asperities;

vi. The ploughing action in the case of PP was identified and it was possible to interpret its role in terms of an analytical model;

vii. In the cases of PP and PC the temperature is the factor which influences less the friction resistance;

viii. In the case of the PC/ABS blend the effect of the temperature is more important than the effect of the contact pressure in the friction force.

Methods for characterising the friction environment in the ejection of injection mouldings

ix. The development of the friction force and the resulting coefficient of friction were evaluated by two different test methods, the Mouldfriction prototype (Portugal) and the PCCL instrumented mould (Austria);

x. In the testing programmes with these two methods the behaviour of the same PC and PC/ABS were compared in terms of similar temperatures and contact pressure conditions;

xi. The metal probes used in the two test methods had different surface topography, the PCCL instrumented mould probe roughness range being in the lower spectrum of practical applications;

xii. For the two systems and in the low roughness range the friction force and the coefficient of friction tendencies were similar.

Contributions to the development of a model that interprets the ejection of injection mouldings

xiii. Given the relevance of the replication in the injection moulding process and subsequent ejection from the mould, a mixed approach model was developed to understand the contribution of each of the mechanisms involved;

xiv. The ploughing and deformation terms can be interpreted by numerical simulation:

xv. The ploughing contribution can be predicted by analytical modelling;

xvi. To this moment the adhesion component can only be inferred from the combination of experimental data and the numerical simulation of the ploughing and deformation contributions.

xvii. The analytical model for the ploughing mechanism developed is dependent on the temperature as is based only on the mechanical properties of the plastics part at the temperature of ejection;

xviii. The ploughing and deformation mechanisms can be jointly interpreted by finite element numerical simulation;

xix. It was possible to verify by the numerical simulation that PP does not deform plastically when in sliding contact against the metallic surfaces with low roughness. Only elastic deformation occurs whatever the contact conditions tested;

xx. The ploughing and deformation terms vary linearly with roughness, and the contribution of deformation is more relevant than ploughing;

xxi. The effect of the adhesion in the friction force is dominant for small roughness. At higher values of the surface roughness the other mechanisms become more important.

Experimental validation of the proposed way to predict the coefficient of static friction

xxii. Experimentally it is difficult to isolate and quantify the exact contributions of each component (ploughing, deformation and adhesion) to the global friction force;

xxiii. The coefficient of friction of PC and PC/ABS shows the same variation trends when temperature, contact pressure and surface roughness vary;

xxiv. In the PCCL instrumented mould the variation of the coefficient of friction was more pronounced than in the Mouldfriction prototype.

RECCOMENDATIONS FOR FURTHER WORK

The mechanisms of friction in the demoulding process of plastics materials was studied, and needs and limitations for the development of models that describe this friction process were pointed out in this study. Based on the results and experience gained throughout this work, the following aspects are suggested for future work:

- Study of the effects of strain rate and shear strength on the friction force;
- Development of an equipment and/or test method, integrated or not in the Mouldfriction prototype, for the assessment of the adhesion component;
- Improvement of the model developed by including more variables to make it more sensitive to the roughness range in industrial environments;
- Extension of the study to other materials, both in mouldings and moulding blocks, particularly the non-metallic materials used in hybrid moulds.

REFERENCES

Amirsadeghi, A., J. J. Lee*, et al.* (2011). Polymerizarion shrinkage and adhesion in UV-nano print litography. IMEC2011 - International Mechanical Engineering Congress & Exposition. ASME. Denver, Colorado, USA.

An, C.-C. and R.-H. Chen (2005). An Experimental Study of Demolding Properties on Stereolithography Tooling. Join ASME/ASCE/SES Conference on Mechanics and Materials. Louisiana, USA.

Antunes, F. and D. Rodrigues (2008). "Numerical simulation of plasticity induced crack closure: Identification and discussion of parameters." Engineering Fracture Mechanics **75**(10): 3101-3120.

Antunes, J., J. Fernandes*, et al.* (2008). "Reverse analysis in depth-sensing indentation for evaluation of the Young's modulus of thin films." Philosophical Magazine **88**(3): 313-325.

Apichartpattanasiri, S., J. N. Hay*, et al.* (2001). "A study of the tribological behaviour of polyamide 66 with varying injection-moulding parameters." Wear **251**(1-12): 1557-1566.

Araújo, B. J., A. J. Pontes*, et al.* (2003). "Development of efficient ejection systems for injection moulds / Desenvolvimento de sistemas de extracção eficientes para moldes de injecção." O Molde **56**.

Araújo, B. J. and A. S. Pouzada (2002). "Design of ejection systems for injection moulds." O Molde **54** 36-41.

Attia, U. M. and J. R. Alcock (2011). "A review of micro-powder injection moulding as a microfabrication technique." Journal of Micromechanics and Microengineering **21**(4): 043001.

Bataineh, O. M. and B. E. Klamecki (2005). "Prediction of Local Part-Mold and Ejection Force in Injection Molding." Journal of Manufacturing Science and Engineering **127**(3): 598-604.

Bayer, R. G. (2002). Wear Analysis for Engineers. New York, HNB Pub.

Becker, H. and C. Gärtner (2008). "Polymer microfabrication technologies for microfluidic systems." Analytical and Bioanalytical Chemistry **390**(1): 89-111.

Benabdallah, H. S. (2007). "Static friction coefficient of some plastics against steel and aluminum under different contact conditions." Tribol. Int. **40**(1): 64-73.

Berger, G. R., W. Friesenbichler*, et al.* (2008). A new practical measurement apparatus for demolding forces and coefficients of friction in injection molding. PPS-24 - Polymer Processing Society 26th Annual Meeting. Salerno, Italy.

Bhagavatula, N., D. Michalski*, et al.* (2004). "Modelling and verification of ejection forces in thermoplastic injection moulding." Model. Simul. Mater. Sci. Eng. **12**: S239-S254.

Bhushan, B. (2002). Introduction to Tribology, John Wiley & Sons, Inc.

Blau, P. J. (1992). ASM Handbook, Volume 18 - Friction, Lubrication, and Wear Technology, ASM International.

Blau, P. J. (1996). Friction Science and Technology, Marcel Dekker, Inc.

Blau, P. J. (2001). "The significance and use of the friction coefficient." Tribol. Int. **34**(9): 585-591.

Bowden, F. P. (1952). "Introduction to the Discussion: The Mechanism of Friction." Proceedings of the Royal Society of London. Series A, Mathematical and Physical Sciences **212**(1111): 440-449.

Bowden, F. P. and L. Leben (1939). "The Nature of Sliding and the Analysis of Friction." Proceedings of the Royal Society of London. Series A, Mathematical and Physical Sciences **169**(938): 371-391.

Bowden, F. P. and D. Tabor (1986). The friction and lubrication of solids. Oxford, Clarendon Press.

Burke, C., R. Malloy*, et al.* (1991). "An experimental-study of the ejection forces encountered during injection-molding." In Search of Excellence /: 1781-1787.

Cedorge, T. and J. Colton (2000). "Draft angle and surface roughness effects on stereolithography molds." Polymer Engineering & Science **40**(7): 1581-1588.

Charmeau, J.-Y., M. Chailly*, et al.* (2008). "Influence of mold surface coatings in injection molding. Application to the ejection stage." International Journal of Material Forming **1**(1 Supplement): 699-702.

Chen, J.-Y. and S.-J. Hwang (2013). "Design and fabrication of an adhesion force tester for the injection moulding process." Polymer Testing **32**(1): 22-31.

Colton, J. S., J. Crawford*, et al.* (2001). "Failure of rapid prototype molds during injection molding." Cirp Annals-Manufacturing Technology **50**(1): 129-132.

Cotell, C. M., J. A. Sprague*, et al.* (1994). ASM Handbook, Volume 05 - Surface Engineering, ASM International. **5**.

Crawford, R. J. (1998). Plastics Engineering. Oxford, Elsevier Science.

Cunha, L., M. Andritschky*, et al.* (2002). "Performance of chromium nitride and titanium nitride coatings during plastic injection moulding." Surface and Coatings Technology **153**(2-3): 160-165.

Dearnley, P. A. (1999). "Low friction surfaces for plastic injection moulding dies--an experimental case study." Wear **225-229**(Part 2): 1109-1113.

Delaney, K., D. Kennedy*, et al.* (2010). A Study of Friction Testing Methods Applicable to Demoulding Force Prediction for Micro Replicated Parts. Matrib 2010. Croatia.

Delaney, K. D., G. Bissacco*, et al.* (2010). A Study of Demoulding Force Prediction Applied to Periodic Mould Surface Profiles. Society of Plastic Engineers' ANTEC 2010. Orlando, Florida.

Delaney, K. D., G. Bissacco*, et al.* (2012). "A Structured Review and Classification of Demolding Issues and Proven Solutions." International Polymer Processing **27**(1): 77-90.

Delaney, K. D., D. Kennedy*, et al.* (2011). Development of a friction testing apparatus for demoulding force prediction. International Manufacturing Conference - IMC28. Dublin, Ireland.

Delaney, K. D., D. Kennedy*, et al.* (2011). Investigating polymer-tool steel interfaces to predict the work of adhesion for demoulding force optimisation. MTSM 2011. Split.

Derdouri, A., F. Ilinca*, et al.* (2005). Microinjection Molding of Microstructures - Experimental and Numerical Simulation C8 - Proceedings of the 2005 AIChE Annual Meeting.

Dowson, D. (1998). History of Tribology, Wiley.

Ebnesajjad, S. (2006). Surface Treatment of Materials for Adhesion Bonding. NY, William Andrew Publishing.

Engelmann, P., K. Hayden*, et al.* (2000). "Understanding wear mechanisms: The key to mold life." Technical Papers of Society of Plastics Engineers **46**: 952-956.

Engelmann, P., K. Hayden*, et al.* (2002). "Undercutting mold performance: ejection wear." Technical Papers of Society of Plastics Engineers **48**: 850-854.

Ferreira, E. C., M. F. Costa*, et al.* (2004). "Comparative study, by optical techniques of the interface polymer/steel in replication conditions." Mater. Sci. Forum **455-456**: 467-471.

Ferreira, E. C., C. R. Laranjeira*, et al.* (2003). Influência da temperatura e da rugosidade no coeficiente de atrito, na extracção de peças injectadas em plástico. II Iberian Congress of Tribology, Valencia, Spain.

Ferreira, E. C., N. M. Neves*, et al.* (2001). Friction properties of thermoplastics in injection molding. ANTEC 2001. Dallas/USA.

Ferreira, E. C., N. M. Neves*, et al.* (2002). Analysis of Parameters determining the friction properties of thermoplastics in injection molding. ANTEC 2002. S. o. P. Engineers.

Fleischer, J. and A. M. Dieckmann (2006). "Automation of the powder injection molding process." Microsystem Technologies-Micro-and Nanosystems-Information Storage and Processing Systems **12**(7): 702-706.

Gadelmawla, E. S., M. M. Koura*, et al.* (2002). "Roughness parameters." Journal of Materials Processing Technology **123**(1): 133-145.

Gao, J., W. D. Luedtke*, et al.* (2004). "Frictional Forces and Amontons' Law: From the Molecular to the Macroscopic Scale." J. Phys. Chem. B **108**(11): 3410-3425.

Giboz, J., T. Copponnex, *et al.* (2007). "Microinjection molding of thermoplastic polymers: a review." Journal of Micromechanics and Microengineering **17**(6): R96.

Gonçalves, M. W., G. V. Salmoria, *et al.* (2007). "Study of tribological properties of moulds obtained by stereolithography." Virtual Phys. Prototyp. **2**(1): 29 - 36.

Griffiths, C., S. Dimov, *et al.* (2010). "Investigation of surface treatment effects in micro-injection-moulding." The International Journal of Advanced Manufacturing Technology **47**(1): 99-110.

Griffiths, C. A., S. S. Dimov, *et al.* (2008). Micro-Injection moulding: surface treatment effects on part demoulding. Multi-Material Micro Manufacture. S. Dimov and W. Menz. Cardiff, Whittles Publishing Ltd.

Griffiths, C. A., S. S. Dimov, *et al.* (2007). "The effects of tool surface quality in micro-injection moulding." Journal of Materials Processing Technology **189**(1-3): 418-427.

Guo, Y., G. Liu, *et al.* (2007). "Study of the demolding process-implications for thermal stress, adhesion and friction control." Journal of Micromechanics and Microengineering **17**(1): 9.

Guo, Y., G. Liu, *et al.* (2007). "Analysis of the demolding forces during hot embossing." Microsystem Technologies-Micro-and Nanosystems-Information Storage and Processing Systems **13**(5): 411-415.

Haragas, S., L. Tudose, *et al.* (2008). "On the demolding force calculation in the case of plastics thin-wall injected parts." Materiale Plastice **45**(1).

Heckele, M. and W. K. Schomburg (2004). "Review on micro molding of thermoplastic polymers." Journal of Micromechanics and Microengineering **14**(3): R1-R14.

Holmberg, K., A. Matthews, *et al.* (1998). "Coatings tribology--contact mechanisms and surface design." Tribology International **31**(1-3): 107-120.

Hopkinson, N. and P. Dickens (2000). "Predicting stereolithography injection mould tool behaviour using models to predict ejection force and tool strength." International Journal of Production Research **38**(16): 3747-3757.

Hu, W. and S. Masood (2002). "An Intelligent Cavity Layout Design System for Injection Moulds." International Journal of CAD/CAM **2**(1): 69-75.

Hughes, T. J. R. (1980). "Generalization of selective integration procedures to anisotropic and nonlinear media." Int. J. Numer. Methods Eng. **15**(9): 1413-1418.

James, D. I. and W. G. Newell (1980). "A new concept in friction testing." Polymer Testing **1**(1): 9-25.

Jansen, K. M. B., R. Pantani, *et al.* (1998). "As-molded shrinkage measurements on polystyrene injection molded products." Polymer Engineering & Science **38**(2): 254-264.

Jansen, K. M. B. and G. Titomanlio (1996). "Effect of pressure history on shrinkage and residual stresses—injection molding with constrained shrinkage." Polymer Engineering & Science **36**(15): 2029-2040.

Jeon, J. and A. Bramley (2007). "A friction model for microforming." The International Journal of Advanced Manufacturing Technology **33**(1): 125-129.

Kim, D. E. and N. P. Suh (1991). "On microscopic mechanisms of friction and wear." Wear **149**(1-2): 199-208.

Kim, D. E. and N. P. Suh (1993). "Frictional behavior of extremely smooth and hard solids." Wear **162-164, Part B**: 873-879.

Kinsella, M. E. (2004). Ejection force and static friction coefficients for rapid tooled injection mold inserts. Manufacturing Directorate in the Air Force Research Laboratory, The Ohio State University.

Kinsella, M. E., B. Lilly*, et al.* (2005). "Experimental determination of friction coefficients between thermoplastics and rapid tooled injection mold materials." Rapid Prototyp. J. **11**(3): 167-173.

Ko, S.-L. and D. A. Dornfeld (1991). "A Study on Burr Formation Mechanism." Journal of Engineering Materials and Technology **113**(1): 75-87.

Kurt, M., O. Saban Kamber*, et al.* (2009). "Experimental investigation of plastic injection molding: Assessment of the effects of cavity pressure and mold temperature on the quality of the final products." Materials & Design **30**(8): 3217-3224.

Kwak, S., T. Kim*, et al.* (2003). "Layout and sizing of ejector pins for injection mould desian using the wavelet transform." Proceedings of the Institution of Mechanical Engineers, Part B: Journal of Engineering Manufacture **217**(4): 463-473.

Kwon, K., A. I. Isayev*, et al.* (2006). "Theoretical and experimental studies of anisotropic shrinkage in injection moldings of semicrystalline polymers." Polymer Engineering & Science **46**(6): 712-728.

Kyuichiro, T. (1995). "Some interesting problems that remain unsolved in my work on polymer tribology." Tribology International **28**(1): 19-22.

Li, K., W. Carden*, et al.* (2002). "Simulation of springback." International Journal of Mechanical Sciences **44**(1): 103-122.

Magny, C. (2002). "Friction laws dedicated to the numerical simulation of deep drawing." Revue de Métallurgie **99**(02): 145-156.

Majewski, C. and N. Hopkinson (2003). "Effect of tool finishing on ejection forces for injection moulded parts made using direct metal laser sintered tools." International Journal of Production Research **41**(3): 581 - 592.

Majewski, C. and N. Hopkinson (2004). "Reducing ejection forces for parts moulded into direct metal laser sintered tools." The International Journal of Advanced Manufacturing Technology **24**(1): 16-23.

Martinho, P. G., L. Cardon*, et al.* (2008). A study of the ejection forces on moulding inserts obtained by RPT techniques, Centimfe - Cefamol.

Menezes, L. F. and C. Teodosiu (2000). "Three-dimensional numerical simulation of the deep-drawing process using solid finite elements." Journal of Materials Processing Technology **97**(1-3): 100-106.

Menges, G., W. Michaeli*, et al.* (2001). How to Make Injection Molds (3rd Edition), Hanser Publishers.

Michaeli, W. and R. Gartner (2006). New Demolding Concepts for the Injection Molding of Microstructures. Journal of Polymer Engineering. **26:** 161.

Michaeli, W., A. Rogalla*, et al.* (2000). "Processing technologies for the injection moulding of hybrid microstructures." Macromolecular Materials and Engineering **279**(1): 42-45.

Myshkin, N. and M. Petrokovets (2004). Mechanical behavior of plastics: surface properties and tribology. Mechanical tribology, materials, characterization, and applications. G. E. L. Totten, Hong. New York, Marcel Dekker**:** 57–94.

Myshkin, N. K., M. I. Petrokovets*, et al.* (2005). "Tribology of polymers: Adhesion, friction, wear, and mass-transfer." Tribology International **38**(11-12): 910-921.

Neto, V. F., R. Vaz*, et al.* (2009). "CVD diamond-coated steel inserts for thermoplastic mould tools - Characterization and preliminary performance evaluation." Journal of Materials Processing Technology **209**(2): 1085-1091.

Oliveira, M., J. Alves*, et al.* (2008). "Algorithms and strategies for treatment of large deformation frictional contact in the numerical simulation of deep drawing process." Archives of Computational Methods in Engineering **15**(2): 113-162.

Oliveira, M., J. Alves*, et al.* (2011). Finite Element Analysis of the Amontons-Coulomb's Model using Local and Global Friction Tests. AIP Conference Proceedings.

Oliveira, M. C., J. L. Alves*, et al.* (2003). "Improvement of a frictional contact algorithm for strongly curved contact problems." Int. J. Numer. Methods Eng. **58**(14): 2083-2101.

Padmanabhan, R., M. Oliveira*, et al.* (2007). Study on the Influence of the Refinement of a 3-D Finite Element Mesh in Springback Evaluation of Plane-Strain Channel Sections. AIP Conference Proceedings.

Padmanabhan, R., M. C. Oliveira*, et al.* (2008). "Numerical simulation and analysis on the deep drawing of LPG bottles." Journal of Materials Processing Technology **200**(1-3): 416-423.

Pereira, F., M. Oliveira*, et al.* (2010). "Finite Element Analysis on the Influence of Material Mechanical Properties in Local Contact Conditions." International Journal of Material Forming **3**: 139-142.

Petrie, E. M. (2000). Handbook of Adhesives and Sealants, McGraw-Hill.

Pham, G. T. and J. S. Colton (2002). "Ejection force modeling for stereolithography injection molding tools." Polymer Engineering & Science **42**(4): 681-693.

Pontes, A. J., A. M. Brito*, et al.* (2004). "Effect of melt viscosity on the ejection force in injection moulds." Advanced Materials Forum Ii **455-456**: 755-758.

Pontes, A. J., E. C. Ferreira*, et al.* (2004). Tribological aspects during ejection in injection moulds. RPD 2004 Rapid Product Development. Marinha Grande, Portugal.

Pontes, A. J., M. J. Oliveira*, et al.* (2002). Studies on the influence of the holding pressure on the orientation and shrinkage of injection molded parts. ANTEC 2002. San Francisco/USA.

Pontes, A. J., R. Pantani*, et al.* (2001). Prediction of ejection forces in tubular moldings in amorphous polymers. ANTEC 2001. Dallas/USA**:** paper 927.

Pontes, A. J., R. Pantani*, et al.* (2002). On the prediction of ejection forces for tubular moldings. ANTEC 2002. San Francisco/USA**:** paper 534.

Pontes, A. J. and A. S. Pouzada (2004). "Ejection force in tubular injection moldings. Part I: Effect of processing conditions." Polymer Engineering and Science **44** 891-898.

Pontes, A. J., A. S. Pouzada*, et al.* (2005). "Ejection force of tubular injection moldings. Part II: A prediction model." Polym. Eng. Sci. **45**(3): 325-332.

Pontes, A. J., M. P. Queiros*, et al.* (2010). "Experimental assessment of hybrid mould performance." The International Journal of Advanced Manufacturing Technology **50**(5-8): 441-448.

Pouzada, A. S., E. C. Ferreira*, et al.* (2006). "Friction properties of moulding thermoplastics." Polymer Testing **25**(8): 1017-1023.

Ribeiro Jr., A. R., N. Hopkinson*, et al.* (2004). "Thermal effects on stereolithography tools during injection moulding." Rapid Prototyping Journal **10**(3): 176-180.

Sabino-Netto, A. C. (2008). Desenvolvimento e avaliação de compósito de resina epóxi reforçado com fibras de aço na fabricação de blocos moldantes para moldagem por injeção. Engenharia Mecânica. Florianópolis, Universidade Federal de Santa Catarina. **Tese de Doutorado**.

Sabino-Netto, A. C., G. V. Salmoria*, et al.* (2008). "Friction Properties of Steel Fibre Reinforced Epoxy Composites Used in Moulding Blocks of Hybrid Moulds." Mater. Sci. Forum **587-588**: 217-221.

Sander, M. (1991). A Practical Guide to the Assessment of Surface texture, Mahr Feinprüf.

Sasaki, T., N. Koga*, et al.* (2000). "An experimental study on ejection forces of injection molding." Precis. Eng. **24**(3): 270-273.

Schaller, T., M. Heckele*, et al.* (1999). Microfabrication of a mold insert made of hardened steel and first molding results. ASPE 14th Annual Meeting Proceedings, Monterey, California.

Schmidt, L., J. Opfermann, *et al.* (1981). "Influence of processing conditions during injection molding of thermoplastics parts on structure and mechanical properties." Polymer Engineering Reviews **1**(1): 1-17.

SINO. (2011). "Mold surface roughness, Molds finishing." Retrieved 12 november, 2012, from http://www.cnmould.com/blog/mold-surface-roughness-316.html.

Song, Z., B. You, *et al.* (2008). "Study on demolding temperature in thermal imprint lithography via finite element analysis." Microsystem Technologies **14**(9): 1593-1597.

Straffelini, G. (2001). "A simplified approach to the adhesive theory of friction." Wear **249**(1-2): 78-84.

Suh, N. P. (1986). Tribophysics. Englewood Cliffs, NJ, Prentice-Hall.

Suh, N. P., M. Mosleh, *et al.* (1994). "Control of friction." Wear **175**(1-2): 151-158.

Tabor, D. (1981). "Friction - The present State of Our Understanding." J. Lubr. Technol. **103**: 169-179.

Teixeira, J. J. P. (2001). Fundamentos Físicos do Corte dos Metais.

TESA. (2012). "Surface Roughness Testing." Retrieved 12 november, 2012, from http://tesatool.com/pdf_files/catalog_surface.pdf.

Titomanlio, G. and K. M. B. Jansen (1996). "In-Mold Shrinkage and Stress Prediction in Injection Molding." Polym. Eng. Sci. **36**(15): 2041-2049.

van Beek, A. (2006). Advanced engineering design - Lifetime performance and reliability, Delft University of Technology Mechanical Engineering, www.engineering-abc.com.

Van Stappen, M., K. Vandierendonck, *et al.* (2001). "Practice vs. laboratory tests for plastic injection moulding." Surface and Coatings Technology **142-144**: 143-145.

Viana, J. C., N. Billon, *et al.* (2004). "The thermomechanical environment and the mechanical properties of injection moldings." Polym. Eng. Sci. **44**(8): 1522-1533.

Viana, J. C., A. M. Cunha, *et al.* (2001). "The effect of the skin thickness and spherulite size on the mechanical properties of injection mouldings." Journal of Materials Science **36**(18): 4411-4418.

Wang, H., K. K. Kabanemi, *et al.* (2000). "Numerical and experimental studies on the ejection of injection-molded plastic products." Polymer Engineering & Science **40**(3): 826-840.

Wang, Z., K. S. Lee, *et al.* (1996). "Optimum ejector system design for plastic injection moulds." Int. J. Comp. Appl. Technol. **9**(4): 211-218.

Warren, T. L. and D. Krajcinovic (1996). "A fractal model for the static coefficient of friction at the fiber-matrix interface." Composites Part B: Engineering **27**(5): 421-430.

Westphal, M. G., A. S. Pouzada, *et al.* (2006). "Performance and friction properties of injection hybrid moulds with stereolitography moulding zones." Advanced Materials Forum III **514-516**: 1673-1677.

Worgull, M., M. Heckele, *et al.* (2005). "Large-scale hot embossing." Microsystem Technologies **12**(1): 110-115.

Worgull, M., J. Hétu, *et al.* (2008). "Hot embossing of microstructures: characterization of friction during demolding." Microsystem Technologies **14**(6): 767-773.

Worgull, M., J. F. Hétu, *et al.* (2006). Characterization of friction during the Demolding of Microstructures Molded by Hot Embossing. Symposium on Design, Test, Integration and Packaging of MEMS/MOEMS, Stresa, Italy.

Worgull, M., K. Kabanemi, *et al.* (2008). "Modeling of large area hot embossing." Microsystem Technologies **14**(7): 1061-1066.

Worgull, M., K. K. Kabanemi, *et al.* (2007). Modeling of Large Area Hot Embossing. Symposium on Design, Test, Integration and Packaging of MEMS/MOEMS.

Wriggers, P. (2006). Computational Contact Mechanics, Springer-Verlag Berlin Heidelberg.

Wu, C.-H. and W.-J. Liang (2005). "Effects of geometry and injection-molding parameters on weld-line strength." Polymer Engineering & Science **45**(7): 1021-1030.

Yang, J., Y. Zhao, *et al.* (2005). "Temperature-compensated high pressure FBG sensor with a bulk-modulus and self-demodulation method." Sensors and Actuators A: Physical **118**(2): 254-258.

Yoshikazu, K., S. Kenji, *et al.* (2001). "Relationship between Core Surface Roughness and Ejection Force for Injection Molding." Journal of the Japan Society of Precision Engineering **67**(3): 510-514.

Zambelli, G. and L. Vincent (1998). Matériaux et contacts: une approche tribologique. Lausanne, Presses polytechniques et universitaires romandes.

Zentay, P., Z. Zoller, *et al.* (1999). "Model for the calculation of demoulding force for polyurethane parts." Periodica Polytechnica Ser. Mech. Eng. **43**(2): 197-212.

Zhang, S., P. D. Hodgson, *et al.* (2003). "A finite element simulation of micro-mechanical frictional behaviour in metal forming." Journal of Materials Processing Technology **134**(1): 81-91.

Zhang, S. W. (1998). "State-of-the-art of polymer tribology." Tribol. Int. **31**: 49-60.

APPENDIXES

APPENDIX 1 – MATERIALS

F. RAMADA - AÇOS ESPECIAIS terça-feira, 9 de Outubro de 2007

Classe Aços e Ligas não Ferrosas para Moldes

ORVAR 2M ø⊏

EuroNorm	AISI	SS	AFNOR	DIN	W.Nr.
X40CrMoV5-1-1	H 13	2242	Z 40 CDV 5	X 40 CrMoV 5 - 1	1.2344

C	Si	Mn	Cr	Mo	Ni	V	W	Outros
0,39	1,00	0,40	5,30	1,30		0,90		

	Forjam. (ºC)	Recozim. (ºC)	Redução Tensões ºC	Cement. (ºC)	Têmpera (ºC)	Meio de Arrefec.	Revenido (ºC)
		850	650		980	1 2	180
					1030	3 4	700

Cores de Identificação	Fornecimento Estado	Dureza (HB) Máx.	R_m Kg/mm2	$R_{P_{0.2}}$ Kg/mm2	A (%) $L_0 = 5d_0$
/ERMELHO-AMARELO-VERMELHO	RECOZIDO	**255**			

Aplicações

Fieiras para Extrusão de Aluminio. Moldes para Termoplásticos.

R_m - TENSÃO DE ROTURA $R_{P_{0.2}}$ - TENSÃO LIMITE CONVENCIONAL DE PROPORCIONALIDADE A 0,2%

A - EXTENSÃO APÓS ROTURA

* - DUREZA NO ESTADO RECOZIDO

▲ - CARACTERÍSTICAS MECÂNICAS DO NÚCLEO APÓS TRATAMENTO TÉRMICO (diam. 30mm)

1 - SOBREPRESSÃO (F. VÁCUO) 2 - MARTÊMPERA 3 - AR 4 - ÓLEO 5 - ÁGUA

N - TEMPERATURA PARA TÊMPERA DE NÚCLEO ■ - NORMALIZAÇÃO

C - TEMPERATURA PARA TÊMPERA DA ZONA CEMENTADA

* - CERTIFICAÇÃO DOS NIVEIS DE LIMPEZA MICROESTRUTURAL • - OBTIDO POR PULVEROMETRIA

ESR - AFINADO POR REFUSÃO SOB ESCÓRIA ELECTROCONDUTORA

Observações /Notas

Notas

- As composições químicas indicadas, correspondem a valores médios para cada qualidade.
- De igual modo são indicadas algumas características mecânicas; apenas as impressas a **Bold** fazem parte da especificação do material.
- A legenda é referente à classe a qual este material pertence. Nem toda a simbologia pode ser aplicável a este materia

BÖHLER Steel M333 - Corrosion resistant plastic mould steel with the best polishability for products which require an outstanding surface finish

Physikalische Eigenschaften / Physical properties		
Elastizitätsmodul bei / Modulus of elasticity at	20 °C 68 °F	216 x 10^3 N/mm² 31.3 x 10^3 KSI
Dichte bei / Density at	20 °C 68 °F	7,7 kg/dm³ 0.278 lbs/in³
Wärmekapazität bei / Specific heat capacity at	20 °C 68 °F	460 J/(kg.K) 0.110 Btu/lb°F
Wärmeleitfähigkeit bei / Thermal conductivity at	20 °C 68 °F	23,1 W/(m.K) 13.35 Btu/ft h°F
Magnetisierbarkeit vorhanden / Magnetic properties magnetic		

Wärmeausdehnung zwischen 20 °C und ... °C Thermal expansion between 20 °C (68 °F) and ... °C (°F)					
100 °C	200 °C	300 °C	400 °C	500 °C	
10,50	11,00	11,00	11,50	12,00	10^{-6} m/(m.K)
210 °F	390 °F	570 °F	750 °F	930 °F	
5.83	6.11	6.11	6.39	6.67	10^{-6} in/in°F

Elastizitätsmodul, 10^3 N/mm² / Modulus of elasticity, 10^3 KSI					
20 °C	100 °C	200 °C	300 °C	400 °C	500 °C
216	212	205	198	190	180
68 °F	210 °F	390 °F	570 °F	750 °F	930 °F
31.3	30.7	29.7	28.7	27.6	26.1

Quelle / Source: Materials Center Leoben Forschung GmbH, ÖGI

BÖHLER M340 - Corrosion resistant plastic mould steels with good wear resistance and good grainability.

Physikalische Eigenschaften / Physical properties		
Elastizitätsmodul bei / Modulus of elasticity at	20 °C 68 °F	219 x 10^3 N/mm² 31.8 x 10^3 KSI
Dichte bei / Density at	20 °C 68 °F	7,7 kg/dm³ 0.278 lbs/in³
Wärmekapazität bei / Specific heat capacity at	20 °C 68 °F	460 J/(kg.K) 0.110 Btu/lb°F
Wärmeleitfähigkeit bei / Thermal conductivity at	20 °C 68 °F	18,2 W/(m.K) 10.52 Btu/ft h°F
Magnetisierbarkeit vorhanden / Magnetic properties magnetic		

Wärmeausdehnung zwischen 20 °C und ... °C Thermal expansion between 20 °C (68 °F) and ... °C (°F)					
100 °C	200 °C	300 °C	400 °C	500 °C	
10,88	10,78	11,21	11,61	11,90	10^{-6} m/(m.K)
210 °F	390 °F	570 °F	750 °F	930 °F	
6.04	5.99	6.23	6.45	6.61	10^{-6} in/in°F

Elastizitätsmodul, 10^3 N/mm² / Modulus of elasticity, 10^3 KSI					
20 °C	100 °C	200 °C	300 °C	400 °C	500 °C
219	215	209	201	193	183
68 °F	210 °F	390 °F	570 °F	750 °F	930 °F
31.8	31.2	30.3	29.1	28.0	26.5

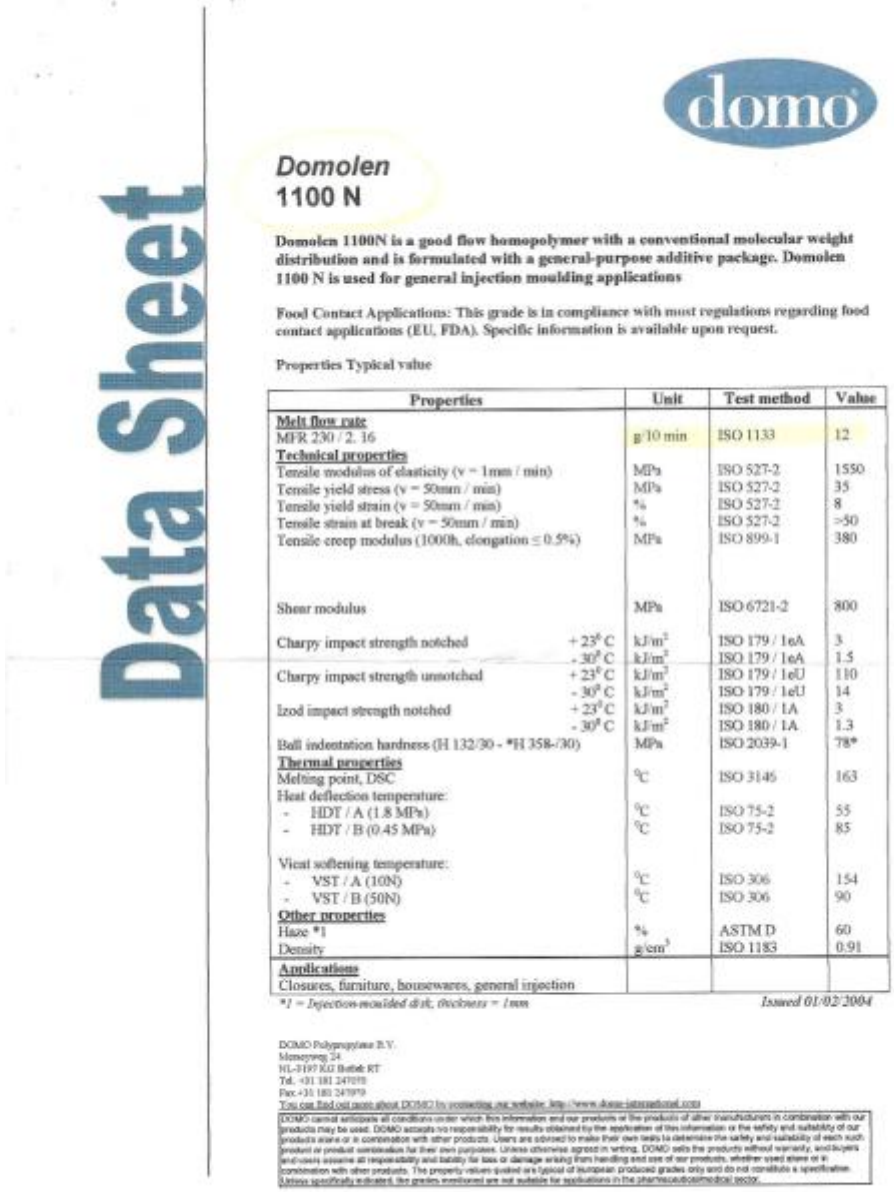

Data Sheet

domo

Domolen 1100 N

Domolen 1100N is a good flow homopolymer with a conventional molecular weight distribution and is formulated with a general-purpose additive package. Domolen 1100 N is used for general injection moulding applications

Food Contact Applications: This grade is in compliance with most regulations regarding food contact applications (EU, FDA). Specific information is available upon request.

Properties Typical value

Properties		Unit	Test method	Value
Melt flow rate				
MFR 230 / 2. 16		g/10 min	ISO 1133	12
Technical properties				
Tensile modulus of elasticity (v = 1mm / min)		MPa	ISO 527-2	1550
Tensile yield stress (v = 50mm / min)		MPa	ISO 527-2	35
Tensile yield strain (v = 50mm / min)		%	ISO 527-2	8
Tensile strain at break (v = 50mm / min)		%	ISO 527-2	>50
Tensile creep modulus (1000h, elongation ≤ 0.5%)		MPa	ISO 899-1	380
Shear modulus		MPa	ISO 6721-2	800
Charpy impact strength notched	+ 23° C	kJ/m²	ISO 179 / 1eA	3
	- 30° C	kJ/m²	ISO 179 / 1eA	1.5
Charpy impact strength unnotched	+ 23° C	kJ/m²	ISO 179 / 1eU	110
	- 30° C	kJ/m²	ISO 179 / 1eU	14
Izod impact strength notched	+ 23° C	kJ/m²	ISO 180 / 1A	3
	- 30° C	kJ/m²	ISO 180 / 1A	1.3
Ball indentation hardness (H 132/30 - *H 358-/30)		MPa	ISO 2039-1	78*
Thermal properties				
Melting point, DSC		°C	ISO 3146	163
Heat deflection temperature:				
- HDT / A (1.8 MPa)		°C	ISO 75-2	55
- HDT / B (0.45 MPa)		°C	ISO 75-2	85
Vicat softening temperature:				
- VST / A (10N)		°C	ISO 306	154
- VST / B (50N)		°C	ISO 306	90
Other properties				
Haze *1		%	ASTM D	60
Density		g/cm³	ISO 1183	0.91
Applications				
Closures, furniture, housewares, general injection				

**1 = Injection-moulded disk, thickness = 1mm*

Issued 01/02/2004

DOMO Polypropylene B.V.
Meneweg 24
NL-5107 KG Raamt RT
Tel. +31 181 247070
Fax.+31 181 247079
You can find out more about DOMO by consulting our website: http://www.domo-laboratories.com

PANLITE L-1225 Z100 TEIJIN Human Chemistry, Human Solutions

Type of material: Polycarbonate resin
Characteristics: Low viscosity; Clear
Good UV resistance (aquired SAE standard)
Processing Method: Injection molding

Property	Unit	Test Method ISO / ASTM	Measurement Condition	L-1225Z 100
Melt volume flow rate	cm^3/10min	ISO 1133	300°C load 1.2kg	11
Density	kg/m^3	ISO 1183	-	1200
Water absorption rate	%	ISO 62	in water 23°C 24h	0.2
Light transmission	%	ASTM D1003	thickness 3mm	88
Refractive index	-	ASTM D542	-	1.585
Tensile modulus	MPa	ISO 527-1 and 527-2	1mm/min	2400
Tensile stress at yield	MPa	ISO 527-1 and 527-2	50mm/min	61
Tensile stress at yield	MPa	ISO 527-1 and 527-2	5mm/min	-
Tensile strain at yield	%	ISO 527-1 and 527-2	50mm/min	6
Tensile stress at yield	%	ISO 527-1 and 527-2	5mm/min	-
Nominal tensile strain at break	%	ISO 527-1 and 527-2	50mm/min	>50
Nominal tensile strain at break	%	ISO 527-1 and 527-2	5mm/min	-
Tensile stress at break	MPa	ISO 527-1 and 527-2	50mm/min	-
Tensile stress at break	MPa	ISO 527-1 and 527-2	5mm/min	-
Tensile strain at break	%	ISO 527-1 and 527-2	50mm/min	-
Tensile strain at break	%	ISO 527-1 and 527-2	5mm/min	-
Flexural modulus	MPa	ISO 178	2mm/min	2400
Flexural strength	MPa	ISO 178	2mm/min	94
Charpy Impact Strength	kJ/m^2	ISO 179	unnotched	NB
Charpy Impact Strength	kJ/m^2	ISO 179	notched	71
Load-deflection temperature	°C	ISO 75-1 and ISO 75-2	1.80MPa	128
Load-deflection temperature	°C	ISO 75-1 and ISO 75-2	0.45MPa	141
Vicat softening temperature	°C	ISO 306	50°C/h 50N	148
Mold shrinkage	%	In house method	parallel	0.5-0.7
Mold shrinkage	%	In house method	vertical	0.5-0.7
Coefficient of linear expansion	$\times 10^{-4}$/°C	ISO 11359-2	parallel	0.7
Coefficient of linear expansion	$\times 10^{-4}$/°C	ISO 11359-2	vertical	0.7
Specific inductive capacity	-	IEC 60250	100Hz	3.1
Specific inductive capacity	-	IEC 60250	1MHz	3
Dielectric loss tangent	$\times 10^{-4}$	IEC 60250	100Hz	10
Dielectric loss tangent	$\times 10^{-4}$	IEC 60250	1MHz	90
Volume resistivity	Ω·m	IEC 60093	-	>1×1013
Surface resistivity	Ω	IEC 60093	-	>1×1015
Withstand voltage	MV/m	IEC 60243-1	short time test	30
Tracking resistance	-	IEC 60112	-	250
Flammability	-	UL 94	-	V-2 (0.40mm)
Flammability	-	UL 94	-	HB (1.9mm)
Temperature index	°C	UL 746B	electric 1.47mm	125
Temperature index	°C	UL 746B	impact 1.47mm	115
Temperature index	°C	UL 746B	non-impact 1.47mm	125

RonfalinC130 natural

Typical values at 23°C	Test method	Unit	Specimens	Values
Properties				
Abbreviated term	ISO 1043			PC/ABS
Density	ISO 1183	g/cm³		1.15
Reinforcing filler content		%		
Water absorption equilibrium @ 23°C	DIN 53 495/L	%		0.2
Water absorption, 24hr @ 23°C/50% rh				0.6
Processing				
Methods; moulding M,Extrusion E, Blow m M				M
MVR 260/5	ISO 1133	cm³/10min	Compound	20
Pre-drying temperature / time		°C / hr		105/3
Melt temperature, injection moulding		°C		230/250
Mould temperature		°C		40/60
Moulding shrinkage		%		0.5
Flammability				
UL 94 rating at 1.6mm	UL 94	class		HB
Automotive materials (thickness of d> 1mm)	FMVSS 302	class		
Mechanical properties				
Tensile modulus	ISO 527-2	Mpa	ISO 3167	2400
Yield stress (V= 50 mm/min)	ISO 527-2	Mpa	ISO 3167	50
Yield strain (V= 50 mm/min)	ISO 527-2	%	ISO 3167	
Flex strength	ISO 178	Mpa		85
Shear modulus	ISO 6721-2	MPA		
Charpy notched impact 23°C	ISO 179/1eU	KJ/m²		40
Charpy notched impact -30°C	ISO 179/1eU	KJ/m²		25
Izod notched impact strength, method A 23°C	ASTM D 256	J/m		500
Izod notched impact strength, method A -30°C	ASTM D 256	J/m		200
Ball indentation hardness H 358/30	ISO 2039-1	MPa		105
Thermal properties				
Deflection temperature 1.8 Mpa (HDT A)	ISO 75-2	°C		110
Deflection temperature 0.45 Mpa (HDT B)	ISO 75-2	°C		130
Vicat softening temperature VST/A/50	ISO 306	°C		
Vicat softening temperature VST/B/50	ISO 306	°C		130
Coefficient of linear expansion 923-80) °C	DIN 53752	10⁴/K		0.79
Thermal conductivity	DIN 52612	W/(m·K)		0.2
Electrical properties				
Dielectric constant at 100Hz / 1MHz	IEC 250			
Dissipation factor at 100Hz / 1MHz	IEC 250	10^{-4}		
Volume resistivity	IEC 93			>10^{16}
Surface resistivity	IEC 93			>10^{14}
Dielectric strength	IEC 243/1	KV/mm		>25
CTI, solution A	IEC 112	V		>250
CTI, solution B	IEC 112			

Reformulated using the latest generation ABS feedstock

JGP Perrite

Tel: +44(0) 1925 810608

APPENDIX 2 – PUBLICATIONS

CONTRIBUTIONS TO THE MODELLING OF EJECTION IN INJECTION MOULDING

M. Correia[1], C. Capela[1], A.S.Pouzada[2] and A.S.Miranda[3]
1 School of Technology and Management, Polytechnic Institute of Leiria, Leiria, Portugal
2 Institute for Polymers and Composites, University of Minho, Guimarães, Portugal
3 Dept. Mechanical Engineering, University of Minho, Guimarães, Portugal
asm@dem.uminho.pt

Abstract

The quality of parts produced by injection moulding may be affected during the ejection stage of the moulding cycle. At this stage the parts are mechanically forced to separate from the moulding surfaces. The ejection force depends on the shrinkage of the polymer on to the core and on the friction properties of the contacting surfaces at the moment of extraction. As during moulding there is a replication of the part over the mould surface the ejection process is also dependent on the plastic deformation of the moulded material. The duration of the extraction process is very short in time, thus the friction coefficient relevant for modelling the process is the static coefficient of friction. This study shows an overview of the understanding of the mechanism of ejection in injection moulding and proposes an interpretation of the factors that influence directly the process. These analyses are relevant for developing a model that will consider phenomenological factors, such as the polymer shrinkage, the friction properties at the ejection stage and the plastic deformation of the polymer.

Introduction

Today thermoplastics are the most widely used materials for applications ranging from non-critical packaging products to very demanding technical parts. These parts are frequently made by injection moulding. In the injection moulding cycle, the mechanical process of ejection of the parts may affect their quality; at this stage the parts are mechanically forced to separate from the moulds. This ejection force may be quite high if the parts are moulded over deep cores.

The design of the ejection system depends on factors such as the draft angles, the surface finish, and the properties of the moulding material at the ejection temperature [1]. The geometry and the location of the ejector pins depend significantly on the shape of the part and the architecture of the cooling system. Nevertheless, the most important factor for designing the ejection system is the ejection force that varies with materials and the processing conditions [2]. The ejection system must not fail during production, since this will lead to the interruption of the production run or the damage of the mould [3].

The friction forces that develop between the polymer surface and the moulding surface of the mould results from the polymer shrinkage part onto the mould. Furthermore the polymer surface tends to replicate the mould texture, this may becoming an additional problem in the ejection stage. The more intimate contact caused by the shrinkage and the replication, in the case of chemical affinity between the moulding and mould materials, may originate adhesion that has to be overcome upon ejection.

The optimisation of the injection mould systems requires that the frictional behaviour of the mouldings during ejection is known and predictable [1-3]. The study in which this work is included aims at identifying the influencing factors relevant to the ejection of injection mouldings. These include the moulding shrinkage, the mechanical properties of the contacting materials and how the coefficient of friction depends on all the other parameters (Fig. 1).

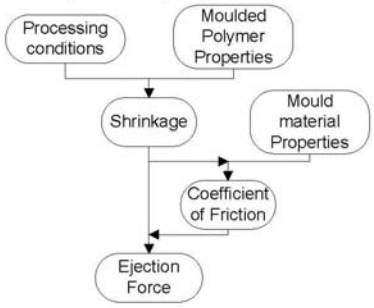

Fig. 1. Factors relevant to ejection in injection moulding

Factors that influence ejection force

Economics impose that the moulded parts are ejected as soon as they are dimensionally stable, to shorten cycle times. As ejection occurs while parts are at elevated temperatures, excessive or unbalanced demoulding forces may cause

localized and gross deformation of the part, leading to part inefficiency [4].

The attempts to model the ejection of injection moulded parts during the last decades started from the basic equation for the friction force (equation [1]).

$$F_E = \mu \times P \times A \qquad [1]$$

In this equation μ is the coefficient of friction between the mould and the part, ***P*** is the contact pressure between the part and the mould core, which depends mostly on the shrinkage, and ***A*** is the area of the contact.

Shrinkage

During the injection moulding process (Fig. 2), the polymer undergoes a complex thermo-mechanical history that has influences on the properties of the material in the part, its microstructure and the final dimensions with respect to the impression dimensions [5].

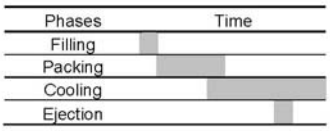

Fig. 2. Phases of the injection moulding process

The shrinkage of the moulding is an aspect of utmost engineering importance as it influences not only the dimensional accuracy of the product but also its ejection process from the mould. In the case of semi-crystalline materials where the shrinkage tends to be higher than in amorphous polymers the prediction of shrinkage justifies complex consideration of the processing conditions and the molecular structure of the material [6].

The shrinkage is affected by the flow-induced residual stresses and orientation, the flow-induced crystallization and the heat transfer. These factors are influenced by processing parameters such as packing pressure, packing time, melt temperature, mould temperature, injection speed, and material properties as well as geometric constrains [7]. The anisotropic shrinkage cannot be predicted based only on volume shrinkage. It is greatly influenced by ejection temperature, is material dependant, and is very different in amorphous and semicrystalline polymers. Deep gates, long holding times, and high holding pressures in the injection moulding process can compensate for shrinkage of the part [2, 8].

Replication

During the solidification process the plastic part shrinks on to the core while in a molten or very deformable state. As a consequence the moulding surface tends to replicate the topography of the moulding block core (Fig 3) [9].

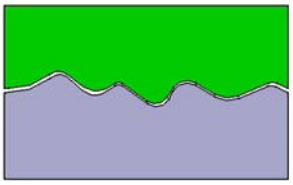

Fig. 3. Replication on the mould

The replication effect is not usually considered in tribology studies and processes but plays a fundamental role in the ejection process of injection mouldings [1].

Mechanical Properties

The mechanical properties of the materials involved in the ejection of moulded polymers may vary substantially for some orders of magnitude. Typically moulding blocks are made from alloy steels with elastic modulus around 200 GPa, whereas the plastics mouldings are in the order of 1-2 GPa. In specific cases of rapid tooling, which is a field that is gathering increasing interest [8, 10] non metallic materials with modulus of around 10 GPa are typical. This wide variation of the data coupled with the replication that occurs in injection moulding may definitely determine the tribological mechanisms associated to the ejection process.

Coefficient of friction

Friction is affected by many factors: material, environmental, interface condition, operating conditions. Some of those factors are difficult to assess and control. That is why friction becomes so complex to simulate in laboratory tests or to reproduce by theoretical modelling.

The friction force is the tangential force opposite to the movement, established in dry or in wet lubrication. Thus, friction is not a property of the materials alone, but a systemic reply as a function of the state of the surface and of the interfacial mean. Conceptually, the friction force is defined as the ratio of two forces acting, respectively, parallel and perpendicular to the interface between bodies under relative motion [11] (see Fig. 4).

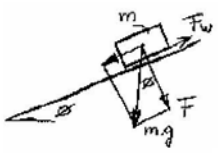

Fig. 4. From the notes made by Leonardo Da Vinci (1452-1519)

The quantity known as the friction coefficient has long been used in science and engineering. The coefficient of friction (μ) is given by the quotient of the friction force by the normal reaction.

$$\mu = \frac{F_w}{F_n} \qquad [2]$$

where F_w is the friction force; F_n is the normal contact force.

Suh et al [12] presented friction as composed of three mechanisms: asperity deformation, adhesion and ploughing of the interface. The overall friction coefficient was then given by the weighed sum of these three components (Equation 3).

$$\mu = \mu_d f_d + \mu_a f_a + \mu_p f_p \qquad [3]$$

Warren and Krajcinovic [13] presented a fractal model for the static coefficient of friction. In equation 4 the normal reaction is f_i and the shear force q_i required to cause the *i*-th asperity to slip, is obtained using the Bowden and Tabor model for a narrow slider riding over a single pointed asperity. The local normal at the contact point is inclined at an angle α_i assuming the surface to be one-dimensional. The coefficient of friction component μ_a is attributed primarily to adhesion, and to a lesser extent to the underlying smaller scale roughness (Equation 4).

$$\mu_i = \frac{q_i}{f_i} = \frac{\mu_a + \tan\alpha_i}{1 - \mu_a \tan\alpha_i} = \\ = \mu_a + \tan\alpha_i = \mu_a + \alpha_i \qquad [4]$$

Sraffelini [14] verified that for a metal pair of a tribological system, the average asperity junction is inversely proportional to the material yield pressure (p_Y) (Equation 5). The main aspect was to consider the average shear strength of each junction (τ_m) as dependent on the effective work of the adhesion. There exists a irreversible phenomena (plastic deformation) that occur during sliding.

$$\mu = \frac{\tau_m}{p_Y} \frac{1}{\sqrt{1 - 12(\tau_m / p_Y)^2}} \qquad [5]$$

Benabdallah [15] proposed a model that considers the coefficient of static friction (μ_s) dependent of the real area of contact (A_R) and of the normal load (F_n). Assuming that the low range increase in normal load does not affect the number of asperities initially in contact, which in turn imply a power law relationship between A_R and F_n, the decrease of μ_s with F_n is justified by equation 6 where τ_0 and α are constants depending mainly to the material.

$$\mu = \frac{\tau_0}{F_n} A_r + \alpha \qquad [6]$$

The results suggest that assuming low range increase in normal load does not affect the number of asperities initially in contact, which in turn imply a power law relationship between A_r and F_n, the decrease of μ_s with F_n is justified by Equation 6. On the contrary, at relatively higher loads μ_s approaches a constant value due to the linear relationship of A_R with F_n that prevails in this condition. This also implies that at this stage, the interfacial shear strength of the micro-junctions becomes independent of the normal load.

Friction between the thermoplastic part and the injection mould core depends on the mechanical interaction between the two surfaces (shrinkage, mould roughness), but also on an adhesive component inherent to the properties of the two materials at the processing conditions [8] and on the properties of the mating surfaces. The adhesive force is a result of atomic forces established between the contacting surfaces of the two materials.

Wang *et al.* [16] carried out a numerical and experimental study for the determination of the ejection force using boxes of polycarbonate resin. The Wang study explains that during solidification the box conforms to the mould core geometry, while it deforms right after ejection. The core provides constraining forces to prevent free shrinkage and warpage of the box before it is ejected. During ejection, friction forces are induced at the mould-part interface, so the ejection force provided by the ejector pins is basically to overcome friction and to remove the box (Fig. 5).

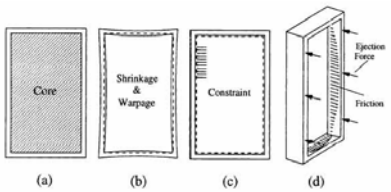

Fig. 5. Mechanism of part ejection during injection moulding of plastics: (a) before ejection; (b) after ejection, (c) constraint by mould; (d) ejection [16].

Therefore the analysis of the ejection process must be based on the constraining and friction forces resulting from mould-part interaction during solidification and ejection.

Ferreira *et al.* developed a special prototype apparatus for testing thermoplastics in as-moulding conditions [17]. The testing procedure included heating the specimens to the corresponding processing temperatures, applying a normal load (so that the specimen replicated the mould surface), cooling to ejection temperature and then pulling the specimen. The effect of the polishing direction, surface roughness and temperature on the coefficient of friction was studied. Results showed that the testing temperature and the surface roughness have a significant effect on the coefficient of friction for polycarbonate. For polypropylene, none of these parameters have a significant effect on the coefficient of friction, except possibly the interaction of polish direction and roughness. The coefficient of friction obtained for both polymers are higher than already published values.

Ejection Force

The relevance of the coefficient of friction in the ejection of injection mouldings has been evidenced in the work of many researchers. In particular Pontes and co-workers [2, 3, 18-20] have analysed some of the aspects associated to this process, namely the processing conditions and the shrinkage. Their studies have been focused on tubular mouldings where the shrinkage effects tend to be more evident.

Recent studies have been analysing the ejection process in hybrid moulds with cores manufactured in non-metallic materials. In these circumstances it has become evident that the adhesion process between the mould and the moulding materials is important in the ejection process, especially when the materials have similar Hildebrand solubility parameters [11].

Guidelines for a model

The studies that were mentioned herein suggest that the tribological mechanism related to the ejection of injection mouldings include aspects related to the mechanical interaction between the mould and the moulding materials, and also, in specific cases, chemical adhesion between the materials.

A general model for describing that tribological situation must include the mechanical aspects that consider the replication that is associated to the injection of the polymer in the mould. That model must also include the chemical reactions likely to occur and leading to the adhesion of the moulding to the mould.

The model must consider the formation of the moulding debris that result from the fracture of the asperities that were 'welded' to the mould by adhesion or could not go over the mould relief (Fig 6).

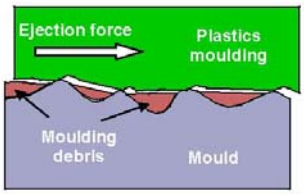

Fig. 6. Adhesion and moulding erosion during ejection

In the cases of adhesion it is likely the occurrence of higher ejection force that will result from the mechanisms of deformation and of fracture of asperities of the plastic part. Thus in the cases where adhesion is likely to occur higher coefficients of friction are likely to be detected in tests carried out according to the test method suggested in [1].

As the wear of the plastics moulding is likely to occur the influence of the roughness parameter(s) must play a fundamental role in the model to develop and will be interlinked with the shear strength of the moulding material.

The influence of the shrinkage, as determinant of the contacting pressure and therefore of the level of replication, must be also taken into account. An additional complexity arises from the shrinkage being strongly dependent from the type of injection flow and the processing conditions (injection and ejection temperature, holding pressure and time).

The direction of polishing also affects the ejection. This influence is further enhanced by the replication effect.

In conclusion it is foreseeable that a model for describing the ejection process of injection mouldings does not depend only on the intrinsic properties and topography of the surfaces in contact but strongly on the processing conditions that will be used in the production of the parts.

Keywords

Friction, ejection forces and injection moulding.

References

[1] A. S. Pouzada, E. C. Ferreira, A. J. Pontes - Friction properties of moulding thermoplastics, Polymer Testing 25 (2006).
[2] A.J. Pontes, R. Pantani, G. Titomanlio, A. S. Pouzada - On the prediction of ejection forces for tubular moldings, ANTEC 2002 Conf, San Francisco: May 2002. paper 534.
[3] B. J., Araújo, A. S. Pouzada, Design of ejection systems for injection moulds, O Molde, 54 (2002).
[4] N. Bhagavatula, D. Michalski, B. Lilly, G. Glozer - Modelling and verification of ejection forces in thermoplastics injection moulding, Modelling Simult. Mater. Sci. Eng., 12 (2004).
[5] G. Titomanlio, K. M. B. Jansen - In-mold shrinkage and stress prediction in injection molding, Polym. Eng. Sci.,36 (1996).
[6] A.J Pontes.; M.J. Oliveira; A.S.Pouzada - Studies on the influence of the holding pressure on the orientation and shrinkage of injection molded parts, ANTEC 2002 Conf, San Francisco: May 2002. paper 98.
[7] K. Kwon, A. I. Isayev, K.H. Kim, C. van Sweden - Theoretical and experimental studies of anisotropic shrinkage in injection moldings of semicrystalline polymers, Polym. Eng. Sci., 46 (2006).
[8] M.E. Kinsella - Ejection force and static friction coefficients for rapid tooled injection mold inserts, PhD thesis. The Ohio State University (2004).
[9] E.C. Ferreira, M.F. Costa, C.R. Laranjeira, M.J. Oliveira, A.S.Pouzada - Comparative study, by optical techniques of the interface polymer/steel in replication conditions, Mat. Sci. Forum, 455-456 (2004).
[10] M.W. Gonçalves, G.V. Salmoria, A.S. Pouzada, - Study of tribological properties of moulds obtained by stereolithography, Virt. Phys. Protot., accepted (2007).
[11] P.J. Blau, The significance use of the friction coefficient, Tribology International 34 (2001).
[12] N.P. Suh, M. Mosleh, P.S. Howard - Contol of friction, Wear,175 (1994).
[13] T. L. Warren, D. Krajcinovic - A fractal model for the static coefficient of friction at the fiber-matrix interface, Composites: Part B 27B (1996).
[14] G. Straffelini - A simplified approach to the adhesive theory of friction, Wear 249 (2001).
[15] H. S. Benabdallah - Static friction coefficient of some plastics against steel and aluminium under different contact conditions, Tribology International, 40 (2007).
[16] H. Wang, K.K. Kabanemi, G. Salloum - Numerical and experimental studies on the ejection of injection-molded plastic products, Polym. Eng. Sci., 40 (2000).
[17] E.C. Ferreira, N.M. Neves, R. Muschalle, A.S. Pouzada - Friction properties of thermoplastics in injection molding, ANTEC 2001 Conf, Dallas: May 2001. paper 26.
[18] A.J. Pontes, R. Pantani, G. Titomanlio, A.S. Pouzada - Prediction of ejection forces in tubular moldings in amorphous polymers, ANTEC 2002 Conf, San Francisco: May 2002. paper 60.
[19] A.J. Pontes, A. S. Pouzada - Ejection force in tubular moldings. Part I: Effect of Processing Conditions, Polym. Eng. Sci., 44 (2004).
[20] A.J. Pontes, A.S. Pouzada, Ejection force in tubular moldings. Part II: A prediction model, Polym. Eng. Sci., 45 (2004).

Int J Adv Manuf Technol
DOI 10.1007/s00170-011-3573-2

ORIGINAL ARTICLE

Analysis of friction in the ejection of thermoplastic mouldings

Mario Simoes Correia · Antonio Sousa Miranda · Marta Cristina Oliveira · Carlos Alexandre Capela · Antonio Sergio Pouzada

Received: 12 April 2011 / Accepted: 7 August 2011

Abstract The ejection force of injection-moulded thermoplastics depends on the contact conditions at the moment of ejection. Replication of the polymer part surface occurs onto the mould surface during injection of the melt. Ejection takes place in a very short time, hence the static coefficient of friction must be considered for modelling the ejection process. To understand the contribution of the mechanisms involved in the friction during the ejection stage, a mixed approach was followed: analytical simulation of the ploughing, numerical simulation of the deformation, and experimental inference of the adhesion. The relevance of roughness, temperature and contact pressure in the coefficient of friction was evidenced.

M. S. Correia · C. A. Capela
ESTG–School of Technology and Management,
Polytechnic Institute of Leiria,
Leiria, Portugal

A. S. Miranda
CT2M–Centre for Mechanical and Materials Technologies,
University of Minho,
Guimarães, Portugal

M. C. Oliveira
CEMUC–Mechanical Engineering Centre
from University of Coimbra,
Coimbra, Portugal

C. A. Capela
CDRSP–Centre for Rapid and Sustainable Product Development,
Polytechnic Institute of Leiria,
Leiria, Portugal

M. S. Correia (✉) · A. S. Pouzada
Institute for Polymers and Composites/I3N, University of Minho,
Guimarães, Portugal
e-mail: mario.correia@ipleiria.pt

Published online: 26 August 2011

Keywords Static friction · Polymer · Injection moulds

1 Introduction

Thermoplastics are common materials in modern applications from noncritical packaging products to technical parts. Injection moulding is the most used process due to its flexibility for complex shapes and fast production. During this process, the polymer undergoes a complex thermomechanical history, which influences the mechanical properties and the final dimensions (with respect to the corresponding mould dimensions) of the part [1]. The process encompasses four stages: filling, packing, cooling and ejection. Ejection is critical when complex geometry parts are produced and distortion or denting is caused by the ejectors [2]. The correct design of the ejection mould system requires that the frictional behaviour of the contacting surfaces during ejection is known and predictable [3–5]. The most important factor for designing this system is the ejection force that varies with materials, processing conditions and geometry [5, 6]. The ejection system must not fail during the production since this will lead to the interruption of the production run or to mould damage. The mechanical properties of the materials involved in the injection moulding of polymers may vary substantially for some orders of magnitude. Typically, moulding blocks are made from alloy steels with elastic modulus around 200 GPa, whereas the plastics mouldings present elastic modulus in the order of 1–2 GPa. This high difference of mechanical properties coupled with the replication of the mould surface topography, which occurs in injection moulding determine the tribological mechanisms associated to the ejection process, which involves both elastic and plastic deformation. In specific cases of rapid tooling,

which is a field that is gathering increasing interest [7, 8], nonmetallic materials with elastic modulus around 10 GPa are used for the moulding blocks (core and cavity). In these cases, the tribological mechanisms may include also chemical adhesion phenomena.

There is an increasing interest in understanding polymer tribological behaviour because of the growing application of these materials in friction surfaces [9]. In the specific context of understanding the ejection of polymers since the earlier studies by Menges and Bangert [10], experimental work was developed to measure the friction force required for ejection [8, 11–14].

The ejection force depends on the friction properties of the contacting surfaces at the onset of extraction. In this tribological situation, the contact is very complex since the part surface is formed against the moulding surface in the mould. Thus, during ejection, the friction forces that develop between the polymer and the moulding surface result from the polymer shrinkage onto the mould. The shrinkage occurs during the solidification and cooling of the plastics part and as a consequence, the moulding surface tends to replicate the topography of the moulding block surface [15]. This replication brings about an additional problem in the ejection since the replication effect is not usually considered in tribological studies and processes in spite of playing a fundamental role in the ejection process of injection mouldings [3]. Due to the replication of the metallic topography on the plastic part, there is an interlocking between the two surfaces making the roughness characterization very important [16]. The effective contact surface increases as a result from the more intimate contact caused by the combined shrinkage and replication; in the case of chemical affinity between the moulding and mould materials, further adhesion is promoted and it must be overcome upon ejection [3].

Understanding the ejection in injection moulding implies the consideration of a number of process variables and material properties that influence the shrinkage, which is responsible for the contact force between the surfaces and of the coefficient of friction that ultimately determines the magnitude of the ejection force (Fig. 1).

Economics impose that the moulded parts are ejected as soon as they are dimensionally stable to shorten the cycle time. This stability increases with the mechanical stiffening when the temperature reduces. However, if ejection occurs at very low temperature, excessive or unbalanced demoulding forces may cause localised and gross deformation of the part leading to part inefficiency [4, 14]. If, for the sake of cycle time reduction, the ejection is performed at a higher temperature gross distortion of the moulded part may result.

Suh et al. [17] interpreted friction as resulting from three mechanisms: asperity deformation, adhesion and ploughing

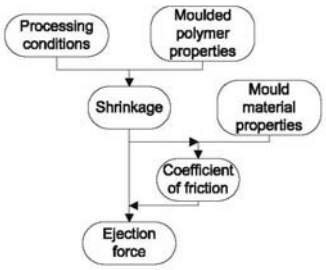

Fig. 1 Factors relevant to ejection in injection moulding [16]

of the interface. Thus, the overall coefficient of friction is given by the weighed sum of these three components:

$$\mu = W_{\text{deform}}\mu_{\text{deform}} + W_{\text{adhesion}}\mu_{\text{adhesion}} + W_{\text{plough}}\mu_{\text{plough}} \quad (1)$$

where, μ_{deform}, μ_{adhesion} and μ_{plough} are the deformation, adhesion and ploughing components of the coefficient of friction, respectively, and W_{deform}, W_{adhesion} and W_{plough} are the corresponding time-dependent weighting factors.

Following this interpretation of the coefficient of friction, Ferreira et al. [18] considered the case of ejection of plastics and proposed that the static coefficient of friction should include the contribution of deformation and ploughing $\mu_{\text{static}}=\mu_{\text{deform}}+\mu_{\text{plough}}$ and suggested that the kinetic coefficient of friction was governed by the ploughing only, $\mu_{\text{kinetic}} = \mu_{\text{plough}}$.

The consideration of adhesion in the tribological behaviour of contacting surfaces has not received as wider attention as the other two mechanisms. Recently, Gao et al. [19] made some considerations on the adhesion contribution in terms of the number of inter-atomic or intermolecular

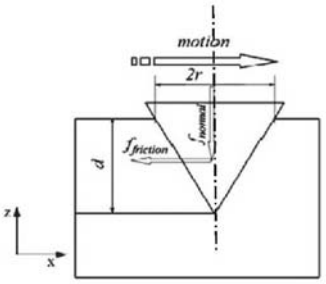

Fig. 2 Conical asperity geometry and elementary forces

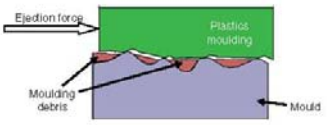

Fig. 3 Abrasion of the polymeric material [16]

bonds that are broken and reformed while the surfaces slide over each other. In the actual context of injection moulding of thermoplastics, evidence of the relevance of the adhesion mechanism has been shown associated to the intermolecular bonds, as is the case of moulds with highly polished surface (Ra<0.05 μm) [20] or to the chemical affinity of the two materials [7].

In this paper, the interpretation of the ejection mechanism in injection moulding is made through a mixed approach (theoretical and numerical) following previous works by Suh et al. [17] and Ferreira et al. [18]. This interpretative analysis considers the three contributors for the friction force: ploughing (F_{plough}), deformation (F_{deform}) and adhesion ($F_{adhesion}$):

$$F_{friction} = F_{plough} + F_{deform} + F_{adhesion} \quad (2)$$

An analytical model is proposed for the ploughing contribution. From the numerical simulation of ploughing and deformation, the adhesion component is inferred from experimental data.

2 Friction force based on geometrical aspects

2.1 Analytical model

Roughness is the major variable in the friction force developed during the ejection stage, since it influences directly the ploughing and deformation components of friction in the contact between the hard mould steel and the soft plastics.

To simulate the contact in this analysis, the hard tool surface was represented by an array of conical asperities. The indentation of the hard asperity on the soft surface was characterised by the indentation radius, r, and the indentation depth, d, as shown in Fig. 2. In this figure, the two elementary forces, normal force (f_{normal}) and friction force ($f_{friction}$) involved in the contact mechanism of one single asperity are also shown.

The ploughing term associated to a conical asperity has been discussed by Tabor [21] who did not consider the mechanical properties of the contacting pair. Now, both roughness and mechanical properties are taken into account. Considering Ra as the arithmetical mean roughness and S the local mean peak spacing, each asperity is geometrically defined in terms of the height:

$$d = 2 \times Ra \times S, \quad (3)$$

and the cone radius:

$$2r = S \quad (4)$$

Therefore, the cross-sectional area (A_z) of a triangular indentation formed by the conical asperity is:

$$A_z = S \times Ra \quad (5)$$

The ploughed groove results from the plastic deformation associated to the yield stress of the polymeric material, σ_y. The resistance of each asperity to the relative motion, or elementary ploughing force, f_{plough}, is the product of the surface pressure, S_0, by the cross-sectional area, A_z. Upon yielding, it can be considered that the pressure is equivalent to the compressive yield stress, which is very dependent on temperature. Thus, the elementary ploughing force is:

$$f_{plough} = A_Z \times \sigma_y = S \times Ra \times \sigma_y \quad (6)$$

For the whole apparent contacting surface, assuming that S is the mean spacing of profile irregularities, the maximum

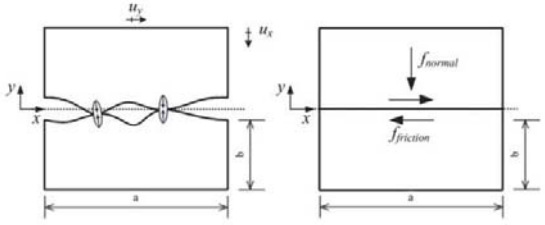

Fig. 4 Micro-asperities relative motion and resultant homogenised forces

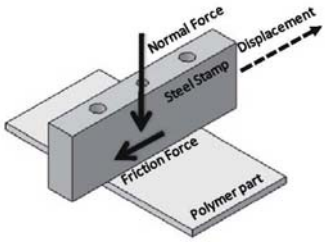

Fig. 5 Scheme of the steel stamp and the polymeric part in the friction test

ploughing component of the ploughing force (F_{plough}) is the sum of all the elementary forces acting on each asperity. Defining the peak count, P_c, as an integer giving the number of peaks per unit area and multiplying by the elementary ploughing force, results in Eq. 10:

$$F_{plough} = P_c \times S \times Ra \times \sigma_y \tag{7}$$

For determining P_c, a "peak" is defined relatively to upper and lower thresholds of the arithmetical Ra. Equation 7 defines the maximum value for the resistance force to sliding motion that should be expected if the engaging of the asperities is maintained. This can result from the ploughing mechanism that causes abrasion of the polymeric material as shown in Fig. 3.

2.2 Numerical model

The assessment of the elementary forces associated to friction in the ejection process can be done using the finite element method. In this numerical simulation, a representative volume element under homogeneous boundary conditions was considered. This element includes the contact geometry with the surface profile. If the model considers only deformations applied in the normal direction, the computational homogenization procedure yields a homogenised contact law for the contact pressure. To derive

Table 1 Conditions used in the friction tests

Surface roughness [μm]		Contact Pressure [MPa]	Temperature [°C]
S	*Ra*		
283.6	0.039	4.3	50
79.6	0.052		
61.4	0.588	4.9	65
71.4	1.952	5.6	80

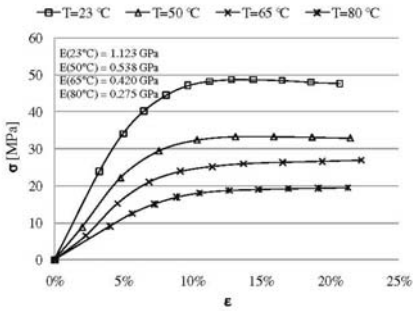

Fig. 6 Compression test stress–strain curves at different deformation temperatures

a friction law, the model must also take into account the sliding or tangential motion. For the numerical simulation of the micro-mechanical model, it is necessary to define a general contact law for the contact forces in the normal and tangential directions. The friction law results either from a constitutive relation describing the deformation in the contact area and/or the elastic plastic response of the solid, which is related to ploughing and deformation. The numerical simulation of this type of microstructure allows computing the normal and tangential contact forces on the rough surfaces, which only occur in some parts of the micro-asperities as depicted in Fig. 4. The sum of these forces allows to determine the resultant force on the entire contact surface [22].

The homogenization procedure involved the following steps: (1) discretization of the representative volume element taking into account the roughness characteristics and (2) application of a homogeneous deformation pattern to the boundary of the blocks in the normal and tangential directions. As a first step, a normal displacement is applied until the prescribed normal force is reached. After that, the relative

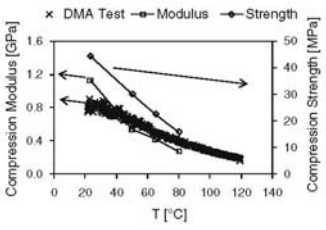

Fig. 7 Mechanical properties determined using compressive tests and DMA analysis

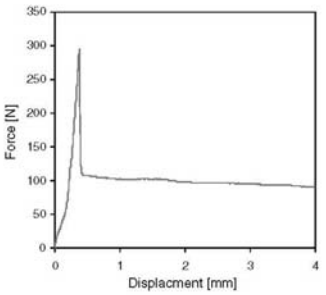

Fig. 8 Friction force evolution for a surface roughness of 0.588 μm; contact pressure, 4.9 MPa, test temperature, 65°C

displacement is incrementally applied in the tangential direction keeping the normal displacement fixed.

In the present case, the adopted finite element model had only one elementary asperity in order to compare the elementary force with that determined with the previous model. Considering the very different mechanical properties of the mould and the moulded polymer, the elementary asperity is considered as rigid and modelled with Bézier surfaces. Since the injection process always involves surface replication, it was assumed that the polymeric part topography will be exactly the same as the mould. The replication occurs as a result of the applied normal contact force. Therefore, a stress field is induced in the polymeric part in this first deformation stage. In this simulation, the indentation step was taken into account before the evaluation of the deformation stage.

The simulations were performed with the in-house finite element Deep-Drawing 3D Implicit (DD3IMP) code, specifically developed to simulate sheet metal-forming processes [23]. The Signorini condition is used to model the unilateral

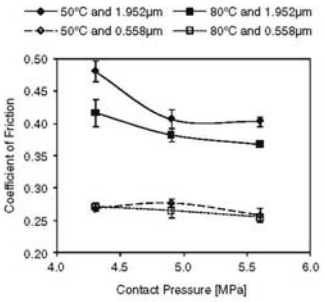

Fig. 9 Variations of coefficient of friction with the contact pressure

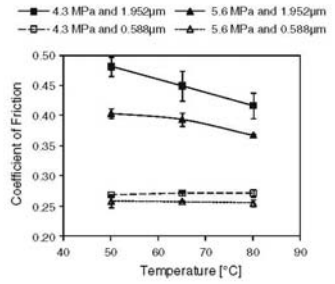

Fig. 10 Variations of coefficient of friction with the temperature

contact conditions and the friction contact problem between the tool and the deformable body was modelled with the Coulomb's classical law, adopting an evolutional law that takes into account the effect of the local pressure on the local coefficient of friction. The contact with friction is considered by an augmented Lagrangian approach [24]. Deformable bodies are discretized with 3D solid finite elements. In the present study, a traditional trilinear eight-node hexahedral finite element associated with a selective reduced integration scheme was adopted [25].

It should be mentioned that to derive a friction law, one needs to perform the numerical simulation for different normal contact forces and sliding distances. The numerical simulation of only one elementary asperity is considered in this study to estimate the two friction force components (ploughing and deformation) following the approach suggested by Wriggers [22]. Numerical simulations were actually performed with a null friction coefficient for the different elementary asperities analysed in this study, as Jeon and Bramley did considering several asperities [26]. Each numerical experiment still takes some time due to the problem dimension [22]. Also, it is necessary to consider different geometries to obtain a statistical representative distribution of the microgeometries. However, the objective in this work was to gain some insight into the behaviour of the micro-asperities of the contact interface.

This numerical model allows estimating the two components (ploughing and deformation) of the friction force as show in the equation:

$$f_{\text{num}} = f_{\text{plough}} + f_{\text{deform}} \tag{8}$$

The same approach from Section 2.1 was followed to achieve the numerical global result. The elementary numerical force is multiplied by the peak count to obtain the global numerical force:

$$F_{\text{num}} = P_c(f_{\text{plough}} + f_{\text{deform}}) \tag{9}$$

Table 2 Experimental data used in the simulation

Temperature [°C]	Compression modulus [GPa]	Strength in compression [MPa]
23	1.129	44.3
50	0.538	30.1
65	0.420	22.6
80	0.275	16.0

3 Experimental

3.1 Materials

The material used in the tools was an AISI H13 1.2344 tool steel, Ramada Orvar 2 M (F. Ramada, Portugal). The contacting surfaces of the metallic tools were made by electrical discharge machining method.

A polypropylene homopolymer, Domolen 1100 N of MFR 12 g/10 min (230°C/2.16 kg; DOME Polypropylene, The Netherlands) was used to mould the plastics test pieces.

3.2 Samples

Rectangular plates of 62×31×2 mm were moulded using a Krauss Maffei KM-60 210 injection moulding machine of 600 kN clamping force (Krauss Maffei AG, Germany).

From these injection mouldings, small blocks were cut with 5×6×2 mm for mechanical characterization by dynamic mechanical analysis (DMA), 50×10×4 mm for the determination of the elastic modulus in compression and 10×10×4 mm for the strength.

3.3 Test methods

The mechanical properties of the moulded material in compression were determined using a universal testing machine Zwick Z100 (Zwick, Germany) with a controlled temperature environment chamber. The compression tests were performed according to the ISO 604 standard.

The DMA Triton model Tritec 2000 (Triton Technology, UK) was used to evaluate the variation of the elastic modulus of the polymeric material with the temperature according to the DIN53457 standard.

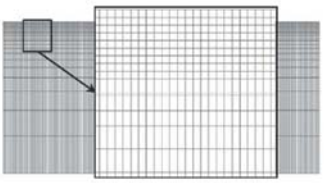

Fig. 11 Finite element mesh and detail

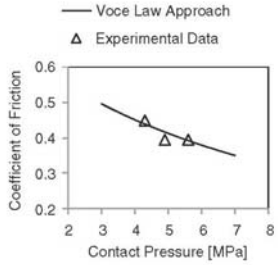

Fig. 12 Variation of coefficient of friction with contact pressure

The roughness of the steel surfaces was measured with a Perthometer M2 (Mahr GmbH, Germany). The cut-off length was selected according to the DIN 4768 standard.

The friction tests were carried out using prototype equipment, fitted on a universal testing machine Instron 4505 (Instron Corp., USA), with a load cell of 1 kN at a crosshead displacement rate of 10 mm/min following the method proposed by Pouzada et al. [3]. A scheme of the test parts is shown in Fig. 5.

In a first stage, the steel stamp was heated up to 150°C. Then, the stamp was pressed against the polymeric part at the recommended contact pressure and this is maintained until the end of the process. After 2 min of the contact, presure is applied and the replication of the surface in the polymeric part is obtained. After this 2-min period, the system was cooled down until the required test temperature, which corresponds to the one used in the ejection stage. The system

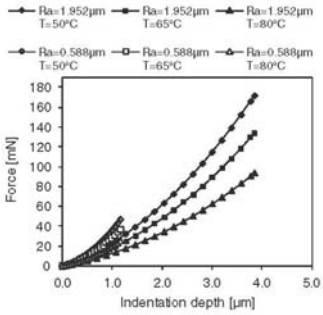

Fig. 13 Variation of the indentation force with test temperature

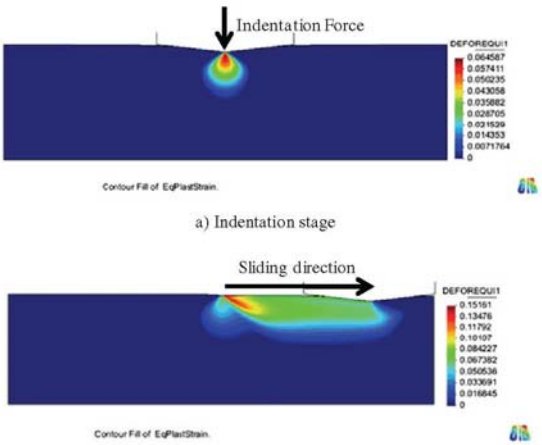

Fig. 14 Equivalent plastic strain for 65°C and *Ra*=1.952 μm

a) Indentation stage

b) Displacement stage

is maintained at this temperature for 2 min. Then the relative displacement was started with a velocity of 10 mm/min until a total displacement of 4 mm is achieved.

The variables (roughness) and test conditions (contact pressure and test temperature) used are described in Table 1. The values selected for the contact pressure are common with this polypropylene [3, 5, 11] and the testing temperature is within the common range of ejection temperatures for this material.

4 Results

4.1 Mechanical properties

Compressive tests were performed at four different temperatures. The chosen temperatures were the same as those selected for the ejection of the moulded part. The stress–strain curves of the polymer (Domolen 1100 N) are summarised in Fig. 6.

The elastic modulus and the strength compressive data, as well as the evolution of the elastic modulus with temperature obtained from DMA are summarised in Fig. 7. These data confirm a good adjustment between the elastic modulus data obtained by DMA and conventional compression testing. This information is relevant to obtain data; in particular, temperatures higher than those achievable when using an environment chamber with a universal testing machine.

4.2 Friction tests

A typical trace of the friction force evolution during a test is shown in Fig. 8. The force increases until a maximum value is attained corresponding to the onset of ejection, the static friction force. Then, the relative motion between parts begins and the force decreases to a lower value corresponding to the kinetic friction force. In the injection mould design, this force is not important because of the draft angles that usually are introduced in the design of the parts, the contact force decreases rapidly when ejection starts.

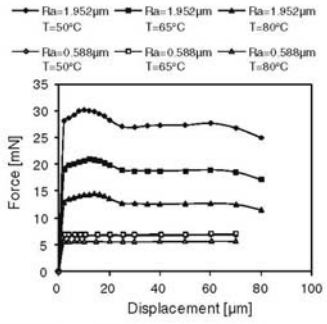

Fig. 15 Evolution of friction force during the displacement stage

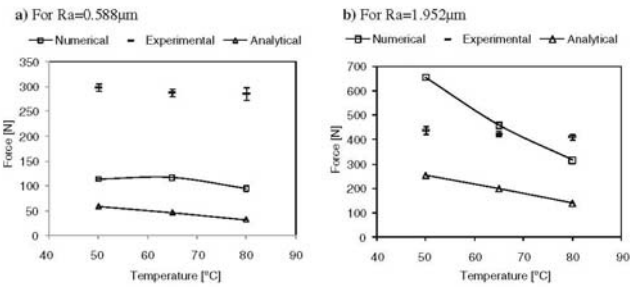

Fig. 16 Predicted friction force by analytical and numerical modelling versus experimental data

The variations of the coefficient of friction with contact pressure and temperature, for variable surface roughness, are shown in Fig. 9. It can be observed that the global trend of the coefficient of friction is mainly dictated by the surface roughness.

In Fig. 10, the variation of the coefficient of friction with temperature is shown. It is worth noting that for low roughness, the effect of temperature is hardly noticeable.

4.3 Simulation

In the finite element method simulations with the DD3IMP code, the geometry of the elementary asperities was defined based on the measured roughness variables described in Section 2.1 and presented in Table 1. The mechanical properties and the coefficient of friction determined experimentally were used as input. Some of the experimental data in Fig. 7 are tabulated in Table 2.

The slave deformable body was discretized with a high-density mesh (Fig. 11), which considers plane strain conditions. This strategy was adopted to allow a comparison with the analytical model already introduced, although it is known that a real microgeometry is always a two-dimensional surface [22]. The base of the slave body was fixed.

The polymer was considered as elastic perfectly plastic material, taking into account the mechanical properties presented in Table 2. The parallelepiped 0.1-mm long block has a width of a=0.23 mm and a height of b=0.06 mm. The polymer was considered to be isotropic. Regarding the coefficient of friction, the simulations were performed assuming an evolutional law for this parameter. The adopted evolutional law takes into account the effect of local contact pressure on the local coefficient of friction:

$$\mu = B - (B - A)\exp(-mp^n) \tag{10}$$

where, A, B, m, and n are parameters of the best fit of the Voce type law to the observed dependence of the coefficient of friction on the contact pressure, p (Fig. 12). It must be noted that this law has four parameters and that only three experimental were results are available. Thus, the parameters were identified by best fitting and considering saturation behaviour for high-contact pressure values in order to minimise numerical problems (A=0.75, B=0.0, m=27.0, n=0.72).

In Fig. 13, the evolution of the indentation force for the two highest values of roughness, Ra is observed. The maximum force corresponds to a displacement equal to the double of Ra.

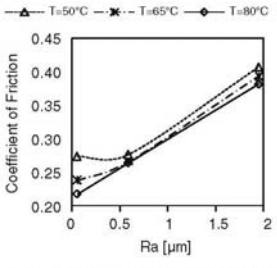

Fig. 17 Experimental coefficient of friction as a function of roughness and temperature. Contact pressure of 4.9 MPa

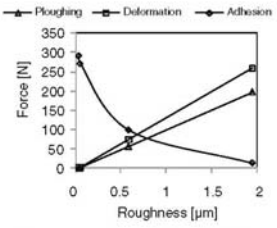

Fig. 18 Friction force components contribution (P=4.9 MPa and T=65°C)

At the end of the indentation stage and only for the surface with the highest roughness, there is some irreversible deformation of the polymer (Fig. 14a). For the lower values of roughness, the polymer is kept in the elastic regime at the end of the indentation process.

The situation at the end of the displacement stage is shown in Fig. 14b. For the highest roughness case, the equivalent plastic strain increases due to the friction force. The strain increase is higher for lower temperatures since the mechanical resistance increases.

Figure 15 shows the simulation of the friction force evolution during the displacement stage as predicted by the numerical simulation. As it would be expected, the increase in roughness results in an increase of the friction force.

4.4 Can friction in ejection be predicted?

Based on the experimental and the previous numerical results, Eqs. 7 and 9 were applied to estimate the ejection force. The experimental data for the case of the higher surface roughness in Fig. 16 are compared with results of the analytical model and of the numerical simulation. For the lowest value of roughness, the friction model and simulation could not describe the actual tribological process. In fact, when the mould surfaces are smoother, the polymer deforms only elastically as it was seen in the numerical simulations. In both prediction cases, the adhesion component of the ejection force was not considered and this may help to justify the large difference between experimental data and the models.

The coefficients of friction worked out from the experimental data show an increase in the lower region of the surface roughness (Fig. 17). This increase of the coefficient of friction is due to increased adhesion which results from the more intimate contact (higher pressure) and nonpermanent deformation when the roughness amplitude is small.

A full method to predict the ejection force in injection moulding should include the three terms referred to in Eq. 2. In this study, it was possible to establish an analytical model for the ploughing term and account for ploughing and deformation by numerical simulation. When the surface roughness *Ra* is clearly higher than 1 μm, this approach allowed estimating with acceptable precision the contribution of the ploughing and deformation terms of the ejection force. In the case of smoother surfaces, large deviations were observed which may be attributed to the nonconsideration of the adhesion contribution. The increasing role of the adhesion contribution for average roughness lower than 0.5 μm can be evidenced by subtracting the ploughing and deformation contribution from the experimental data as shown in Fig. 18. In this figure, the estimated contribution of each term is also depicted. It is possible confirm the importance of the adhesion component especially at low values of roughness. When the average roughness increases, the deformation and ploughing components are preponderant and the adhesion contribution becomes residual.

5 Conclusions

In injection moulding, the ejection of the moulded part is associated to a tribological process where on top of the usual sliding process there is the contribution of the replication of the plastics part on the moulding surface. In this singular tribological situation, there is physical interlocking of the two surfaces especially when the roughness is high.

Experimental tests highlighted the influence of roughness, temperature and contact pressure on the friction force upon demoulding a commercial polypropylene.

For average roughness *Ra* of the mould surface above 0.5 μm, it was observed that the friction force increases with the surface roughness and the contact pressure and reduces with increasing temperature. This tendency could be observed in the numerical simulation where the ploughing and deformation terms were considered. It was also possible to predict the contribution of the ploughing component by analytical modelling considering the asperities as conical entities. The ploughing and deformation terms vary linearly with roughness, the contribution of deformation being more relevant than ploughing.

Conversely, when the roughness drops to values associated to polished surfaces (below *Ra*=0.5 μm) the predictions fail by not considering the contribution of the adhesion force term associated to intermolecular forces. This deviation rapidly increases with reducing roughness.

More experimental work, with metallic stamps with lower roughness, should be carried out for a better understanding of the mechanisms of adhesion.

Acknowledgements MS Correia thanks the Polytechnic Institute of Leiria for the financial support and leave of lecturing during the research period. The authors thank the support from the Portuguese Foundation for Science and Technology to MS Correia through the grant SFRH/PROTEC/49301/2008.

References

1. Viana JC, Billon N, Cunha AM (2004) The thermomechanical environment and the mechanical properties of injection moldings. Polym Eng Sci 44(8):1522–1533
2. Araújo BJ, Pouzada AS (2002) Design of ejection systems for injection moulds. O Molde 54:36–41

3. Pouzada AS, Ferreira EC, Pontes AJ (2006) Friction properties of moulding thermoplastics. Polym Test 25(8):1017–1023
4. Bhagavatula N, Michalski D, Lilly B, Glozer G (2004) Modelling and verification of ejection forces in thermoplastic injection moulding. Model Simul Mater Sci Eng 12:S239–S254
5. Pontes AJ, Pouzada AS, Pantani R, Titomanlio G (2005) Ejection force of tubular injection moldings. Part II: a prediction model. Polym Eng Sci 45(3):325–332. doi:10.1002/pen.20275
6. Pontes AJ, Titomanlio G, Pouzada AS (1999) The influence of processing conditions in the ejection forces of injection moulded parts. Paper presented at the PPS 15th Annual Meeting. Hertogenbosch/The Netherlands
7. Gonçalves MW, Salmoria GV, Ahrens CH, Pouzada AS (2007) Study of tribological properties of moulds obtained by stereolithography. Virtual Phys Prototyp 2(1):29–36
8. Kinsella ME, Lilly B, Gardner BE, Jacobs NJ (2005) Experimental determination of friction coefficients between thermoplastics and rapid tooled injection mold materials. Rapid Prototyp J 11(3):167–173
9. Zhang SW (1998) State-of-the-art of polymer tribology. Tribol Int 31:49–60
10. Menges G, Bangert H (1981) Measurement of coefficient of static friction as a means of determining opening and demolding forces in injection molds. Kunststoffe 71(9):552–557
11. Berger GR, Friesenbichler W, Scofer G, Freudenschuss G (2008) A new practical measurement apparatus for demolding forces and coefficients of friction in injection molding. Paper presented at the PPS-24 Polymer Processing Society 26th Annual Meeting. Salerno, Italy. June 15–19
12. Dearnley PA (1999) Low friction surfaces for plastic injection moulding dies—an experimental case study. Wear 225–229 (2):1109–1113
13. Sasaki T, Koga N, Shirai K, Kobayashi Y, Toyoshima A (2000) An experimental study on ejection forces of injection molding. Precis Eng 24(3):270–273
14. Pontes AJ, Pouzada AS (2004) Ejection force in tubular injection moldings. Part I: effect of processing conditions. Polym Eng Sci 44:891–898
15. Ferreira EC, Costa MF, Laranjeira CR, Oliveira MJ, Pouzada AS (2004) Comparative study, by optical techniques of the interface polymer/steel in replication conditions. Mater Sci Forum 455–456:467–471
16. Correia M, Capela C, Pouzada AS, Miranda AS (2007) Contributions to the modelling of ejection in injection moulding. Paper presented at the PMI 2007 International Conference on Polymers and Moulds Innovations. Gent, Belgium.
17. Suh NP, Mosleh M, Howard PS (1994) Control of friction. Wear 175(1–2):151–158
18. Ferreira EC, Laranjeira CR, Gomes JR, Miranda AS, Pouzada AS (2003) Influência da temperatura e da rugosidade no coeficiente de atrito, na extracção de peças injectadas em plástico. In: II Iberian Congress of Tribology, Valencia, Spain
19. Gao J, Luedtke WD, Gourdon D, Ruths M, Israelachvili JN, Landman U (2004) Frictional forces and Amontons' law: from the molecular to the macroscopic scale. J Phys Chem B 108 (11):3410–3425. doi:10.1021/jp0363621
20. Pontes AJ, Ferreira EC, Pouzada AS (2004) The effect of temperature and surface roughness on the coefficient of friction between thermoplastics and moulding surfaces. Paper presented at the PPS Americas Reg. Meeting. Florianópolis, Brazil.
21. Tabor D (1981) Friction—the present state of our understanding. J Lubr Technol 103:169–179
22. Wriggers P (2006) Computational contact mechanics, 2nd edn. Springer, Berlin
23. Menezes LF, Teodosiu C (2000) Three-dimensional numerical simulation of the deep-drawing process using solid finite elements. J Mater Process Technol 97(1–3):100–106
24. Oliveira MC, Alves JL, Menezes LF (2003) Improvement of a frictional contact algorithm for strongly curved contact problems. Int J Numer Methods Eng 58(14):2083–2101. doi:10.1002/nme.845
25. Hughes TJR (1980) Generalization of selective integration procedures to anisotropic and nonlinear media. Int J Numer Methods Eng 15(9):1413–1418
26. Jeon J, Bramley A (2007) A friction model for microforming. Int J Adv Manuf Technol 33(1):125–129. doi:10.1007/s00170-006-0608-1